Stability of block mattress under non-uniform flow downstream of sluice gate

By

Tian Ye

Master of Science

in Civil Engineering and Geosciences

Delft University of Technology,

to be defended publicly on Thursday October 12, 2017 at 11:30 AM.

Supervisor:	Prof. dr. ir. W.S.J. Uijttewaal	TU Delft
Thesis committee:	Ir. H.J. Verhagen	TU Delft
	Ing. C. Kuiper	TU Delft
	Jean-Pierre Quataert,	Holcim

TU Delft

Holcim

Acknowledgement

This report presents the working has been done for my graduation thesis, as a closure of master study in Hydraulic engineering in Delft Technology of University. The research topic is proposed by company Holcim and the research work is done in TU Delft.

The study started with the problem found by Holcim that the design formula for block mattress only limitedly functioning. Based on the problem identifying by Smyrnis (2017), flume experiments have been done in the water lab in civil faculty, TU Delft. For the purpose of optimizing the design formula in a quantitative way, a detailed study has been conducted.

I would like to give thanks to many people offered help during my thesis. I would like to thank my graduation committee, prof. dr. ir. W.S.J. Uijttewaal, Ir. H.J. Verhagen, Ing. C. Kuiper, from TUD and Mr. Jean-Pierre Quataert from company Holcim for the support and inspirations they gave me during the thesis. Apart from the academic knowledge I learned, the approaches to solve problems are essentially valuable to me.

I would also like to thank Mr. S. De Vree. and the staff at water lab for their patient assistance. Moreover, special thanks to my coworker for this research Xabi Arrieta Ortubay. It was both efficient and pleasant working with you.

List of Figures

List of Tables

List of Symbols

Roman symbols

A	Area	[m^2]
a	Flow acceleration	[m/s^2]
C_D	Drag coefficient	[-]
C_F	Friction coefficient	[-]
C_L	Lift coefficient	[-]
D	Characteristic dimension (Pilarczyk)	[m]
d	Stone diameter	[m]
D_{n50}	Median nominal diameter	[m]
F_D	Drag force	[N]
F_F	Friction force	[N]
F_G	Gravity force	[N]
F_L	Lifting force	[N]
g	Gravitational acceleration	[m/s^2]
h	Water depth	[m]
h_m	Jongeling characteristic length	[m]
k	Turbulence kinetic energy	m^2/s^2
K_h	Water depth parameter (Pilarczyk)	[-]
K_T	Turbulence parameter (Pilarczyk)	[-]
k_s	Equivalent roughness	[m]
k_s^+	Non-dimensional equivalent roughness	
l_m	Mixing length l_m	[m]
Q	Flow idscharge	[l/s]
Q_i	Raupach quadrant	[-]
r_i	Relative turbulence intensity	[-]
R_e	Reynolds number	[-]
u	Streamwise velocity	[m/s]
u_*	Shear velocity	[m/s]
u^+	Non-dimensional streamwise velocity	
u_{fail}	Failure streamwise velocity	[m/s]
u_{peak}	Peak of streamwise velocity associated with failure	[m/s]
v	Transverse velocity	[m/s]
V	Volume	[m^3]
w	Vertical velocity	[m/s]
x	Streamwise coordinate	m
y	Transverse coordinate	m
y^+	Non-dimensional transverse coordinate by shear velocity	
z	Vertical coordinate	m

Greek symbols

α	Empirical constant (Various uses)	[-]
α	Turbulence magnification factor derived based on peak velocities	[-]
β	Empirical constant (Various uses)	[-]
Δ	Relative density	[-]

δ	Error	[-]
κ	Von-Kartman constant	[-]
ρ	Water density	[Kg/m^3]
ρ_s	Solid density	[Kg/m^3]
φ	Stability parameter (Pilarczyk)	[-]
τ	Shear stress	[N/m^2]
τ_t	Turbulence viscosity or eddy viscosity	[N/m^2]
Ψ	Shield parameter	[-]
Ψ_{Lm}	Stability parameter (Jongeling)	[-]
Ψ_{WL}	Stability parameter (Hofland)	[-]
$\Psi_{u-\sigma[u]}$	Stability parameter (Hoan)	[-]

Mathematical symbols

σ_x	Standard deviation
$\bar{x}$	Average over time
$\overline{x'^2}$	Square root average
x'	Fluctuating part of x around $\bar{x}$
$\lvert x \rvert$	Absolute value
$\langle x \rangle_L$	Spatial average of x over L
$\overline{u'w'}$	Reynold stress

Abbreviations

2D	Two-dimensional
3D	Three-dimensional
ADV	Acoustic Doppler velocimeter
BFS	Backwards facing step
EMS	Electromagnetic Magnetic velocimeter Sensor
QSF	Quasy-steady forces
LDV	Laser Doppler velocimeter
TWP	Turbulence wall pressures

Abstract

Downstream of hydraulic structures, the flow is normally of turbulence. This will cause considerable erosions on a gravel bed. To prevent this, block mattress is preferable in many cases. Block mattress is normally a rectangular unit made of concrete blocks joined together by geotextile or polypropylene ropes. Its effective stabilization and feasibility on construction make it commonly used against scouring problems, protecting underwater pipelines and cables. Although adequate research has been done for stone stability, the study on block mattress is rather lagging behind. The currently widely used design formula with dedicated parameters for block mattresses was derived by Pilarczyk. However, it is observed to be partly functioning under non-uniform flow condition, since the turbulence parameter is rather empirical.

Therefore the main purpose of this thesis is to optimize the current design formula (Pilarczyk's) for non-uniform flow condition. In this flow regime, turbulence is of importance for bed material entrainment. Thus this research focused on how to introduce turbulence effect into formula explicitly. To predict the failure of block mattress better, a detailed study on failure mechanism and impact of flow condition over the block mattress edge is necessary.

Jongeling et al.(2003) first combined the turbulent effect and flow velocity in the stone stability formula, in a form of $\bar{u} + \alpha\sqrt{k}$. This method included the turbulence effect explicitly as turbulence kinetic energy, as well as defined the responsible failure structure as the combination of flow velocity and turbulence effect. It is proven to be effective and continue to be used by later researchers. Thus in this thesis, this method representing the turbulence effect is still being used. In this research, the test results from scale model was analyzed following with including Jongeling's approach into Pilarczyk's formula to account for turbulence effect. Therefore, the proposed parameter reads as follows:

$$\Delta D = \frac{\varphi \times 0.035 \times (\bar{u} + \alpha\sqrt{k})^2 \times K_h}{\Phi_s \times 2g \times K_s}$$

The stability parameter φ, turbulence magnification factor α need to be determined. Lacking sufficient previous research, experiments have been done to collect data. In total, three series, four set-ups and 18 failure cases have been recorded. From the obtained data, values of $\alpha = 3.25$ and $\varphi = 0.3$ give best fit.

The new approach, with a safety factor, gives considerably smaller scatter than Pilarczyk's formula. From this thesis, the formula provides α and φ for the flow under sluice gate condition. Together with Ortubay's work on flow over weir structure, the series experiment was pointing a direction of testing different types of hydraulic conditions thus providing a series of α and φ values. it is a robust toll to predict the block mattress behavior since it has the feasibility to represent various flow conditions. Moreover, the series of α and φ values also provides the distribution functions for probabilistic design.

Due to the fact that the flow in the present situation is accelerating, a formula including acceleration term was applied as a way of evaluation. Coincide has been found between two parameters. This not only indicated that the current approach of including turbulence into Pilarczyk's formula is reasonable but also verified the possibility of a wider application range of the former formula.

Study has been done for failure mechanism targeting the last row of block mattress. It was done by synchronizing the recorded failure moment with velocity signal. A responsible flow patter was observed: A sudden increase of flow velocity following by a peak of shear stress. Moreover, for situation that flow under sluice gate, larger flow structure (pressure gradient) was found to be more responsible than turbulence structure. Moreover, the backward facing step was also found can be account for the occurrence of a failure.

Flow properties have been checked to get a better understanding of the interaction between flow and block mattress. Although the flow is from standard open channel flow, logarithmic and wake-log velocity profiles were observed. A clear pattern of mixing length generation showed, and the Bekhmetev distribution was predicted valid for the further downstream region. Moreover, by calibrating shear velocity, a larger value for equivalent roughness than it suggested by Pilarcyk has been found.

Contents

1 Introduction

Erosion of river bed and bank downstream of hydraulic structures, like sluice gate, weir and culvert is a common problem in hydraulic engineering. The block mattress as a solution to prevent the sand bed from scouring, showing its advantages such as higher stability and being able to construct efficiently. However, the current design formula is rather empirical and contains several parameters that are still uncertain.

1.1 Problem definition

For engineering approach, Pilarczyk's formula is widely used to predict the stability of block mattress. However, the accordingly designed block mattress was found to be washed away for instance at the reattachment point of weir structure where the flow is highly turbulent.

Fundamentally, the reason for inaccurate prediction lies in the unknown of failure mechanism. The failure pattern appears to be brittle and very different from that of gavel material. Van Velzen and De Jong (2015) summarized the block mattress behavior under propeller flow. Later Smyrnis (2016) recorded the failure motion in open channel flow. Both experiments recorded a very sudden and expeditious failure of the block mattress. For the purpose of a better understanding, a series of experiments was conducted and this thesis is part of it. Ortubay (2017) continued the research for the flow over weir structure and concluded the maximum of flow velocity is responsible. Although the more in-depth analysis was addressed, no study has been conducted quantitatively. Thus this thesis focused on the flow under sluice gate and more quantitative analysis was applied.

In term of the design formula, originally, Pilarczyk's formula was derived for uniform flow. Whereas the flow downstream of hydraulic structures are normally fierce and non-uniform. Pilarczyk indeed released the fact and introduced turbulence effect as a correction coefficient into the formula. However, the drawback of this approach is fairly obvious and can be concluded as follows: i) the combination of velocity and turbulence effect, i.e. $K_T \times u_{cr}$, is not able to present specific flow conditions. For the flow at the reattachment point of weir structure with nearly zero flow velocity but high turbulence, the formula tends to give fairly small dimensions of block mattress. However, recent researches all concluded that the turbulence is of crucial importance. Thus high instability of designed block mattress can be expected, meaning Pilarczyk's formula tends to give under-dimensional results. On the other hand, for the flow under sluice gate with high velocity but low level of turbulence, the formula gives over-dimensional results. ii) the current turbulence coefficient K_T is considerably uncertain and can only be used as a rule-of-thumb. For the degree of turbulence, Pilarczyk only suggested categories as normal, increased and heavy turbulence. This category is rather vague hence unable to represent different flow conditions. Therefore more representative expression on turbulence effect for various flow conditions into the stability formula is needed.

To reveal engineering problems in practice, physical experiment is proved to be a powerful method. Adequate experiments were done for stone stability study by previous researchers, and sufficient data was collected. In-depth studies on the interaction between flow properties and stone stability were conducted based on those experiments. However, for block mattress, no sufficient information has been collected. Detailed information regarding the cause of failure of block mattress remains unknown, as well as the essential data for stability parameter deriving. Therefore, experiments using scale model will be conducted for the purpose of investigating

the failure mechanisms and measuring turbulence effects, as well as providing a database for later research.

1.2 Objectives and research questions

This research can be seen as the first step to present turbulence effect on block mattress under various flow conditions in a more certain way. The main objectives can be summarized as optimizing Pilarczyk's formula for non-uniform flow conditions. This objective can be subdivided in:

- To derive a stability parameter that introducing turbulence effect into the stability formula
- To investigate the interaction between flow properties and block mattress.

To accomplish these objectives, several research questions come up:

Q1: What are the forces that exerted on the block mattress by the flow?

a. What are the flow properties in the current situation?
b. What flow structures exert what kind of forces on block mattress?

Q2: What is the forces can be expressed by the stability formula?

Q3: What is the responsible flow structure for the failure mechanism?

Q4: What is the most reasonable way to express the turbulence effect?

Q5: What data is needed from the experiments?

a. How many experimental set-up are needed?
b. How many failure cases is considered sufficient?
c. Which locations will be targeted for measuring?

Q6: How to derive required parameters with obtained data?

Q7: How well is the new stability parameter behave?

In this chapter, all the research questions will be conclusively answered in section 8.1. Next, in section 8.2, recommendations for further research will be given.

1.3 Research methodology and outline

In Figure 1.1 the approach of this thesis is displayed graphically. The applied methodology to answer the above research questions is aligned with the outline of this thesis.

Firstly, literature study is presented in Chapter 2 as the start of this thesis. Theoretical background on flow properties, forces on bed materials, the recorded failure patterns of block mattress as well as existing stability formula will be given. Q1, Q6 are able to be solved in this chapter. In Chapter 3, experimental configurations will be described. In this chapter, Q2 will be solved. With the obtained data, detailed studies on flow properties and block mattress failure mechanisms will be conducted in Chapter 4 and 5. In chapter 5, the explicit analysis will be done to solve Q5. The related parameters and proposal of new stability parameter will be derived in Chapter 6. The related Q3 and Q5 will be answered in this chapter. A discussion regarding possible inaccuracy and the limitation of this thesis will be given in Chapter 7. Finally, conclusions and recommendations will be addressed in Chapter 8.

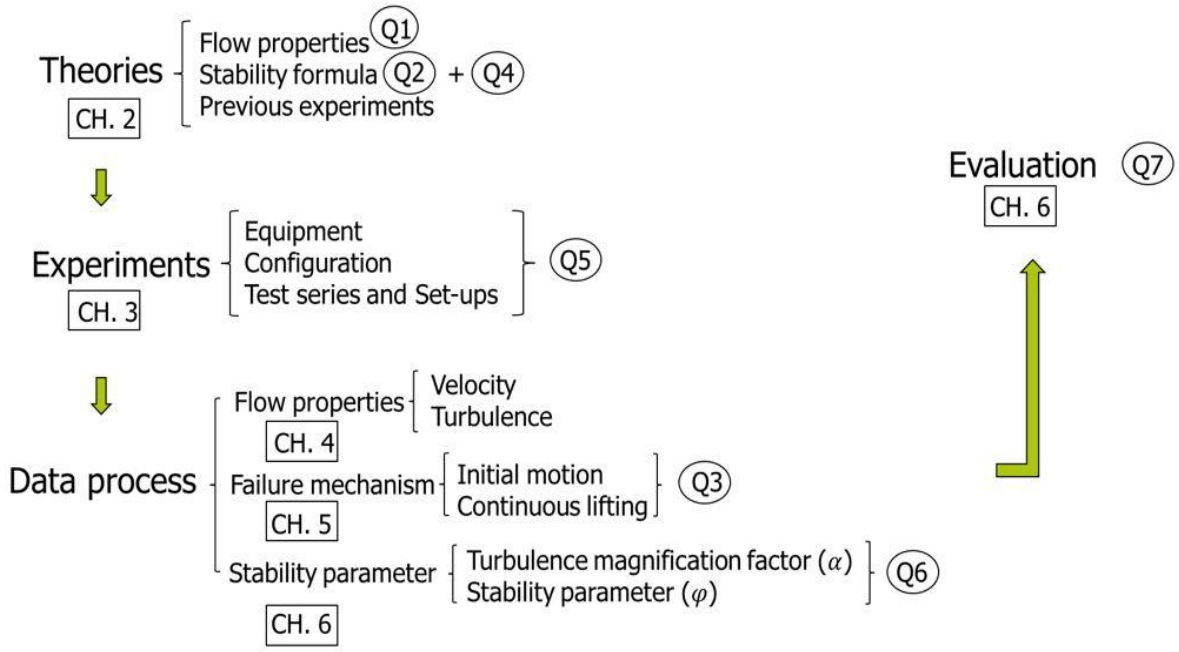

Figure 1.1: Flowchart of thesis outline

2 Literature review

In this chapter, some background information was presented to prepare for the later studying on the interaction between flow and block mattress. Therefore the presented theories were mainly focused on the well-established ones, i.e., fully developed uniform flows theories, forces on the single stone and the stone stability formula. The further extensive work from the existing theories to present case will be conducted in following chapters.

First, in section 2.1, flow and turbulence properties were discussed. This information was used to assess the forces on a single block and so caused failure mechanism in section 2.2. In section 2.3, Pilarczyk's formula, as well as existing stone stability, were presented. Finally, the chapter ended with some concluding remarks in section 2.4.

2.1 Flow properties

In this section, some basic characteristics of flow and turbulence will be discussed. In this thesis, the coordinate was defined as x to be the streamwise coordinate, y the upward coordinate, z transverse coordinate, the and u, v, w are the velocity components in three directions respectively. An over bar is used to represent the stationary mean part (e.g. $\bar{u}$) and a prime represents the fluctuating part (e.g., $u' = u - \bar{u}$).

The uniform open channel flow situation was elaborated to get a basic understanding since the situation is rather profoundly known. The subjects that essential for understanding the hydrodynamic forces on the block mattress were discussed (e.g. velocity distribution, turbulence intensity, turbulence kinetic energy, shear stress etc.). Afterwards, the theories on accelerating open channel flow were addressed, since it represents the flow situation in this thesis.

2.1.1 Uniform open channel flow

Velocity profile

For the case of uniform open channel flow over a rough bed, the vertical distribution of streamwise velocity is distinguished by vertical positions, i.e., viscous sublayer, buffer layer, log-wall layer and outer layer. The typical velocity profile for each layer is summarized as in Table 2.1.

Table 2.1: Velocity distribution in each wall region in open channel flow.

Region	Layer	Velocity distribution	Description
$0 < y^+ < 5$	Viscous sublayer	$u^+ = y^+$	Linear relation behaves well in this region; Viscous effect is the dominant in this region.
$5 < y^+ < 30$	Buffer layer	-	Both viscous and turbulent shear are important in this region; No analytical relation available; normally the velocity profile in this region is

			approximated by extrapolation between viscous sublayer and the log-law layer.
$30 < y^+ < 300$	Log-wall layer	$u^+ = \frac{1}{\kappa} lny^+ + B$	The logarithm law is well known to describe the velocity profile here. The turbulence stress starts to dominate instead of the viscous effect.
$y^+ > 300$	Outer layer	$u^+ = \frac{1}{k} lny^+ + \frac{2\Pi}{k} sin^2(\frac{\pi y}{2h})$	The profile in outer layer has a clear deviation from log law, that should be accounted for by considering a wake function. Coles (1956) proposed this Wake-law distribution, in which Π is the Coles wake strength parameter.

Despite the flow can be distinguished by several layers, the lag law is often used to describe the velocity profile over the whole water depth in open channel flow (Keulegan [1938]). The parameters κ and B were fixed to be 0.41 and 5.29 respectively by Nezu and Rodi [1986].

Turbulence intensity distribution

Nezu and Nakagawa (1993) proposed a universal law for the vertical distribution of turbulence intensity. It reads:

$$\frac{\sigma(u_i)}{u_*} = \alpha_i e^{-\beta_i \frac{y}{h}} \tag{2-1}$$

Where α_i and β are the empirical constants independent of the Reynolds number and the Froude number, i stands for three dimensions. The values of those empirical constants were established as follows:

$$\alpha_u = 2.30, \alpha_v = 1.63, \alpha_w = 1.2. \quad \beta_u = \beta_v = \beta_w = 1.0 \tag{2-2}$$

Shear stress distribution

The shear stress in the turbulent flow is given as follows:

$$\tau = \rho\nu \frac{d\bar{u}}{dy} - \rho\overline{u'v'} \tag{2-3}$$

$-\rho\overline{u'v'}$ is also called Reynolds shear stress, generally much larger than viscous shear stress ($\rho\nu \frac{d\bar{u}}{dy}$). Thus in an equilibrium flow, the shear stress yields as:

$$\tau = -\rho g(h-y)i = -\rho\overline{u'v'} = \rho(1-\frac{y}{h})u_*^2 \tag{2-4}$$

Where h is the water depth, i is the energy slope.

Turbulence viscosity and mixing length

Equation 2-4 is used to derive the turbulence viscosity in open channel flow. Turbulence viscosity or eddy viscosity was introduced by Boussinesq, in analogy with kinematic viscosity ($\tau_v = \rho\nu\frac{d\bar{u}}{dy}$), it reads:

$$\tau_t = \rho\nu_t\frac{d\bar{u}}{dy} \tag{2-5}$$

Later, the concept of mixing length was introduced to solve the closure problem of RANS equation by Prandtl (1875-1953). Following the Prandtl mixing-length hypothesis the velocity that characterizes the turbulent fluctuations is proportional to the velocity difference in the mean flow over a distance lm over which the mixing or transport of momentum takes place, and is given by: $l_m \cdot |\partial U/\partial y|$. By using l_m again as the governing length scale, the eddy viscosity can be written as:

$$\nu_t = l_m^2\left|\frac{d\bar{u}}{dy}\right| \tag{2-6}$$

And effective shear stress as:

$$\tau_t = \rho l_m^2\left|\frac{d\bar{u}}{dy}\right|\frac{d\bar{u}}{dy} \tag{2-7}$$

Till here, the problem of determining the eddy viscosity has now shifted to the determination of the mixing length l_m (Uijttewaal, 2005). Prandtl proposed a linear relation between l_m and the distance to the wall in the wall region. It reads:

$$l_m = \kappa y \tag{2-8}$$

Where the proportional parameter is known as the constant of von Karman κ ($\kappa \approx 0.4$).

The analysis for an open channel flow already has resulted in the Bakhmetev distribution given by:

$$l_m = \kappa h\gamma(1-\gamma)^{\frac{1}{2}} \tag{2-9}$$

Where h is the water depth and $\gamma = y/h$ (Uijttewaal, 2005).

Bed roughness

Considering the bed, in reality, can hardly be smooth, equivalent roughness (k_s) was introduced to describe the bed roughness. Further, to extend the velocity profile from smooth bed to rough bed, equivalent roughness height (y_0) was introduced. The expression for equivalent roughness height in smooth, intermediate and rough bed conditions was listed in Table 2.2:

Table 2.2: Equivalent roughness height for different bed roughness

equivalent roughness k_s	Bed roughness type	equivalent roughness height y_0
$k_s^+ < 5$	Smooth	$0.11\left\|\frac{\nu}{u^*}\right\|$
$5 < k_s^+ < 70$	Intermediate	$0.11\left\|\frac{\nu}{u^*}\right\| + \frac{k_s^+}{30}$
$k_s^+ > 70$	Rough	$\frac{k_s^+}{30}$

Where:

k_s^+: dimensionless equivalent roughness ($k_s^+ = \frac{k_s u_*}{\nu}$) [-]

The study on the value of equivalent roughness was mainly focused on the gravel bad. Nikuradse [1933] argued that for the flow over single layer of glued sand grains, $y_0 = k_s/30$, with $k_s = d_{n50}$, should be applied. Later Hofland (2005) found the y_0 value could go up to $k_s/10$ for a bed with randomly placed stones. In terms of the block mattress, Pilarczyk proposed $k_s \approx 0.05m$ for smooth type and about the height of the rib for articulating mats according to Nikuradse.

Turbulent structures

Despite the fact that the turbulent flow is highly chaotic, certain similar flow patterns can still be observed repeatedly. They are called 'coherent structures'. For the smooth bed, the well-known bursting process is account for the turbulence generation (Robinson, 1991). However, for the rough bed, it is not the case. Raupach [1981] performed a quadrant analysis to study the near-bed turbulence structure. It is found that Q4 ($u' > 0, v' < 0$) and Q2 ($u' < 0, v' > 0$) occur most frequently, since they are linked to the positive Reynolds shear stress ($-u'v'$). Besides, Raupach also argued that the Q4 are the most important events near rough walls, whereas Q2 for smooth walls.

Turbulence wall pressure

Booij (1998) states that pressure fluctuations caused by turbulent eddies could contribute considerably to the forces that initiate motion of bed particles. These pressures are known as turbulence wall pressure (TWP). Hofland (2005) concluded that the situation that TWP works most efficiently to lift a single stone is that the passing eddy has the same size as the project stone.

2.1.2 Accelerating open channel flow

The pressure gradient plays rather an important role in for example the development of boundary layer thus the velocity profile, the turbulence kinetic energy. Figure 2.1 gave a sketch on the flow behavior under different pressure gradient conditions.

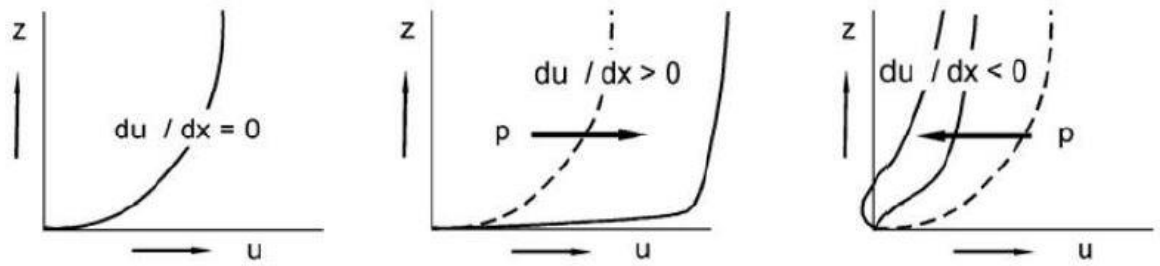

Figure 2.1: The influence of pressure gradients on velocity profiles (from R.S. Steentra 2014)

The flow is accelerating with a favorable (negative) pressure gradient, the development of boundary layer is stretched and grows slower, thus the turbulence production is suppressed. Whereas it is the opposite situation in the decelerating flow. With an adverse (positive) pressure gradient, the thickness of boundary layer increases. The flow separates from the wall, resulting in a large production of turbulence kinetic energy.

The non-uniformity of flow also makes more terms in Navier-Stokes equations non-negligible. For the Reynolds stress derivation (Eq. 2-4), the pressure gradient terms should be added (Nezu & Nakagawa, 1993). It gives new expressions as follows:

$$-\rho\overline{u'v'} + \int_y^h \bar{v}\frac{\partial \bar{u}}{\partial y}dy + \int_y^h \frac{\partial \overline{u'w'}}{\partial z}dy = \rho(1-\frac{y}{h})u_*^2 \qquad (2\text{-}10)$$

Another important conclusion can be drawn from the previous study on accelerating and decelerating flow is that the flow characteristics can be different under different geometries. For example, the relations between velocity and turbulence can be different from different types of acceleration, i.e., bed slope induced or constriction in vertical and horizontal induced acceleration.

2.1.3 Flow under the sluice gate

The energy loss and transfer have been sufficiently studied for this subject. However, for the purpose of this thesis, the flow properties, and hydrodynamic properties are more interesting. Figure 2.2 gave a sketch on the flow under sluice gate structure. The flow transforms from subcritical to supercritical flow, following a hydraulic jump. The position for hydraulic jump moves considerably when raising or lowering the tailwater elevation. The turbulence intensity is severe at the hydraulic jump position, thus any bed protection will be under serious flow attack here. Therefore, acknowledgment of the hydraulic jump position is of importance to the bed protection design. However, this is beyond the scope of this thesis. For this thesis, the condition that block mattress placed between the gate mouth and hydraulic jump will be addressed. This means the supercritical part of flow needs to be studied sufficiently to prepare for the block mattress behavior study. The detailed measured flow features will be given in Chapter 3 *experimental arrangement.*

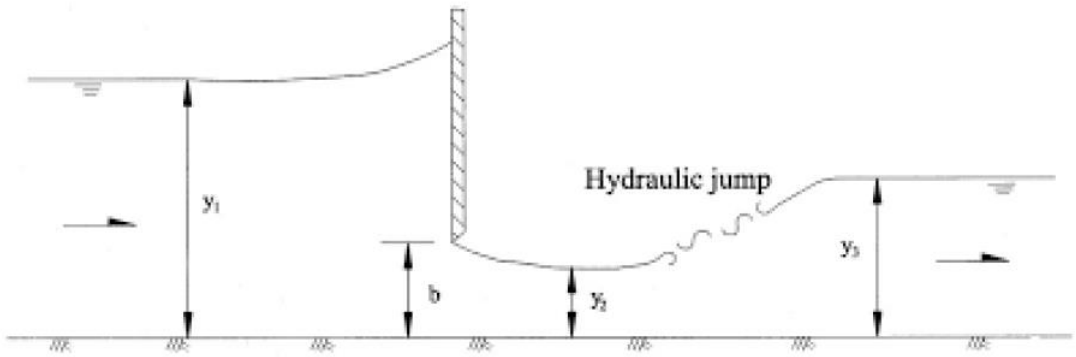

Figure 2.2: Flow under sluice gate

2.2 Block mattress

In this section, firstly the hydrodynamic forces on a single stone were discussed to give a general idea of the flow induced a force on bed materials, as well as to prepare for the force analysis on block mattress. Next, the failure patterns that observed by previous researchers were summarized.

2.2.1 Forces on a single stone

Quasi-steady force

A lift force (F_L) present when the flow velocity above the stone is higher than the velocity under the stone. A drag force (F_D) is caused when the stone exposed to a fluid flow. Figure 2.3 gave an overview on the force terms generated by flow on a single stone.

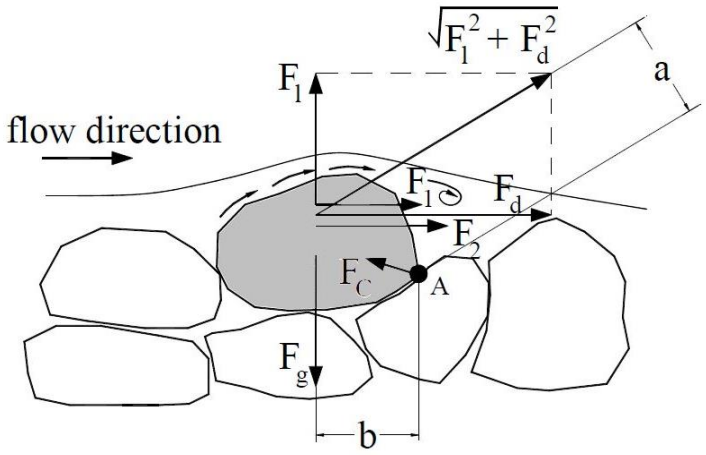

Figure 2.3: Forces acting on particles resting on a bed surface from Hoan [2008]

According to the Bernoulli law, these forces are proportional to the velocities in the vicinity of the stone (Hoan [2008]). The drag force and lift force can be formularized as follows:

$$F_D = \frac{1}{2} C_D \rho A_D u|u| \tag{2-10}$$

$$F_L = \frac{1}{2} C_L \rho A_L u^2 \tag{2-11}$$

Where C_D and C_L are the drag and lift coefficient respectively.A_D and $A_L$is the exposed area of the particle. u is the velocity near the particle. Adequate study has been done to determine the drag and lift coefficients (for detailed the review, see Hofland 2005). The drag coefficient is rather constant if deriving from $u_{0.15}$ (the critical velocity for stone hemispheres at $\Pi/d \approx 0.5$), namely $C_{D\,0.15} \approx 0.23 - 0.3$. As for the lift coefficient, values of 0.15 to 0.22 are found at high Re_*, when the particle is placed between other particles (Einstein & El-Samni, 1949; Xingkui & Fontijn, 1993; Benedict & Christensen, 1972).

The velocity near the particle is used to determine the forces. This velocity always consist of mean and fluctuating part, i.e., $u = \bar{u} + u'$ (Reynolds components). For the local velocity near the particle, the fluctuating part can be at the same magnitude as the man part, thus cannot be neglected. This leads to the mean (as Eq. 2-10 and 2-11) and fluctuating part, so called quasi-steady fluctuating force, as in Eq. 2-12 and 2-13.

$$F_D' \propto \bar{u}u' + \frac{1}{2}u'^2 - \frac{1}{2}\sigma(u)^2 \tag{2-12}$$

$$F_L' = a\bar{u}u' + b\bar{u}v' \tag{2-13}$$

Dynamic drag force

The acceleration, induced by a pressure gradient, also exerts external force to the particle. This dynamic force mainly consists of two parts, the buoyancy force and the net force caused by the accelerating sphere relative to the flow, as shown in Eq. 2-14.

$$F_a = \rho V \frac{D\bar{U}}{Dt} + \rho V C_m \left(\frac{D\bar{u}}{Dt} - \frac{dv_p}{dt}\right) \tag{2-14}$$

Apart from the flow induced net force, the placement of the stone, as well as the geometry, can also be a source of external force. The bed slope plays an important role on the entrainment of stone. The adjacent particles also provide resistance of the project particle. In the case of block mattress, the resistance provided by geotextile cannot be neglected, however not possible to quantify.

2.2.2 Failure mechanism

Regarding the vulnerable position of block mattress, Jol Godbold and Nikki Sackmann (2014) determined that failure occurs mainly to the edge. Van Velzen and De Jong (2015) concluded that the failure is also very sensitive to the placement of block mattress. In addition, they also argued that the critical failure conditions are different between ‘closed edge’ and ‘open edge’.

As for the failure pattern, Smyrnis (2016) observed a clear pattern of block mattress failure. With no upstream obstacle, i.e., free upstream edge, the block mattress fails as a whole in a ‘snake’ shape. Besides, the degree of turbulence plays a more important role than the velocity magnitude. Van Velzen and De Jong (2015) described the failure process as the ‘snow-ball’ effect. The drag force continuously increases with the uplifting of an edge block resulting, eventually causing the mattress to flip over.

In terms of the failure moment, in the experiment of Smyrnis (2016), the failure occurred abruptly which made the definition of failure moment difficult. Van Velzen and De Jong (2015) defined the failure moment as when the block is lifted half of a bl0ck thickness. The reason for this threshold is they observed the block stayed rather stable for a while in this position, namely no falling back nor lifting any further.

Generally and more fundamentally, turbulence structures were found to be essential for the failure occurrence (Hofland 2005). Specifically, the turbulence wall pressure is of importance for the initial motion to happen. Moreover, Steenstra (2014) concluded that the spatial acceleration is responsible. Although all those theory backgrounds are based on stone stability situation, they still provide a version of the interaction between flow and block mattress.

2.3 Existing stability formula

In this section, existing stability formula will be discussed. It started with Pilarczyk’s formula, following with more fundamental formula regarding including the turbulence effect explicitly. Next a summary on all formula was given aiming at their specializations.

Pilarczyk (2001)

$$\Delta D = 0.035 \frac{\varphi}{\Psi_s} \frac{K_T K_h}{K_s} \frac{\langle \bar{u} \rangle_h^{\,2}}{2g} \tag{2-15}$$

Where:

$\Delta = Relative\ density$ [−]

$D = Characteristic\ dimension(thickness)$ [m]

$g = Acceleration\ of\ gravity = 9.81$ [$^{m}/_{s^2}$]

$\langle \bar{u} \rangle_h = Critical\ depth\ averaged\ flow\ velocity$ [m/s]

$\varphi = Stability\ parameter$ [−]

$\Psi_s = Critical\ Shield\ parameter$ [−]

$K_T = Turbulence\ factor$ [−]

$K_h = Depth\ parameter$ [−]

$K_s = Slope\ parameter$ [−]

The formulization of Pilarczyk's formula is based on Shield's stability formula. It introduced the turbulence effect, bed slope influence, and water depth parameter in an implicit quantified way. The empirical coefficient 0.035 was concluded from the data sets on stone stability experiments, thus can be expected not behaving well for block mattress condition. The water depth parameter K_h was studied to be equivalent to C_f for uniform flow. Although the formula is also used for non-uniform flow, the K_h value has not been corrected. The formula distinguished the differences of the failure conditions for block edge and block middle. For different flow conditions, e.g., river bands, hydraulic jump, downstream of stilling basins, the formula also provided suggested turbulence level values. However, the turbulence coefficient is way too implicit, more can be seen as a rule-of-thumb, hence cannot represent all types of flow conditions well. Rock manual in 2015 associated K_T with turbulence relative intensity reads:

$$K_T = \frac{1+3r}{1.3} \tag{2-16}$$

Where $r = \frac{\sqrt{\overline{(u'^2)}}}{\bar{u}}$.

The Jongeling stability parameter

The first approach to include turbulence explicitly was given in Jongeling et al. (2003), using turbulence kinetic energy. It reads:

$$\Psi_{WL} = \frac{\langle (\bar{u}+\alpha\sqrt{k})^2 \rangle_{hm}}{\Delta g d} \tag{2-17}$$

Where:

α: empirical turbulence magnification factor [−]

k: turbulence kinetic energy [m/s]

$\langle .. \rangle_{hm}$: the spatial average over a distance hm above the bed

hm: a certain height above the bed that has influence in the bed ($hm = 5d + 0.2h$) [−]

The original experiments were conducted under several geometries, e.g., flow over a short and long sill, flow under a gate. Afterwards, these flow conditions were calibrated by numerical models. Explicit flow velocity and turbulence intensity were obtained to calculate the stability

parameter. The formula is based on the determination on the incipient motion. However, the accuracy of this determination can be low, hence the rather subjectively defined incipient motion became one of the main defects. Moreover, Hoan (2008) argued that the choosing of $\alpha = 6$ and hm is questionable, since there is no proof that the critical stability parameter has to be a constant value.

The Hofland stability parameter

The Holfland's stability parameter was proposed based on the governing physical mechanisms on particle entrainment. The main idea is the responsible large-scale velocity fluctuation can reach the particle via eddy motions. Besides, a large-scale velocity fluctuations are associated with turbulence kinetic energy and its own horizontal length scale. Therefore, The fluctuations are part of a large rolling structure so that the 'maximum velocity' at the bed can be determined from the velocities from the entire water column above the bed. To find the 'maximum velocity' at the bed, the maximum of local instantaneous velocity is weighed with relative mixing length. The length scale is chosen as the well-known Bakhmetev distribution.

$$\Psi_{Lm} = \frac{\max\left[\langle \bar{u} + \alpha\sqrt{k}\rangle_{Lm}\frac{Lm}{y}\right]^2}{\Delta g d} \tag{2-18}$$

Where $l_m = \kappa h\gamma(1-\gamma)^{\frac{1}{2}}$ (Bakhteve distribution).

A correlation between Holflan's stability parameter and particle entrainment, based on the data of Jongeling et al.(2006) and De Gunst (1999) with a α value of 6.

The Hoan stability parameter

Hoan (2008) proposed a stability parameter built upon the flow velocity and standard deviation of velocity $\sigma_u x$. The main assumption behind the formula is the estimation of maximum (extreme) force. It assumed the flow force exerted on the stone on a bed is proportional to the square of the near bed velocity (u) and the exposed surface area of the stone ($\propto d^2$), with cooperation of Reynolds composition. It reads:

$$F_{max} \propto \rho[\bar{u} + \alpha\sigma(u)]^2 d^2 \tag{2-19}$$

Where $\sigma(u) = \sqrt{\overline{u'^2}}$ and α is turbulence magnification factor. Next a weighing function was come up to represent the turbulence effect near bed, under the assumption that the near bed turbulence structure has the largest influence on stone entrainment just like Holfland did. Finally the formula has the form of:

$$\Psi_{u-\sigma[u]} = \frac{\langle[\bar{u} + \alpha\sigma\,(u)]^2\left(1-\frac{y_b}{h}\right)^{\beta}\rangle_h}{\Delta g d} \tag{2-20}$$

The determination of empirical coefficient was based on the experiments by Hoan (2008). The best correlation lies in the value of $\alpha = 3, \beta = 0.7, H = 0.7h$.

The Remco Steenstra stability parameter

Remco Steenstra argued that clearly the pressure gradient plays an important role in particle entrainment, whereas no single previous formula has taken it into account. Thus a new stability formula including the acceleration term was proposed. The formulation is based on The Dessens stability parameter and Holfland's parameter. It reads:

$$\varphi = \frac{\left(\max\left[<\bar{u}+\alpha\sqrt{k}>_{Lm}\frac{Lm}{z}\right]^2\right)-C_{m:b}\frac{dp}{dx}d_{n50}}{K_\beta \times \Delta g d_{n50}} \quad (2\text{-}21)$$

Where $C_{m:b}$ is the ratio of added mass coefficient to bulk coefficient. The approximation of $a_x \approx \partial p/\partial x$ was used according to Huijsmans (2006). The determination of empirical coefficient α and $C_{m:b}$ was based on the data sets by Jongeling et al. (2003), Dessens (2004), Huijsmans (2006) and Hoan (2008). Numerical models was also used to estimate the acceleration term under different experiment set ups. Finally, the best correlation was found at $\alpha = 3.75$ and $C_{m:b} = 23$ for stone stability.

2.4 Concluding remarks

In this section, a summary of most important effects on stone entrainment and block mattress failure will be given. Although most of the theories are treating the stone stability, they still provide the foundation for the understanding of block mattress behavior.

First of all, due to the purpose of this thesis, the defects of Pilarczyk's formula needs to be diagnosed. The problem emerges when using this formula under non-uniform flow conditions. To be more specific, the formulation of Pilarczyk's formula was based on Shield's formula, which was focusing on uniform flow condition. Although additional parameter representing the non-uniformity (K_T) was included, it can be seen more of a rule-of-thumb. Moreover, the water depth parameter (K_h) was also derived from uniform flow condition. As can be expected, it will be different from non-uniform flow. In addition, the empirical coefficient 0.035 was determined on the data sets of experiments on stone stability. Thus the application to block mattress case is questionable.

Secondly, based on the acknowledgment that turbulence is of importance to the stone entrainment, one can assume that it can also be essential for block mattress stability problems. Therefore, the next step will introduce the turbulence effect into stability formula. To do so, an in-depth understanding of how turbulence works to lift the particle is needed.

Jongeling et al. (2003) was the first attempt to include the turbulence effect explicitly. The combination of mean velocity and corrected turbulence intensity with magnification factor, i.e., $\bar{u} + \alpha\sqrt{k}$, has been widely used since then. Holfland (2005) came up with a detailed theory on the turbulence mechanism. The main idea of it is the responsible large-scale velocity fluctuation can reach the particle via eddy motions. Besides, a large-scale velocity fluctuations are associated with turbulence kinetic energy and its own horizontal length scale. This theory was then accepted and further applied into Hoan's and Remco's formula. Later, Remco's formula managed to include the pressure gradient factor in it, i.e., acceleration and deceleration. Table 2.3 gives a summary on the existing stability formula.

Table 2.3: Summary on existing stability formula

	Formula	Velocity	Turbulence	Steady acceleration force
Block mattress	Pilarczyk	Critical depth-averaged mean velocity	Empirical: as a correction factor K_T	-
			Rock manual: turbulence relative intensity (r)	-
Stone	Jongeling	Both mean and fluctuating part of velocity was taken into account.	Explicitly: turbulence kinetic energy (k)	-
	Hofland	The velocity profile over water depth was used to find the maximum velocity.	Explicitly: turbulence kinetic energy (k)	-
Stone	Hoan	Both mean and fluctuating part of velocity was taken into account. The velocity profile was used.	Explicitly: as a function of the standard deviation of the velocity $\sigma(u)$.	-
	Steenstra	Both mean and fluctuating part of velocity was taken into account. The velocity profile was used.	Explicitly: turbulence kinetic energy (k)	Using the approximation of $a_x \approx \frac{\partial p}{\partial x}$. Thus including the pressure gradient as $C_{m:b}\frac{dp}{dx}d_{n50}$

Apart from the derivation of stability formula, governing mechanism has also been adequately studied. As illustrated by Hofland (2005), quasi-steady force is one of the main accounts for failure motion. A summary of related force term is given in Table 2.4. The magnitude of mean QSF depends on the mean flow velocity. The contribution of fluctuated velocity components is represented by fluctuated QSF. This term reveals the amount of turbulence intensity contribution to failure. Apart from the steady force, special and time-related acceleration can also be related to force terms.

Table 2.4: Hydrodynamic force on coarse particle in water body

Force	Related flow property
Mean QSF	$\bar{u}$
Fluctuated QSF	u', v'
Steady acceleration induced forces	$a \approx {dp}/{dx}$
Time dependent acceleration	$a = {du}/{dt}$

Apart from the force in large scale, according to Hofland (2005), turbulence structures are of importance regarding the initial motion of particles. To study those coherent structures, quadrant analysis is considered useful. It allows an insight on the generation of turbulence structure. For more detailed information on eddy scale, PIV measurement is needed. Those force analysis conducted to single stone provides a clue on how to assess the entrainment of block mattress, which will be taken as a methodology in later chapter 6.

The start point of entrainment assessment is how to define the initial motion. For stone stability, the methods can be summarized as the threshold of motion method and the stone transport method. In comparison, the definition of failure moment for block mattress is rather simple. It is due to the observation by Smyrnis (2016) and Van Velzen and De Jong (2015) that once the failure occurs the whole block mattress will be washed away, so-called ‘snow-ball’ effect. Therefore, Van Velzen and De Jong (2015) defined the failure moment as when the block is lifted half of a block thickness. This threshold will be used for the upcoming experiments.

3 Experimental arrangement

In this chapter, the experimental configurations, techniques as well as data processing methods were employed. In section 3.2, experimental configurations were described. Nest in section 3.3 and 3.4, the block mattress model and techniques are presented. In section 3.5, three experimental series were conducted. The first series focused on the various combinations of flow velocity and turbulence intensity, the second flow properties and the third failure mechanism. This was followed by a discussion on test timing selection. In section 3.7, a brief on data processing methods were given.

3.1 Model setup

3.1.1 Facilities

The experiment was conducted in the water lab of TU Delft. The open-channel flume with a length of 14m, a height of 0.4m, an available width of 0.4m was used. The discharge, to the maximum of 60 l/s, was controlled by the valve to the pump. To simulate the sluice gate, a baffle-like structure was placed upstream of the block mattress. With different opening widths (D) and distances (L) to the mattress, various combinations of flow velocity and turbulence intensity could be obtained, as shown in Figure 3.1.

Few details of the configuration need to be illustrated as follows:

- Glued gravel bed was placed to restore the prototype as much as possible. Three kinds of the slab were provided by the water lab with different roughness. Lacking the information of the real case, the medium roughness, with the grain size of roughly 3mm, was chosen.
- In reality, the front of the mattress usually leveled up by concrete thus being fully protected from direct flow force. To create a clear 2D situation, another two layers of bed layers were placed in front of the mattress with the smooth side upwards.
- In order to avoid the water penetrating underneath the bed layers or along the sidewalls that would hit the block front directly, a board was glued at the end of the slabs.

The experimental configuration is shown in Figure 3.1. The details of the interface between bed and mattress front are shown in Figure 3.2.

The four set-ups were chosen based on the flow condition and the feasibility of measuring. The flow downstream of the structure was fierce and carried a considerable amount of air bubbles. Those bubbles blocked the laser beam and caused the failure of recording. After the rehearsals of couple of settings, the set-ups with D=3cm, L=45cm; D=3cm, L=55cm; D=4cm, L=35cm; D=4cm, L=45cm were finally decided.

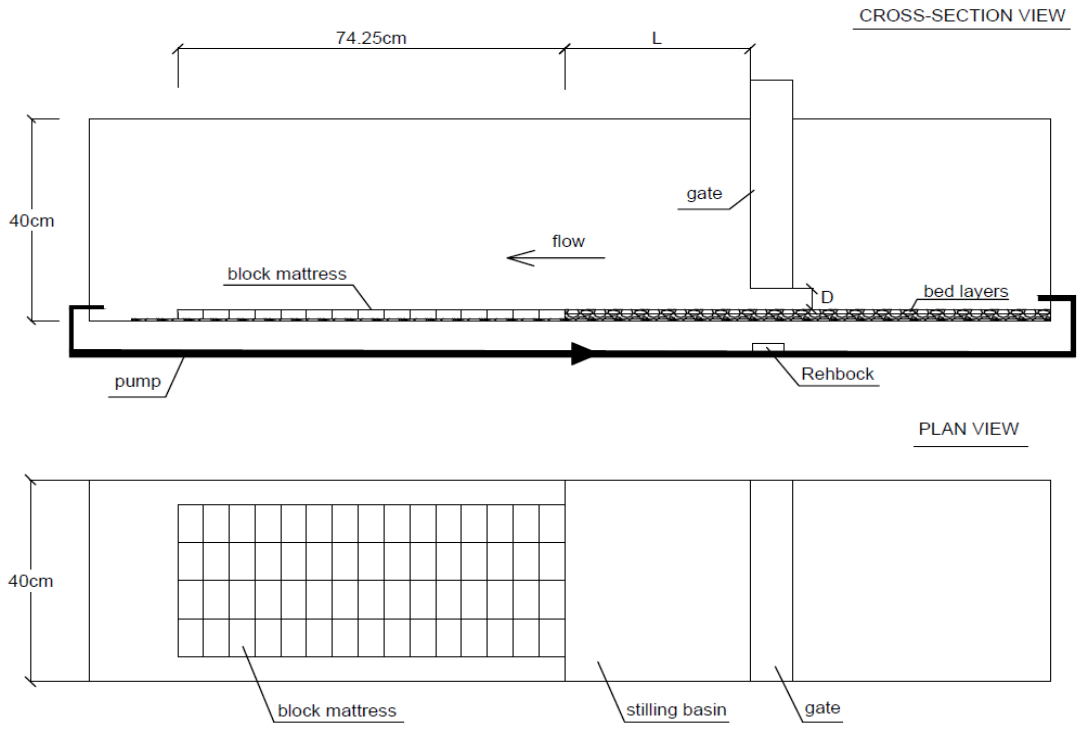

Figure 3.1: Experimental configuration (not to scale)

Figure 3.2: Details of the interface between bed layers and mattress front

Note that the opening width of sluice gate structure D was measured from the top of bed layer to the bottom of the mouth of the structure.

3.1.2 Materials

In this experiment, the block mattresses ('Betomat Type GS-VB') were provided by Holcim. The same model was used in the previous experiment *Stability of a block mattress in propeller-induced loads* done by G. van Velzen and M.P.C. de Jong 2015. The density of block mat is 2312 kg/m^3. All blocks are connected to the geotextile with glue and 2 screws. The dimensions of the whole mat, as well as single stone[G. van Velzen and M.P.C. de Jong 2015], are shown in Figure 3.3.

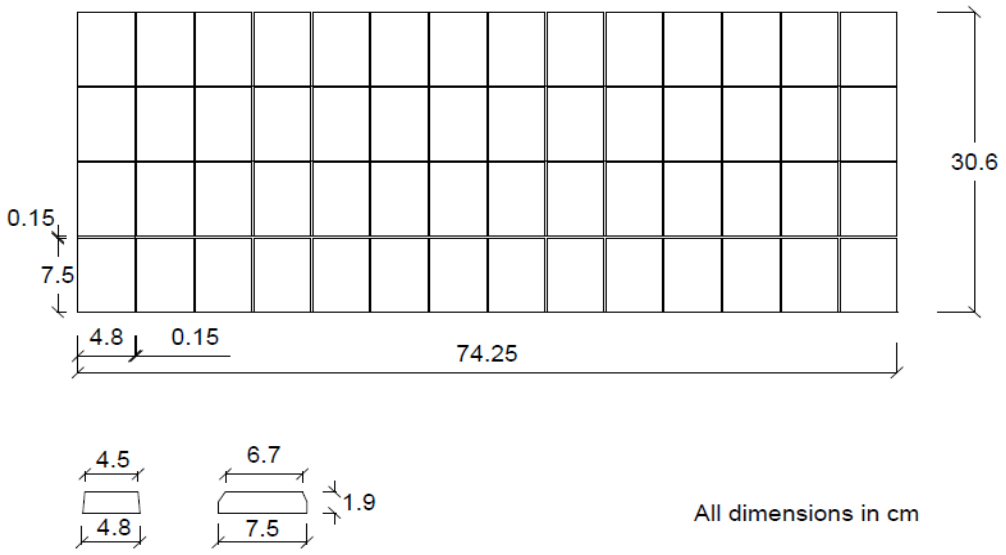

Figure 3.3: Block mattress dimensions

The used geotextile is a PP15 geotextile of Ten Cate Geolon made of polypropylene tape and split fiber yarns. The geotextile properties according to the information from suppliers are summarized in table 3.1.

Table 3.1: Properties of the geotextile

Properties	Value	Unit
Tensile strength	16	kN/m
Elongation at min strength	17	%
Static puncture resistance	2,3	kN
Dynamic perforation	19	mm
Permeability	12	mm/s
O_{90}	250	µm

3.1.3 Scaling

The model mattress is based on the GS-VB-15 produced by Holcim Coastal BV with a prototype thickness of 150mm, corresponding to an approximate scale ratio of 8. Some differences between the model and prototype need to be considered. First of all, the geotextile is not scaled. In the prototype, the concrete connection is used to fix the geotextile to blocks. Whereas, it is achievable for model and replaces by glue and screws connection. Secondly, The density of the model is slightly different from the prototype. Holcim concluded that the density of the model is 2312 kg/m^3 while the prototype's density is 2350kg/m^3. Moreover, some simplifications of the shape were done to ensure the feasibility of the model block fabrication, as shown in Figure 3.4.

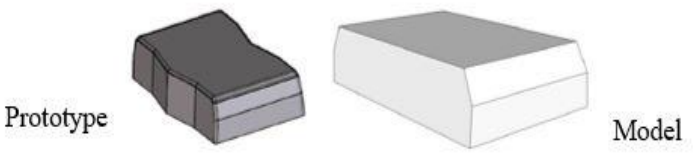

Figure 3.4: Simplification from prototype to model, from Van Velzen and De Jong (2015)

The influence of scale effect on geotextile was pointed out by Van Velzen and De Jong (2015), especially the stiffness and the permeability. Although the most flexible geotextile was chosen for the model mattress, it was still considerably high. The stiffness of the material is a relevant parameter on the resistance against local flapping. According to Van Velzen and De Jong (2015), the contributing resistance of the geotextile against overturning is 7% in the model comparing to the prototype 0.03%. On the other hand, the permeability mainly influences the flow lift force hence the block mattress stability. A more impermeable geotextile at the model leads to a more stable block mattress middle, whereas more vulnerable edges. Considering that the edges are the most critical parts of the mattress, a conservative decision was taken by choosing a more impermeable geotextile at the model.

3.2 Techniques

3.3.1 Flow velocity and turbulence intensity

A Laser Doppler Velocimetry (LDV) was used to measure the flow velocity and turbulence intensity. The streamwise (u) and vertical (v) velocity were measured. There were several instruments provided by the water lab, including Electromagnetic Flow Meter (EMS), Acoustic Doppler Velocimeter (ADV), Particle Image Velocimetry (PIV) and Laser Doppler Velocimetry (LVD), to measure the flow velocity. The reasons for choosing LDV rather than EMS, ADV or PIV are listed as follows:

- LDV provides high accuracy of measurements without interrupting the flow. The sampling frequency can go up to 1000Hz. Besides, the lowest measuring point can go down 0.5 cm above the block mat. Thus it is considered to be the most suitable equipment for this experiment.
- Both EMS and ADV devices need receivers into the water body for measurements, thus will introduce extra turbulence. Due to the fairly high velocities and low water depths during the tests, the influence of the extra turbulence would be significant.
- PIV is specifically used to observe the eddy structures which is less relevant to the main purpose of this thesis, as illustrated in the first Chapter. Moreover, to operate the PIV, an additional optical rail, a PIV camera, a particle dispenser, mirrors etc. are needed. As noted, it is fairly complicated to use a PIV instrument.

With two collimated laser beams intersect that forming a probing volume, the movement of particles in the flow can be fully captured. The signal collected and received by the computer is in the unit of voltage. Thus a calibration from voltage [v] to velocities [m/s] is needed as follows:

$$u=0.096\times beamA-0.096\times beamB \tag{3-1}$$

$$v=0.096\times beamA+0.096\times beamB \tag{3-2}$$

Note that the fixed calibration parameter 0.096 is provided by the Water Lab.

3.3.2 Block Mattress movement

To capture the failure moment of block mattress, a high-speed camera was used. It was synchronized with LDV by the same time series. The external trigger of the camera could go up to 20 Hz. Correspondingly, the sampling frequency of LDV for failure captures was set to be 80Hz, namely four measuring signals for each frame.

The definition of failure was suggested by Van Velzen and De Jong (2015) as the moment when the block is lifted by half of the block thickness. During the experiment, this failure motion is the only failure pattern that happened and the block stayed rather stable after this motion. Therefore, the definition will be continuously used in this thesis. An example of typical failure is shown in Figure 3.5.

Figure 3.5: An example of typical failure moment

3.3.3 The discharge and water depth

The discharge through pump can be read directly from the valve recorder, which was synchronized to LDV records. However, the significant deviation between the valve recorder and real discharge was observed. To calibrate this, the Rehbock was used to obtain the real discharge. It was placed beside the pump under the flume as shown in Figure 1. The work was done by measuring the water level inside the Rehbock, then applying the calibration from water level to discharge as shown in equation 3-3. Note that the water level inside and outside the Rehbock needs 10 minutes to reach equivalence. The record of Rehbock was also synchronized to LVD and camera records. Again, the original signal was in the unit of voltage, thus the relation as equation 3-4 is provided. Since it was more convenient to read the discharge through valve recorder, thus a relation between real discharge and valve discharge was established as equation 3-5.

$$Q = 1000 \times c_e \times 2/3 \times \sqrt{2g} \times b \times h_e^{1.5} \tag{3-3}$$

Where:
Q: the real discharge *(l/s)*
b: width of Rehbock edge $0.442m$
$c_e = 0.602 + 0.083 \times \frac{h_e}{h_b}$;
$h_b = 0.25m$;
$h_e = h_a + 0.0012$;
g: gravity acceleration 9.81 m/s^2;

$$h_a = 38 \times rehbock\ voltage - 129.2 \tag{3-4}$$

$$Q = 5 \times pump\ discharge - 10 \tag{3-5}$$

The water level and distances were measured by a ruler.

3.3.4 Calibration and Accuracy

A summary of calibration and accuracy is shown in Table 3.2.

Table 3.2: Calibration and accuracy

measuring purpose	technique	calibration	accuracy
flow field	LDV	u=0.096×beamA-0.096×beamB	0.001 m/s
		v=0.096×beamA+0.096×beamB	
discharge	Rehboch	ha=38×Rehbock voltage-129.2	0.1 m
		$Q = 1000 \times c_e \times 2/3 \times \sqrt{2g} \times b \times h_e^{1.5}$	0.01 l/s
	Valve record	Q=5× valve discharge-10	0.01 l/s
water level	ruler		0.1 mm
distance			

3.4 Test program

3.4.1 The first series

The first series of experiment was performed to obtain various combinations of flow velocity and turbulence intensity at failure moment. In this series, the LDV, camera and valve discharge recorder were used. Several set-ups were obtained by changing the gate opening width and distance between block mat and gate. A summary of all set-ups is shown in Table 3-2. The measuring point was at 0.6 cm above the last row of block mattress. The intersection point of two laser beams was in the middle of the column. In this series, two subseries were conducted. Firstly, the failure moments were recorded, through which the discharge at the failure moment can be obtained. Secondly, a database contains the flow velocity and turbulence intensity at each discharge were collected. By doing so, the instantaneous flow velocity and corresponding turbulence intensity at the failure moment could be obtained.

The sequence of failure recording was as follows:

- Opened the valve at low discharge, at which the block mat was stable.
- Switched the valve to higher discharge by small increasing steps, 0.5l/s—1l/s.
- Waited for one minute till the discharge was stable after each switch.
- Increased the discharge until the block mat fails.
- Memorized the failure discharge as a reference.
- Repeated step one, till the discharge was close to failure discharge.
- Turned on the camera, start recording.
- Carefully increased the discharge till the block mat failed.
- Stopped the camera records.

Note that, high vulnerability of block mattress to a sudden increase of discharge, i.e. increasing step of 5l/s, was observed. Therefore very small increasing steps were essential.

Having the failure discharge from the previous subseries. The sequence of database collecting was as follows:

- Increased the discharge close to failure discharge, i.e. 3l/s lower.
- Waited until it was stable
- Started LDV recording for two minutes.
- Stopped LDV recording

- Carefully increased the discharge by 0.5 l/s.
- Waited until it was stable and recorded for two minutes, then stopped.
- Repeated step 5 and 6, till the discharge exceeded failure discharge, i.e. 2 l/s higher.
- Stopped recording.

Note that:

- The failure discharge for set-up D4L35 was high enough to generate lots of air bubbles in the water body. This had a significant influence on the velocity recording since the laser light beams are very sensitive to bubbles. The recording signal would drop to zero when air bubbles passing. Under the circumstances, the database for this set-up was recorded till 3 l/s below the failure discharge. Extrapolation was then used to find the corresponding flow velocity and turbulence intensity.
- The last row of block mat was glued together with the row ahead in this subseries. During the failure procedure, the last row will be flipped and block the LDV laser beam. Therefore it was not possible to collect database right on failure discharge. After gluing, no flipping motion observed anymore thus able to collect database.

Table 3.3: Experimental Set-up summary

set-up	Sep-up properties		Failure cases	Failure Discharge (l/s)	Database discharge (l/s)
	D (cm)	L (cm)			
D3L45	3	45	F1--F5	24.54--25.65	21.07--25.60
D3L55	3	55	F1--F5	28.05-28.65	27.95--28.99
D4L35	4	35	F1--F5	37.6--38.2	27.58--35.29
D4L45	4	45	F1--F5	35.75--36.00	35.76--37.48

3.4.2 The second series

The second series was performed to study the flow properties, including velocity distribution, turbulence intensity distribution, shear stress distribution, mixing length profile. The second series has a larger scope than the first one. The first series only focus on the near-bed velocities, whereas in the second series, the measuring points spread along the whole block mat and over the whole water depth. This series was conducted under the hydraulic conditions of set-up D4L35, with a fixed discharge of 30 l/s. The reasons for choosing such condition are as follows:

- The water depth in this test series was the highest among all. Therefore it would allow the maximum vertical measuring positions.
- Any discharge higher than 30 l/s would induce bubble interventions.

The LDV technique was used along with distance measurement (ruler).

The measuring positions along the mat were at the end of the first row (P1); the end of the 3rd row (P2); the end of the 5th row (P3); the end of the 8th row (P4); the end of the 11th row (P5); the middle of the 15th row (P6) separately. For each position, 13 vertical locations were measured. In the lower half of the water body, the distance between two neighboring points was 1mm whereas in the upper half 4mm to 5mm. The sketch of set-up is shown in Figure 3.4.

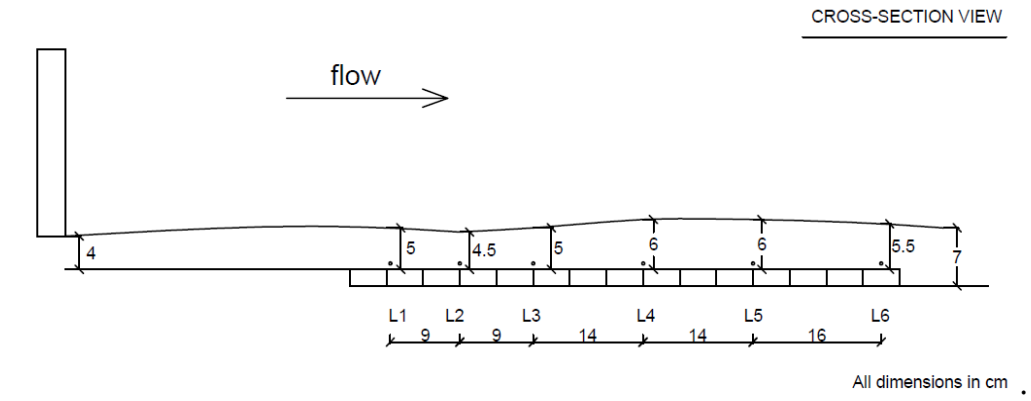

Figure 3.6: The second test series configuration

Note that Local water level fluctuations can be observed.

3.4.3 The third series

This series was performed to study the failure mechanism of the block mat. In this series, LDV technique and water level measurement were used. We focused on studying the backward facing step behind the last block, as well as examining the actual forces acting on it. This series was conducted under the same configurations as the second series.

Since the failures always happened to the last row of block mat, the measuring points were spread around the last row. L1 was placed at the end of the block ahead. L2, L3, L4 were at the front, middle and the end of the last block separately. L5 was placed behind the last block and had the same vertical position as L4. From L6 to L13, they had the same horizontal position but vertical positions varying down by 2.5mm at each step. The sketch is shown in Figure 3.5, with the distance between two neighboring points annotated.

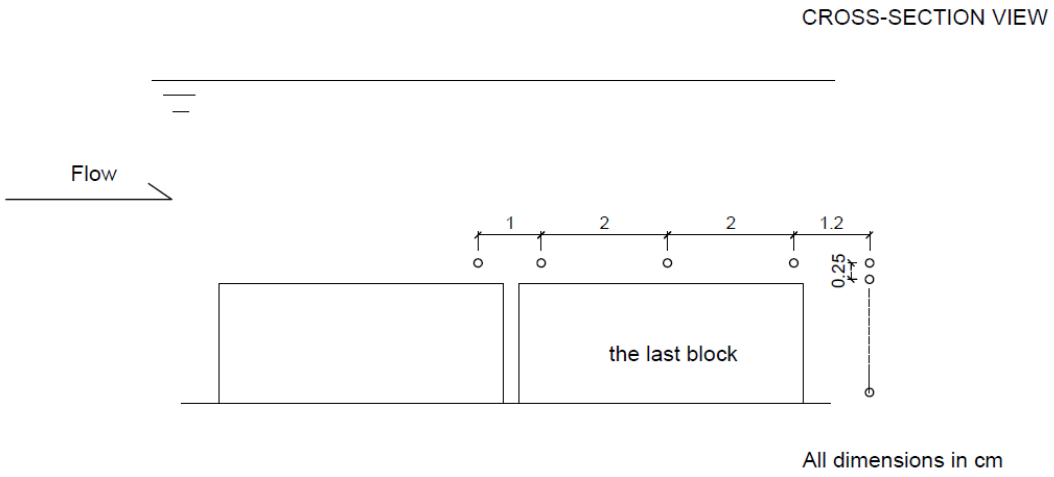

Figure 3.7: The third test series configuration

3.5 Selected time series

In this section, the choice of the signal length for each velocity measurement was discussed. The data obtained from measurement were the mean velocity, turbulence intensity, and Reynolds shear stress. Thus those three were set to be the indicators for test duration choosing. Those three indicators were represented by $u, \sigma(u)^2$ and $\overline{u'v'}$ respectively.

The sample represents quantities better with the increase of test duration, thus a 30-minutes test on velocity measurement using LDV was done. It was set to be a reference to evaluate the appropriateness of possible shorter measuring lengths. On the other hand, the duration should not be so long since the number of tests is rather large. Therefore, a duration of one minute, two minutes and five minutes were examined(Hoan 2008). 50 subseries for each of those three durations were extracted from 30-minutes test arbitrarily. The quantities were compared by the standard value using:

$$\delta x = \frac{x_s - x_0}{x_0} \times 100\% \tag{3-6}$$

Where: δx: relative error of quantity x (x can be $u, \sigma(u)^2$ and $\overline{u'v'}$)

x_s: values obtained from the possible shorter duration series.

x_0: true values, in this case are the values obtained from the 30-minuts test.

The relative errors of three indicators for three test durations are shown in Figure 3.6. Since the relative errors for all indicators of 2-minutes tests are smaller than 5%. Thus the measuring length was set to be 2 minutes.

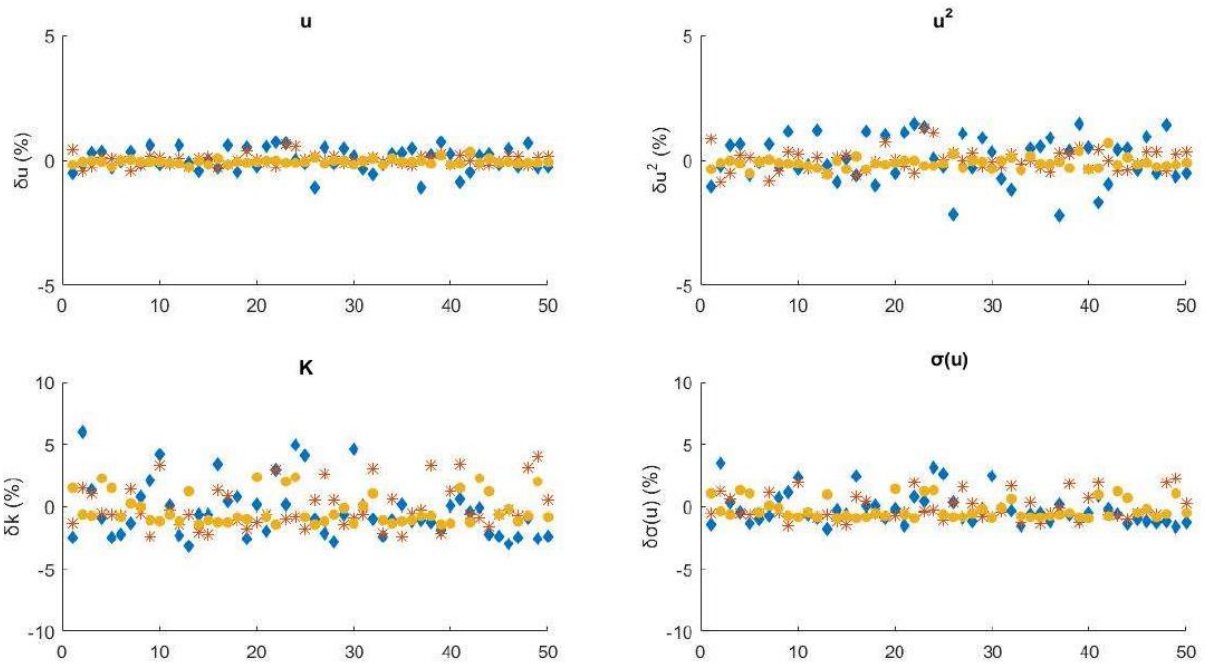

Figure 3.8: The relative errors of 2 minutes(diamonds), 5 minutes (stars) and 10 minutes (circles)

3.6 Data processing methods

3.6.1 Flow quantities

The main flow quantities treated here are water depth, Reynolds number, Froude number and shear velocity. For the sake of simplicity, the flow here is considered uniform flow. Thus the properties can be obtained according to uniform open channel flow.

The mean velocity over water depth was determined as:

$$U = \frac{Q}{Bh} \tag{3-7}$$

Where Q is the discharge (l/s), B is the width of flume (m) and h is the water depth (m).

The Reynolds number was determined as:

$$Re = \frac{Uh}{\gamma} \tag{3-8}$$

Where $\gamma = 1.31 \times 10^{-6} m^2/s$ is the fresh water viscosity at temperature of 10 degree.

The Froude number was determined as:

$$Fr = \frac{U}{\sqrt{gh}} \tag{3-9}$$

The shear velocity, u^* in uniform flow can be calculated as follows:

$$u^* = \frac{U\sqrt{g}}{C} \tag{3-10}$$

Where C is Chezy coefficient determined as:

$$C = 18ln\frac{12R}{k_s} \tag{3-11}$$

Where R is the hydraulic radius, $R = \frac{Bh}{(B+2h)}$; k_s is the equivalent roughness, about the height of the rib for articulating mats(Pilarczyk, K. 1998), thus in this case $k_s = 1.9cm$.

3.6.2 Velocity and turbulence properties

The basic properties of turbulence flow, such like mean velocity, turbulence intensity, and shear stress, can be computed directly from the measuring data. The analysis of other flow properties like turbulent kinetic energy, the eddy viscosity, and mixing length can be obtained base on those basic quantities. One step further, to optimize the stability formula, the computations of turbulence magnification factor, as well as stability parameter, depend on those flow properties obtained previously.

from the data record of measured velocity samples $u(i)$, the mean velocity was computed as:

$$\bar{u} = \frac{1}{N}\sum_{i=1}^{N} u(i) \tag{3-12}$$

Where N is the sample number. In this case, 2-minute test duration with the sampling frequency of 100Hz, N=12000.

The velocity fluctuations is computed as:

$$u'(i) = u(i) - \bar{u} \tag{3-13}$$

The turbulence intensity of u is defined as:

$$\sigma(u) = \sqrt{\overline{(u')^2}} = \sqrt{\frac{1}{N}\sum_{i=1}^{N}[u(i) - \bar{u}]^2} \tag{3-14}$$

The Reynolds shear stress is defined as:

$$-\overline{u'v'} = -\frac{1}{N}\sum_{I=1}^{N}[u(i) - \bar{u}][v(i) - \bar{v}] \tag{3-15}$$

The turbulent kinetic energy is defined as:

$$k = \frac{1}{2}\left(\overline{u'^2} + \overline{v'^2} + \overline{w'^2}\right) \quad (3\text{-}16)$$

Since only two velocity components are available (u and v). The velocity in transverse direction needs to be assumed. Theoretically, in fully developed flow, $\sigma(v) = \sigma(w)$ can be assumed. Additionally, another approximation, $\sigma(w) = \sigma(u)/1.9$, was came up by Hoan measured by EMS. From the recorded data, a relation of $\sigma(v) \approx \sigma(u)/1.8$ can be obtained. It proves that those two assumptions mentioned previously convergent to each other, and appliable to currrent case.

The eddy viscosity is defined as:

$$\gamma_t = \frac{\gamma\frac{du}{dy} - \overline{u'v'}}{\frac{du}{dy}} \quad (3\text{-}17)$$

The mixing length is defined as:

$$l_m = \sqrt{\frac{\gamma_t}{\left|\frac{du}{dy}\right|}} \quad (3\text{-}18)$$

3.6.3 Block mattress movement data

In this thesis, the failure moment is defined as the second that block is lifted by 1cm, namely half of the block thickness. When recording the failure moment, both camera and LDV would be working. Afterward, by checking the frame number of failure moment recorded by the camera, the corresponding failure signal could be found in the LDV records. Thus the failure discharge could be obtained, which was needed to find the velocity and turbulence intensity corresponding to failure moment via the database.

4 Flow characteristics

To have a better understanding of the block mattress stability in non-uniform flow, in this chapter the flow characteristics measured from test series two would be analyzed. Besides the comparison to uniform flow characteristics would be conducted qualitatively. In section 4.1, the measured and calculated flow quantities were presented. In section 4.2, mean velocity profiles were described. Next, in section 4.3, different shear velocity calculating methods were conducted following by the calibration of equivalent roughness. These two chapters provide basis for the study on mixing length distribution in section 4.4. The mixing length gives detailed information on the turbulence effect on block mattress, as well as being used when applying another stability formula for the current situation in Chapter 6. The turbulence intensity data and Reynolds shear stress data were presented in section 4.5 and 4.6 respectively. These two properties give a brief idea on the flow condition, whereas not being included into the stability formula. This chapter ends with some concluding remarks in section 4.7.

4.1 Flow quantities

The main flow quantities are summarized in Table 4.1. Those results were obtained from Test series two, with six locations being measured.

Table 4.1: Summary of flow properties

location	L1	L2	L3	L4	L5	L6
Distance to gate [cm]	41	50	59	73	87	103
h [m]	0.05	0.045	0.05	0.06	0.06	0.055
U [m/s]	1.333	1.481	1.333	1.111	1.111	1.212
Re [-]	41667	41667	41667	41667	41667	41667
Fr [-]	1.9	2.2	1.9	1.4	1.4	1.6
C $[m^{0.5}/s]$	57.6	56.0	57.6	60.2	60.2	59.0
u^* [m/s]	0.072	0.083	0.072	0.058	0.058	0.064

Note:

1. u^* is calculated by equivalent roughness (k_s) method, to give a first impression. Later in section 4.3, more methods were used for calibration.
2. Water surface has local jumps, which resulted in the experimental error up to approximately $\pm 2mm$.

4.2 Mean flow velocity

Figure 4.1 shows the mean streamwise velocity profile for six locations. These results were normalized by using shear velocity that derived by equivalent roughness method, along with the logarithmic function and fitting indicator. See figure 4.2.

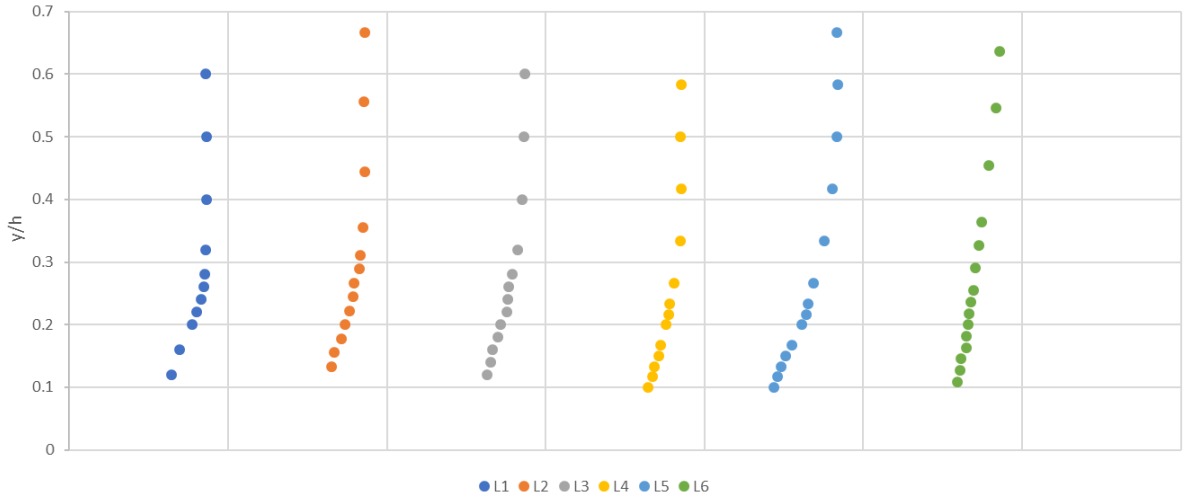

Figure 4.1: Mean velocity profiles

The skewness of the velocity profile at the lower body at L5 is more significant than those in other positions. This may due to the measuring position of L5, which is right above the gap between two blocks. More disturbance is expected to be induced by the gap between neighboring blocks, thus fewer similarities between the results from measured data and from existent open-channel flow turbulence theories should be expected.

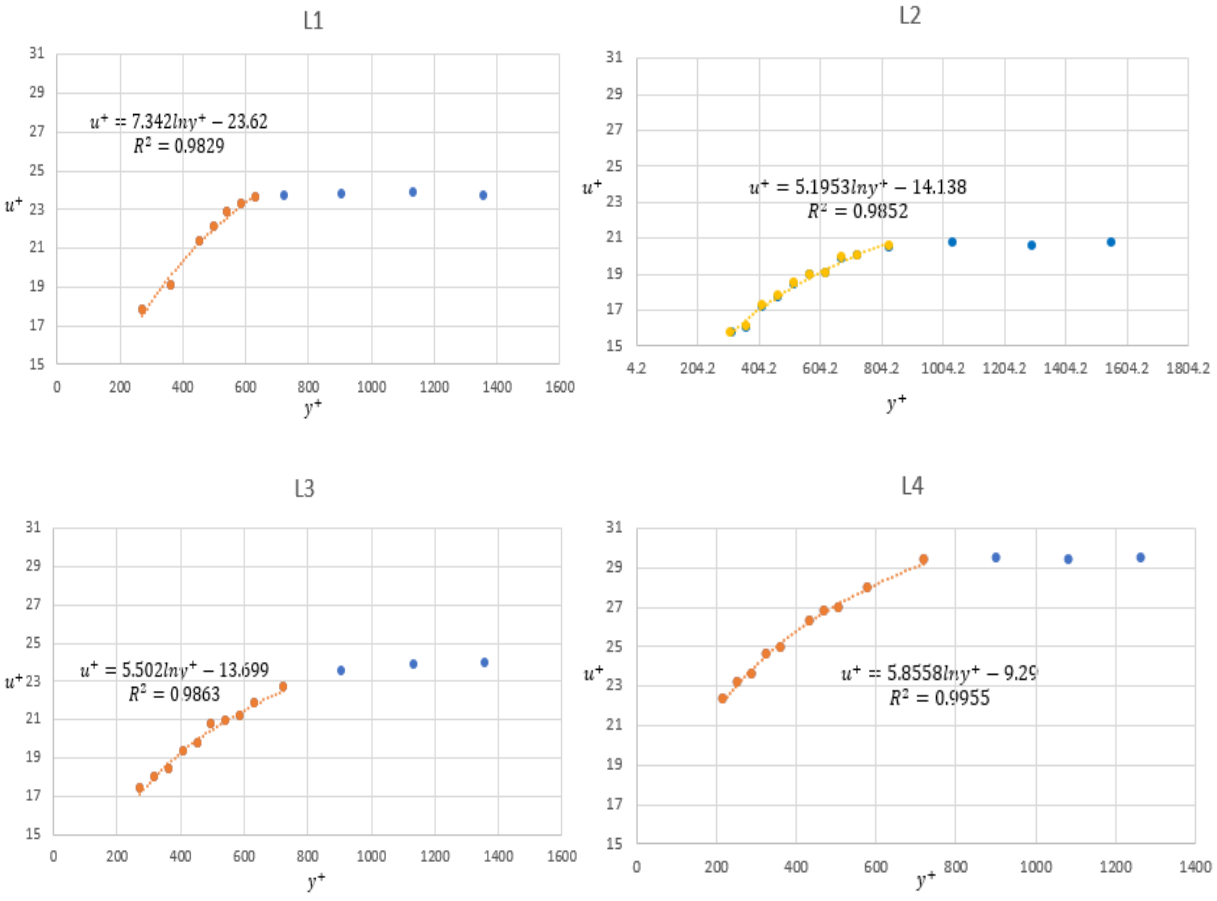

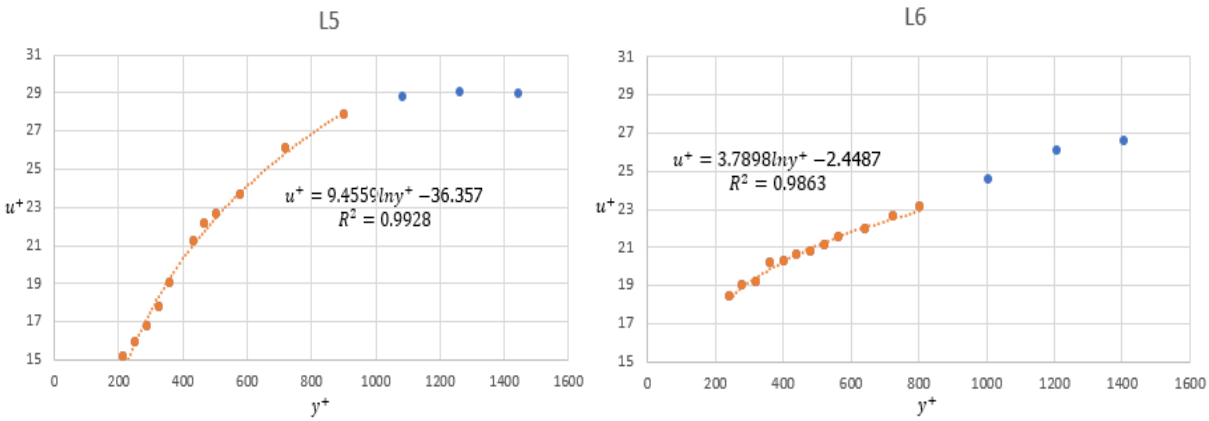

Figure 4.2: The velocity profile with $y = 0$ at the top of block mat

Noted that due to the limitation of LDV, the information of the region within 5mm above the block mat cannot be obtained.

The velocity profile is plotted in log coordinate with $y = 0$ at the top of block mat, as shown in Figure 4.2. Clearly, the function $u^+ = Aln(y^+) + B$ fits very well with the present data (with R^2 very close to 1), indicating that the logarithmic profile can be applied to the lower region. Besides, the outer region can be observed, even though the water depth is very low, 3~4 times of block mat thickness. In this region, the logarithmic profile behaves poorly, instead the clear log-wake law pattern can be observed. Moreover, for L1 to L5, the log-wake law curves indicate the acceleration (flatten trend) feature of flow condition whereas at L6 deceleration (upwards trend).

However, the whole velocity profile moves up and down from L1 to L6 arbitrarily and have contradictories with mean flow velocity derived from mean water depth. According to the mean velocity listed in Table 4.1, the flow should be accelerating from L1 to L2. Whereas in Figure 4.2, the trendline position moves downwards from L1 to L2, which indicates the flow is decelerating. Same goes for L4 to L5. The water level hence the mean velocity stayed constant from L4 to L5. However, from Figure 4.2, the trendline extended to much lower value in L5 comparing to L4. This resulted in the lower mean velocity in L5 than L4. The probable cause of these irregularities could be the choice of local shear velocity. To verify this, different shear velocities obtained by different methods, as illustrated in section 4.3, were used to re-conduct velocity profiles. Figure 4.3 showed the velocity profile by Reynolds shear stress shear velocity, and Figure 4.4 TKE method shear velocity.

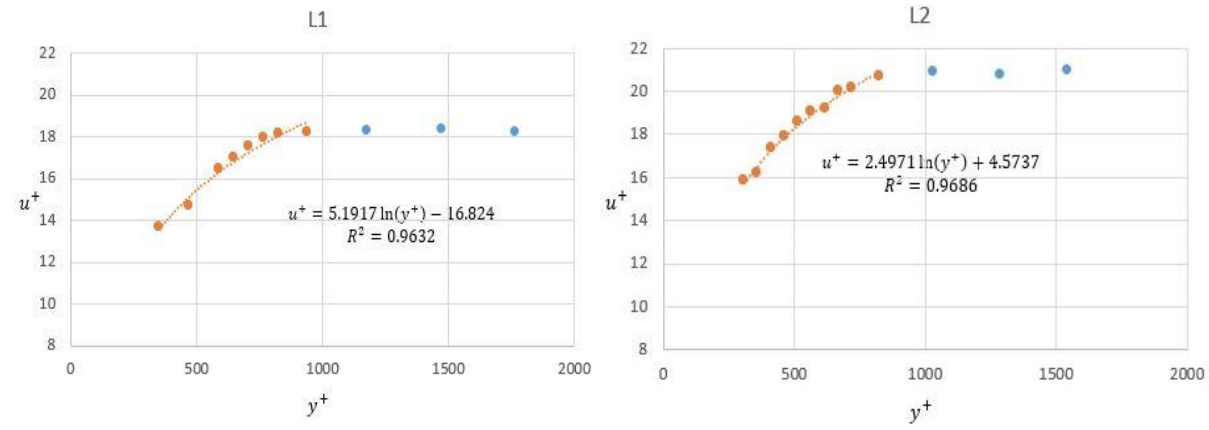

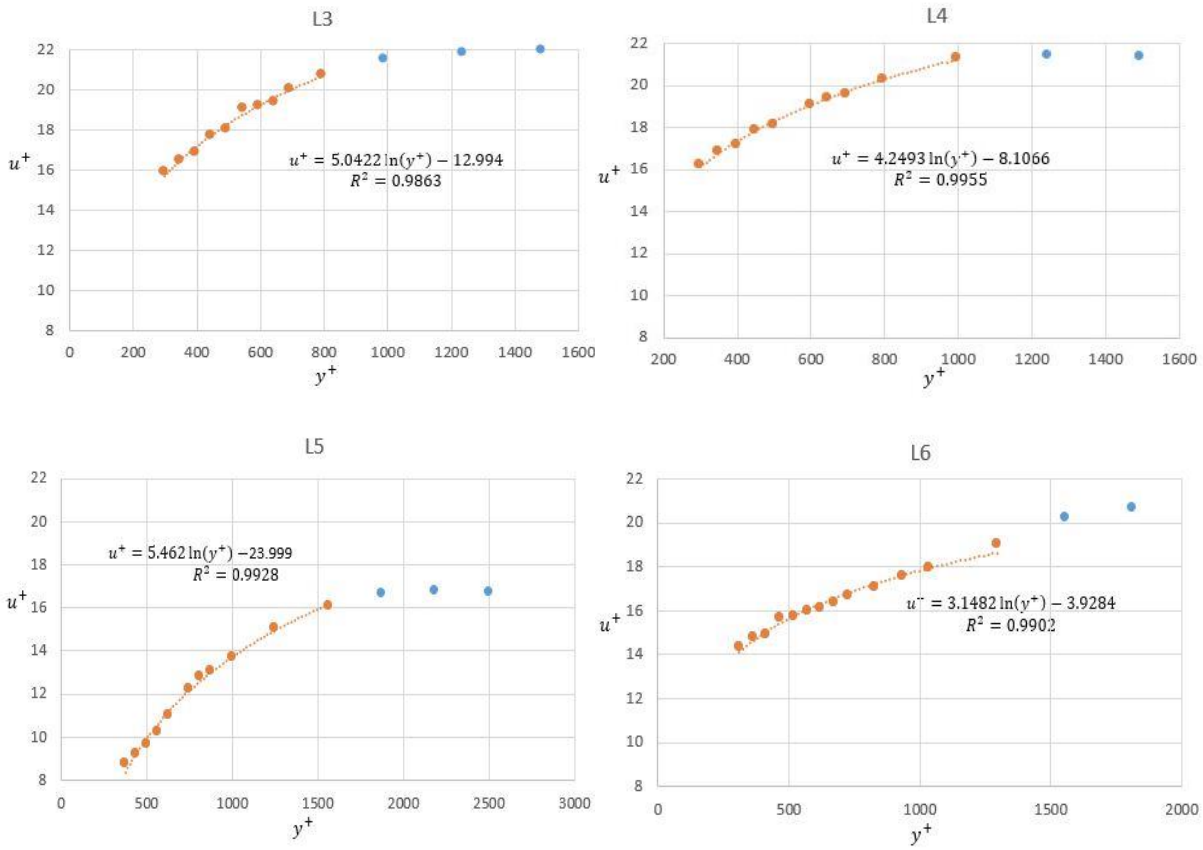

Figure 4.3: The velocity profile derived by Reynolds shear stress shear velocity

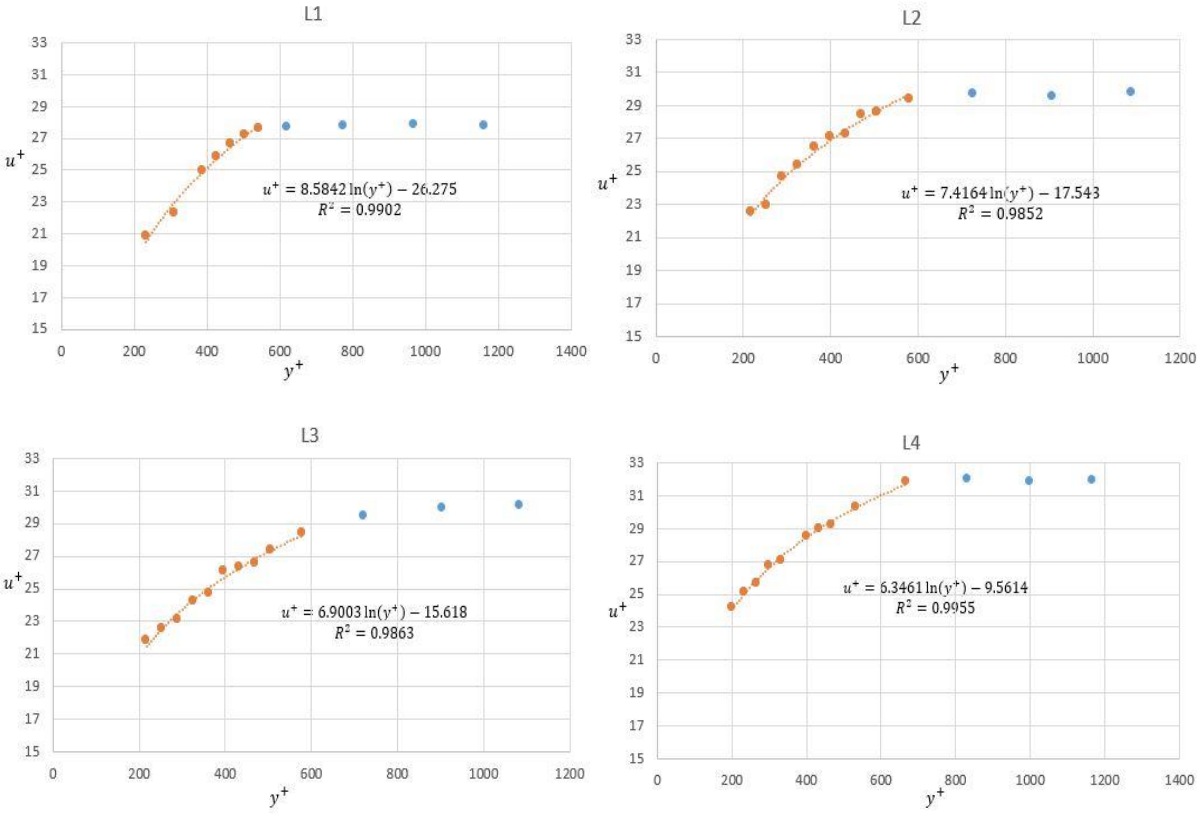

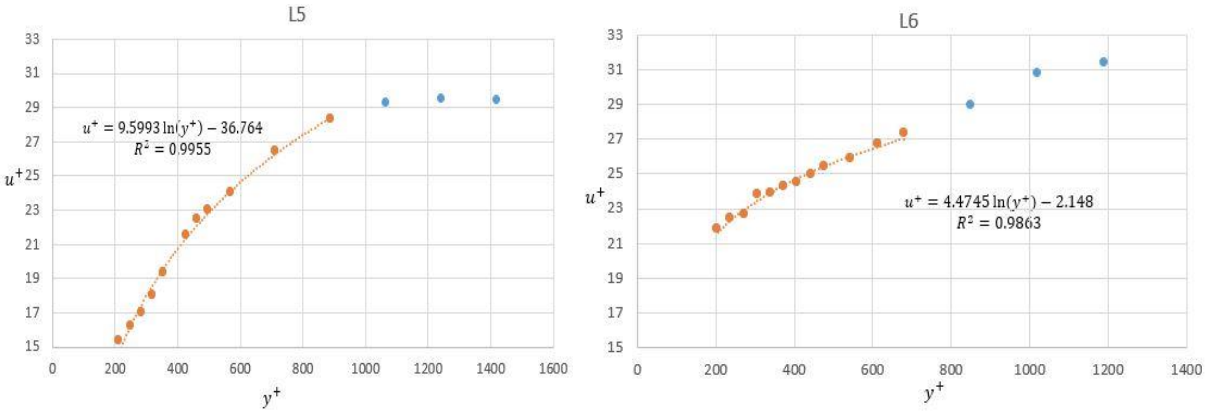

Figure 4.4: The velocity profile derived by TKE shear velocity

For both method, better coincide with depth-averaged velocity is obtained. The flow is indeed accelerating from L2 to L3, as the velocity profile moves upwards. However, the irregularity of L5 still remains.

Another observation is the obtained κ value has deviation from the standard value 0.41, as showed in Table 4.2.

Table 4.2: The κ value from velocity profile with $y = 0$ at the top of block mattress

Location	1	2	3	4	5	6
$\kappa=\frac{1}{A}$	0.136	0.192	0.182	0.171	0.106	0.264

The possible reason for this phenomenon is discussed as follows:

1. The flow is not fully developed yet, i.e. the streamwise velocity is changing along the flow direction, as can be observed from Table 4.1. However, $\kappa = 0.41$ is generally agreed under fully developed flow condition. As can be observed from Table 4.2, the κ value increases along the flow direction, except L5. It can be explained that the flow is growing towards fully developed condition, thus , $\kappa = 0.41$ can be expected further downstream.
2. The κ value highly depends on where the coordinate starts. Since the gaps between two blocks will induce vortex significantly and influence the generation of velocity profile, the top of blovk mattress might not be the real $y = 0$ position. By adjusting y_0 position, $\kappa = 0.41$ might be able to achieve. The adjusted $y = 0$ position is listed in Table 4.3 for six locations, with the fitting indicator R^2.

Table 4.3: The adjusted start of coordinate in vertical direction

	$y = 0$ (cm above block top)	R^2
L1	0.5265	0.9984
L2	0.4574	0.962
L3	0.4774	0.9358
L4	0.4933	0.9472
L5	0.8557	0.9227
L6	0.35	0.9663

As observed, after the $y = 0$ position adjustment, the logarithmic function still fit with the data very well. Again, irregularities showed up in L5 that the $y = 0$ position is relatively far from

the block top. The possible explanation is: Unlike other measuring points are placed above the block surface, the measuring point L5 is right above the gap between two blocks. Thus the data showed irregularities here. The considerable adjusted $y = 0$ position above the block indicates the existence of a layer of disturbance. It is especially the case for L5, where the vortex is stronger.

4.3 Shear velocity and equivalent roughness

Shear velocity u^* is a fundamental velocity scale, especially important to sediment transport dynamics. In section 4.1, a first impression on the shear velocity was given based on the equivalent roughness. However, this equivalent roughness value is lacking a theoretical background. In this section, two more fundamental methods will be used to give more reliable results on shear velocity. Since for engineering approach, it is more handy to use equivalent roughness method, the calibration would be addressed. The methods used here are the Reynolds stress method and the turbulence kinetic energy (TKE) method.

4.3.1 Reynolds stress profile method

The definition of u_* is based on the bed shear stress, τ_w. i.e. $\tau_w = \rho u_*^2$. Physically, for fully developed flow, the total shear stress is $\tau = \rho\nu \frac{d<U>}{dy} - \rho < uv >$. As can be observed from the data, the magnitude of $< uv >$ is 10 to the power of -3; the magnitude of $\frac{d<U>}{dy}$ is 10, with $\nu = 1.31 \times 10^{-6}$, giving the viscous shear stress $\rho\nu \frac{d<U>}{dy}$ ($\sim 10^{-5}$) much smaller than turbulence shear stress $-\rho < uv >$. Thus the total shear stress is further simplified to $\tau = -\rho < uv >$. Therefore the shear velocity can be expressed as:

$$u_* = \sqrt{-\rho < uv >} = \sqrt{-\rho \overline{u'v'}}_{z \to 0} \tag{4-1}$$

As can be observed from the Reynolds stress profile in section 4.6, there is a similar curve to the theoretical one showing the peak of Reynolds stress. This peak value will be considered as the $< uv >_{z \to 0}$ value.

4.3.2 Turbulence kinetic energy (TKE) method

Soulsby (1980) found that the average ratio of shear stress to TKE is constant,

$$|\tau| = C_1 \, \rho \, TKE \tag{4-2}$$

Therefore,

$$u_* = \sqrt{C_1 \, TKE} \tag{4-3}$$

Where C_1 is proportional constant, The value $C_1 \approx 0.19$ was used by MacVicar and Roy (2007) in a gravel bed river, by Rowinski et al. (2005) in a rough-bed open-channel, and by Pope et al. (2006) in river and laboratory studies. Thus in this case, for the block mat the value 0.19 was used. As assumed previously, the flow is fully developed, thus in $y^+ \geq 200$ region, thus we assume $v' = w'$.

As can be observed from the turbulence intensity profile in section 4.5, the curve showed the maximum value would appear at the bottom. This is also validated by John Kim, Parviz Moin and Robert Moser in 1987. Due to the limitation of LDV, the information of very near-bed region is missed, thus Nikora and Goring (2000) suggested using the extrapolation of the TKE profile to the bed, we obtain

$$u_* = \sqrt{C_1 \, TKE}_{z \to 0} \tag{4-4}$$

4.3.3 Results

The estimates of shear velocity u* determined by different methods are shown in Table 4.4.

Table 4.4: The estimates of shear velocity u determined by different methods*

Location	L1	L2	L3	L4	L5	L6
Equivalent roughness method	0.0725	0.0828	0.0725	0.0578	0.0578	0.0643
Reynolds stress method	0.0943	0.0824	0.0791	0.0796	0.1001	0.0829
TKE methods	0.0620	0.0580	0.0578	0.0533	0.0569	0.0545

The Reynolds stress method gave larger value on shear velocity than the equivalent roughness method. This makes sense since the equivalent roughness method approached in a depth-averaged way, whereas the Reynolds stress method more focused on the near-bed area.

The TKE method gave smaller value than the equivalent roughness method and quite a large deviation from the Reynolds stress method. This might be caused by two reasons. Firstly, the assumption that $v' = w'$ is not valid here, since the flow is not fully developed. However, if we check the shear stress profile as illustrated in section 4.6. The curves are very similar to the standard ones. Thus this is unlikely to be the reason that cause the deviation. Secondly, the assumed C_1 value is not valid. The value being used here is based on the gravel bed. However, there are plenty of differences between gravel bed and block mattress. Besides, Kim et al. (2000) found $C_1 = 0.21$ in an estuary by best fit to the data, suggesting that further studies are needed to confirm that this can be considered as a universal constant in hydraulics.

In conclusion, the Reynolds stress method is considered the most reliable method to calculate shear velocity. Due to the reasons that it is a more fundamental method and affected by very few uncertainties. This method will be used to calibrate the equivalent roughness value. The output is listed in Table 4.5.

Table 4.5: Calibrated equivalent roughness length for block mattress

	L1	L2	L3	L4	L5	L6
k_s	4.2 cm	2.0 cm	2.6 cm	5 cm	8.24cm	4.2 cm

By comparing the initial value we used, $k_s = D = 1.9cm$, clearly a larger value needs to be used. Roughly, $k_s \approx 2{\sim}3\ D$ is proposed. The exact value need to be further confirmed by more data.

4.4 The mixing length

Later in Chapter 6, Streeenstr's formula will be applied to the current situation. In that formula, Hofland's stability parameter was used, which includes mixing length distribution in Bakhmetev profile. Thus in this section, the mixing length profiles were computed from experimental data to evaluate the feasibility of applying Bakhmetev profile in current flow condition.

Based on the velocity profiles and shear stress obtained in previous two sections, the mixing length can be determined as:

$$l_m = \sqrt{\frac{\nu\frac{du}{dy} - \overline{u'v'}}{\left|\frac{du}{dy}\right|\frac{du}{dy}}} \tag{4-5}$$

Where ν is kinematic viscosity.

Figure 4.5 shows the distributions of mixing length at six measuring points comparing with Bakhmatev distribution (Eq. 2-9).

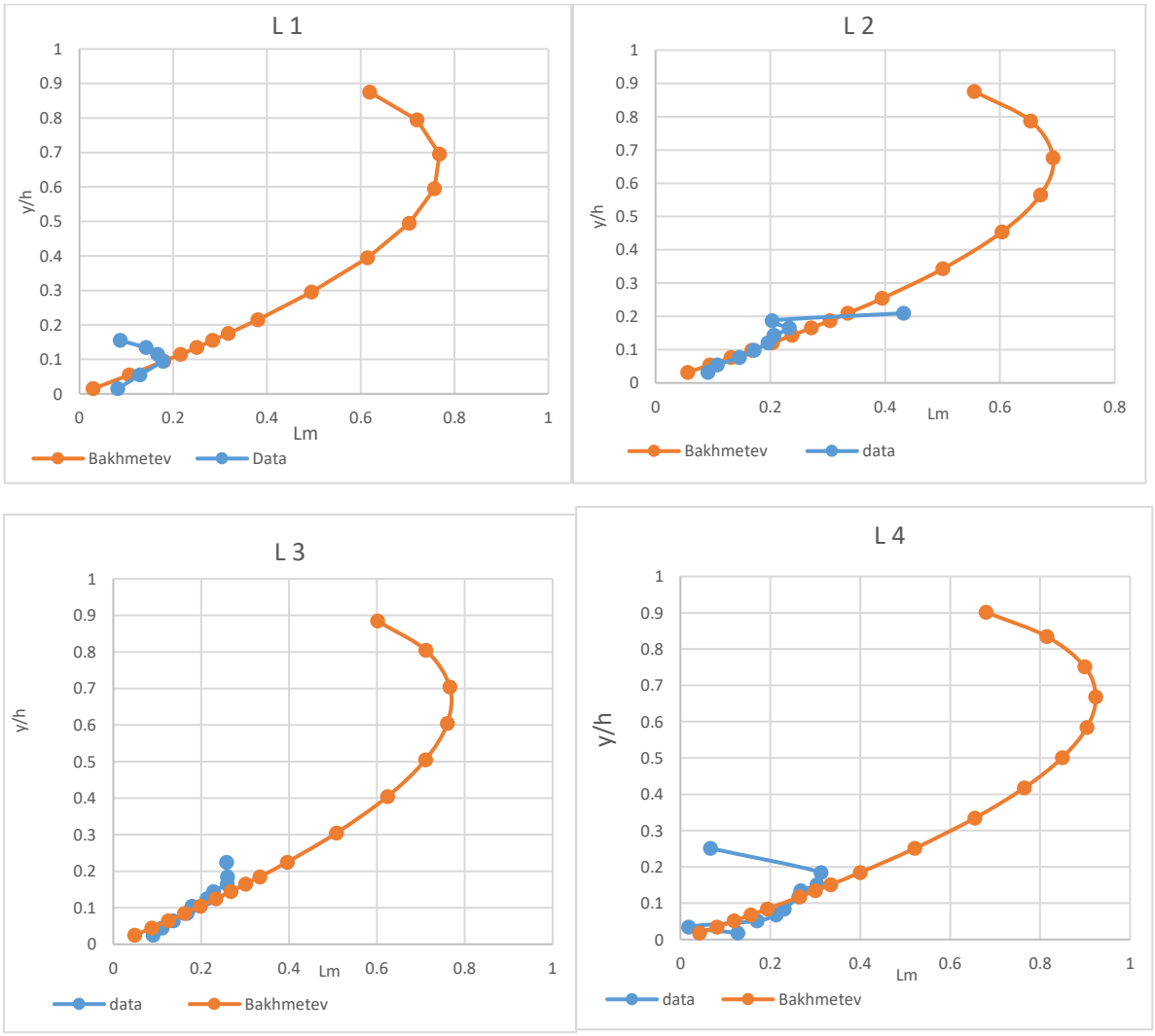

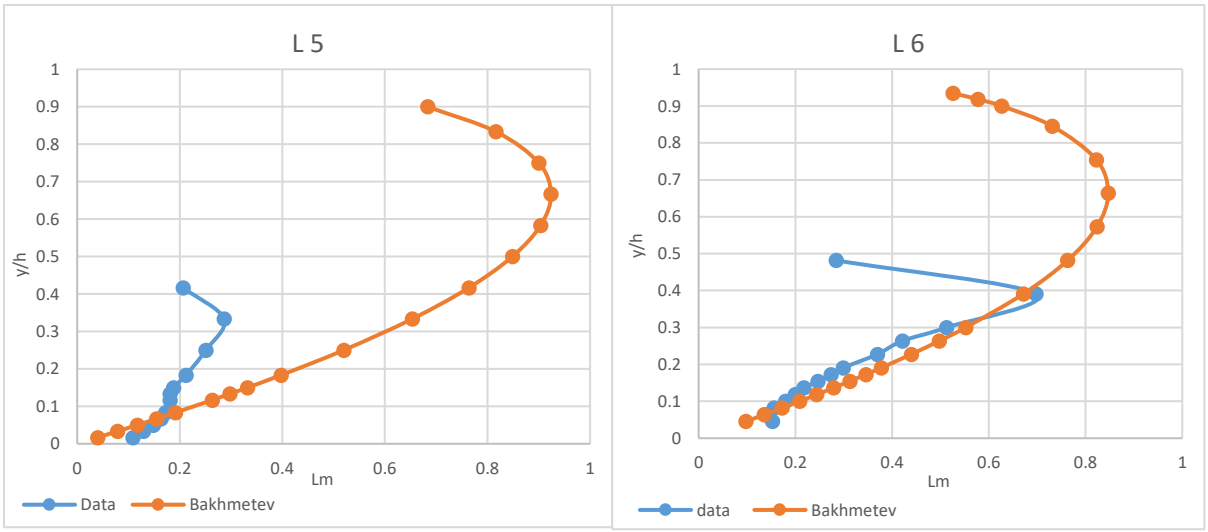

Figure 4.5: Mixing length profile derived from data together with Bakhmetev distribution

Note that the unit of l_m is cm.

The method to derive the mixing length as equation (4-5) is based on the velocity gradient, thus it mainly valid in the region of 0.2h. As can be observed from Figure 4.5, a good agreement between present data and Bakhmetev distribution can be observed in the $y/h < 0.2$ region, except for L5. This is the exact measuring point that showed the irregularities in velocity profile. Like the Bakhmetev distribution, mixing length profiles derived from data also show the transition point, this is most clear in L6. However, this transition point lies much lower to the bottom for the data profile. This can be explained that the boundary layer is still developing under undeveloped flow condition, thus not spreading through the whole water body yet. A clear growing pattern can be observed from L1 to L6, namely that the deviation of transition point between data and Bakhmetev model is shrinking.

4.5 Turbulence intensity data

Figure 4.6 shows the turbulence intensity data in streamwise and vertical directions in six locations. The curves have similarities with the standard ones by John Kim, Parviz Moin and Robert Moser 1986 using numerical models, as seen in Figure 4.5. It verified that the flow is indeed under 2D condition, thus supporting the assumption $v' = w'$.

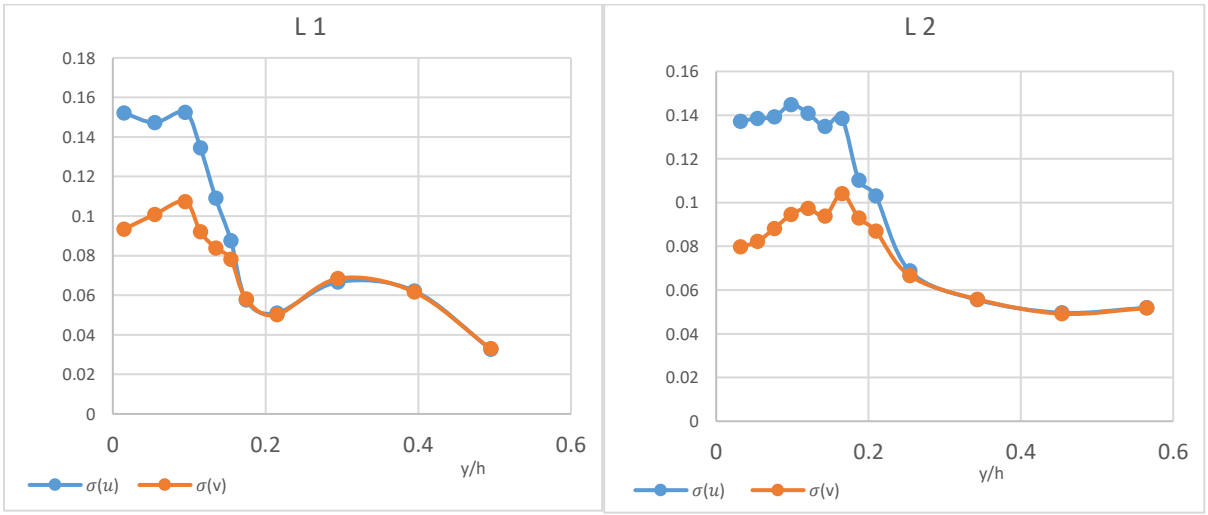

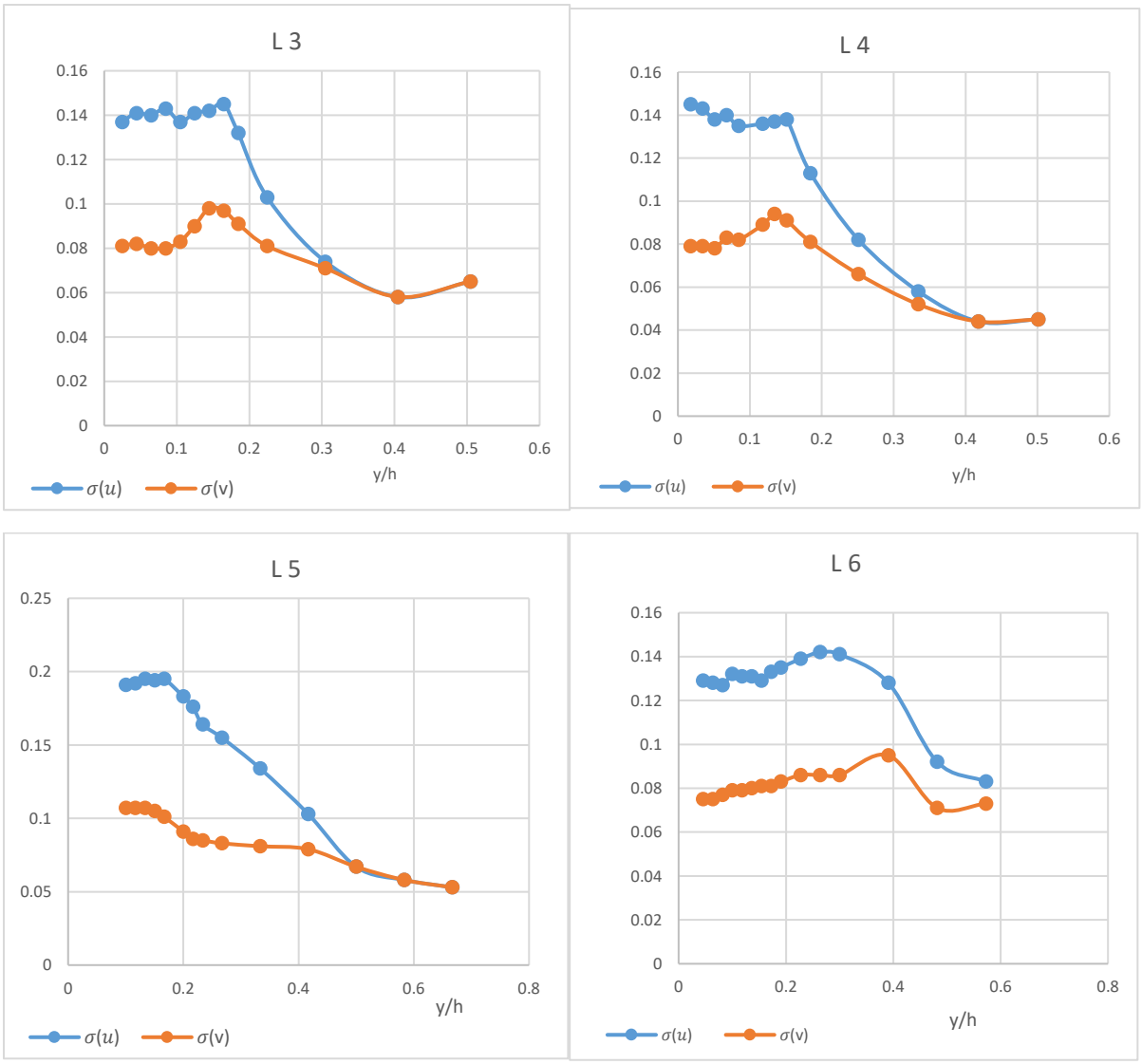

Figure 4.6: Root-mean-square velocity fluctuations in streamwise and vertical direction

4.6 Reynolds shear stress

The figure shows the distribution of Reynolds shear stress $\overline{u'v'}$, with the adjusted y_0 position.

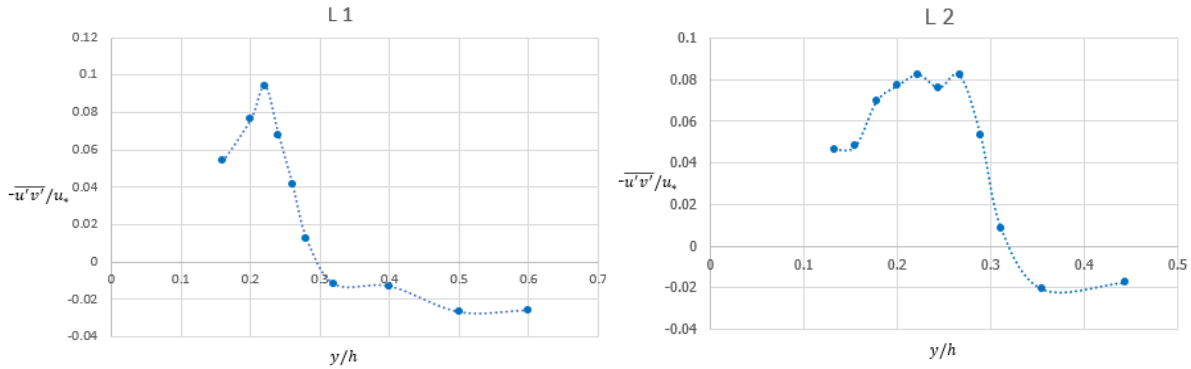

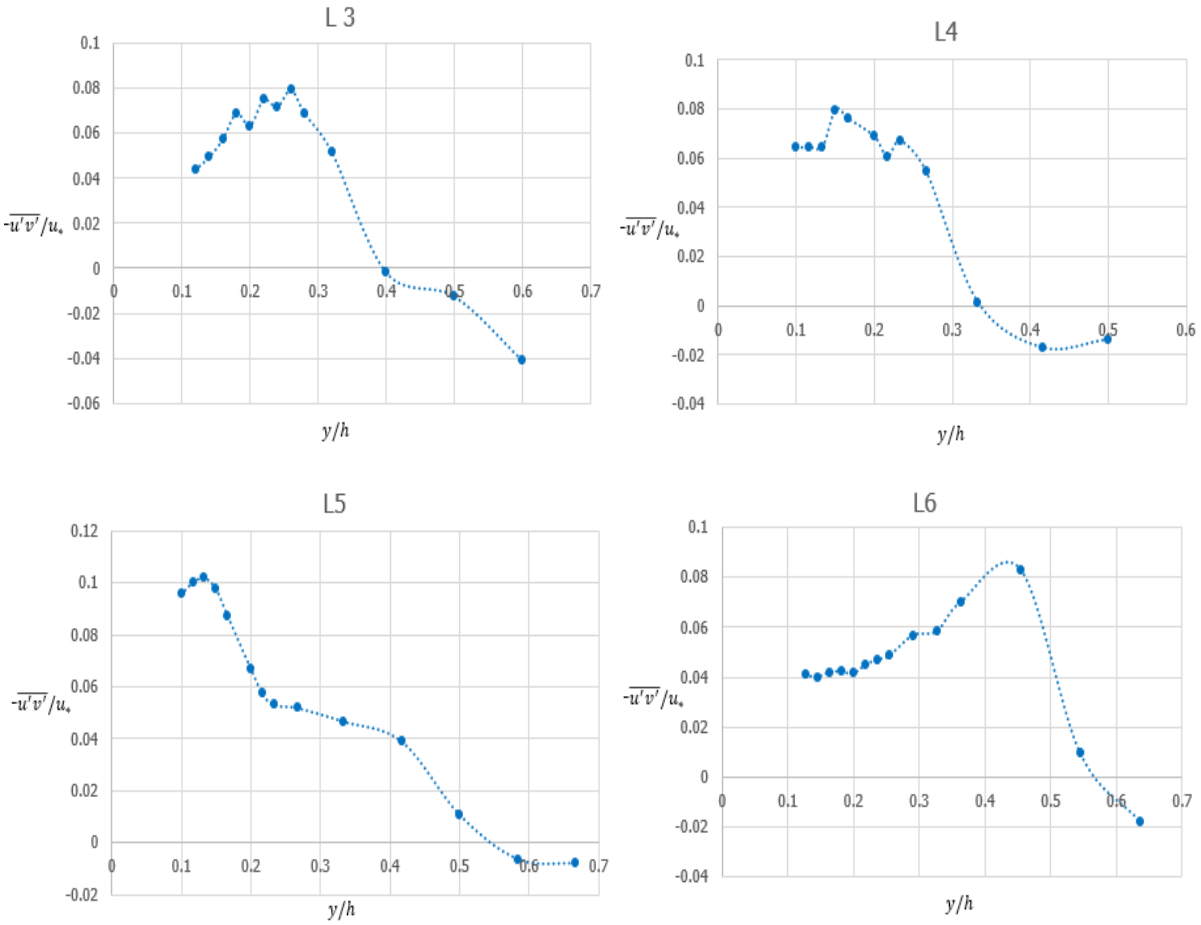

Figure 4.7: Reynolds shear stress computed from data

The profiles show similar curves with the numerical results of Reynolds shear stress profile in turbulence flow by John Kim, Parviz Moin and Robert Moser 1986, as seen in Figure 4.7. A maximum in the Reynolds stress distribution is observed at around $0.15\ y/h$ in L1 to L5, whereas in L6, it is shifted upwards to $0.4y/h$.

The decay of the maximum value position from the standard $0.2y/h$ to present $0.15y/h$ is observed. It might be caused by the accelerating flow condition, or due to the very shallow water condition that the layer is compressed. Besides, it can also be affected by the choice of $y = 0$ position. The upshift at location 6 may be due to longitudinal secondary current, since the L6 is the last block followed by a weir-like structure. This may cause a deviation from the 2D profile and also affect the shear velocity under certain flow conditions (Nezu and Nakagawa, 1993; Albayrak and Lemmin, 2011).

4.7 Conclusion

Despite the fact that the current flow condition is far away from standard open channel flow, namely either uniform nor fully developed, similarities of flow characteristics still exist.

Frist of all, the feature of wall region and the outer region was observed. The logarithmic velocity profile was found in wall region, as well as the wake-log law pattern in the outer region. A deviation of κ values for logarithmic profiles from typical value emerged. This was explained by changing the start of coordinate in vertical direction. A considerable shift of $y = 0$ position

was applied, which indicated a significant layer of disturbance exists. This upshift was especially large for L5, which was placed between two neighboring blocks. It can be expected since the gap of adjacent blocks will introduce severer disturbance.

The velocity profiles using shear velocity that derived by equivalent roughness method showed irregularities. They move up and down from L1 to L6 arbitrarily and have contradictories with mean flow velocity derived from mean water depth. This problem is solved when applying different shear velocity values from two other methods, i.e., Reynolds shear stress method and turbulence kinetic energy method. This reveals that inaccuracy might exist in the choice of equivalent roughness.

In engineering approach, it is indeed more handy to use equivalent roughness for designing. Therefore, the calibration is done in this chapter. It was conducted by comparing shear velocity values obtained by all three methods (Equivalent roughness, Reynolds shear stress and TKE). Since the Reynolds shear stress method behaved best in conducting velocity profiles, it is considered to be the most accurate one. Therefore, the calibration of k_s values can be done by fitting the most accurate shear velocity. As a result, larger values for all positions were obtained compared to the suggested value by Pilarczyk. Whereas more accurate value can only be proposed with more adequate data.

The mixing length distributions showed self-similarity along the flow direction, with a clear growth pattern. In addition, within the region of $0.2h$, the mixing length derived from data shows coincides with bakhmetev model. These two features are of importance for the later stability parameter calculation, which based on the data obtained from experimental set-up 1. In this set-up, the block mattress was placed farther away from the sluice gate (45cm and 55cm) compare to set-up 2 (35cm). It allowed the flow to grow even further. Thus in the Chapter S*tability Parameter,* the Bakhmetev profile would be used.

5 Stability of block mattress

In this chapter, the possible failure mechanism was studied. The methodology applied here is as follows: Firstly, mean steady force analysis was applied to give an impression of the stability. Secondly, the velocity signals with time series ending at failure moment were checked. Next, in order to find a failure pattern, similarities among all sets of velocity signals were studied, along with the corresponding recorded failure images. Afterwards, more detailed analysis, for example, quadrant analysis and dynamic force analysis, was conducted on initial exposure moment as well as failure moment.

The structure of this chapter is as follows. In section 5.1, the initial failure moment will be studied, including force analysis, synchronized velocity signals and recorded images and quadrant analysis. Next, in section 5.2, the process from initial failure moment to actual failure moment will be studied. The analysis focused on the last row of block mattress based on Test series three will be conducted in section 5.3. In this section, another possible failure mechanism will be proposed. Finally, conclusions and discussions will be addressed in section 5.4 and 5.5.

5.1 The initial exposure

Previously, the failure moment was defined as the lifting of half of a block thickness. However as observed from the recorded images, the failure process always starts with initial exposure, as shown in Figure 5.1. The whole process ends with the previously defined failure moment, as shown in Figure 5.2. Thus if any form of failure is definitely unacceptable, the initial failure moment is essential.

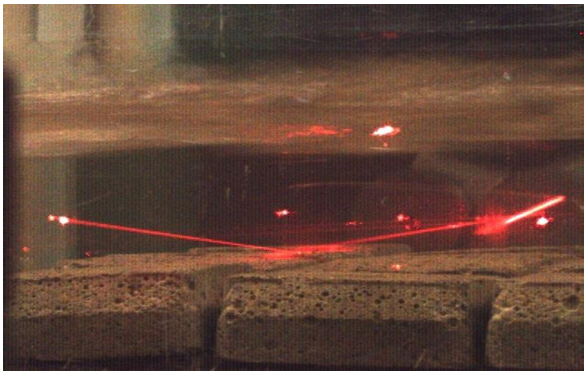

Figure 5.1: The initial exposure of the last row of block mattress

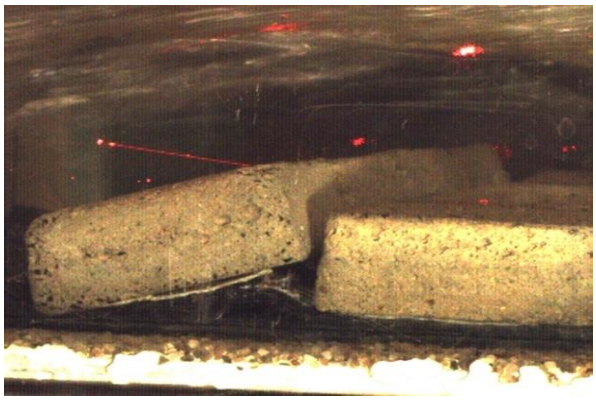

Figure 5.1: The failure moment of the last row of block mattress

5.1.1 Steady forces on a single block

The force analysis was conducted to give a first impression on the stability of block mattress. This analysis focused on the moment right before any exposure, and the object is the last row of block. The velocity used here was the typical critical velocity from the Database (Appendix D). Since there is no exposure area for now, the drag force was considered not playing a role here. Besides, only the steady force was considered for now.

Self-weight:

$$F_G = \rho V g = 1312 kg/m^2 \times 4.5cm \times 7.5cm \times 1.9cm \times 9.81 m/s^2 = 0.83N$$

Mean lifting:

$$F_L = \frac{1}{2} C_L \rho A u^2 = 0.5 \times 0.2 \times 1312 kg/m^2 \times 4.5cm \times 7.5cm \times (1.4 m/s)^2 = 0.87N$$

Note that: flow velocity $u = 1.4 m/s$, $C_L = 0.2$.

Normally, from the recorded data, the velocity corresponding to maximum shear stress is larger than 1.4 m/s. Therefore the resulting lift force is generally larger than the self-weight of a single stone. However, there was no failure observed yet. The reasons were discussed as follows:

1. The lift coefficient has a value of 0.15 to 0.22, when the particle is placed between other particles (Einstein& El-Samni, 1949). Lacking more detailed information, here a midpoint of the domain was chosen.
2. The force by neighboring block as well as geotextile can be seen as a source of stability. However, it is rather impossible to quantify those forces.

In conclusion, the block stays stable under the steady force, taking the force by neighboring block and geotextile into consideration.

5.1.2 The initial exposure moment

As illustrated in section 5.1.1, the block was rather stable under the steady force. Thus there must be other structure that causes the initial exposure. In this section, the synchronized velocity signals and recorded images were analyzed, in order to find the cause of initial exposure. There are 16 failures in different set-ups were recorded, whereas 4 of them can be diagnosed to be interfered by bubbles. The case of interacted velocity signals was shown in Appendix A. This study is based on the test series 1. A summary of failure moment and associated times was presented in Appendix B. Here, all the failure cases were checked individually, instead of taking an ensemble averaging of all of them. The main reason is that some detailed information will be lost if merely the averaged case is studied. Since the structure that responsible for failure is very unknown, the less information missing the better. After carefully checking the signals, two failure patterns were observed:

1. The initial exposure was followed closely by failure moment($\sim 0.25s$).
2. The failure spread rather widely through the time series($\sim 1s$).

The typical synchronized velocity signals and recorded images for the first pattern were presented in Figure 5.3, and the second pattern in Figure 5.4. The corresponding set-ups for recorded failures are D3L55 FAILURE 1 for the first pattern and D4L35 FALURE 1 for the second pattern.

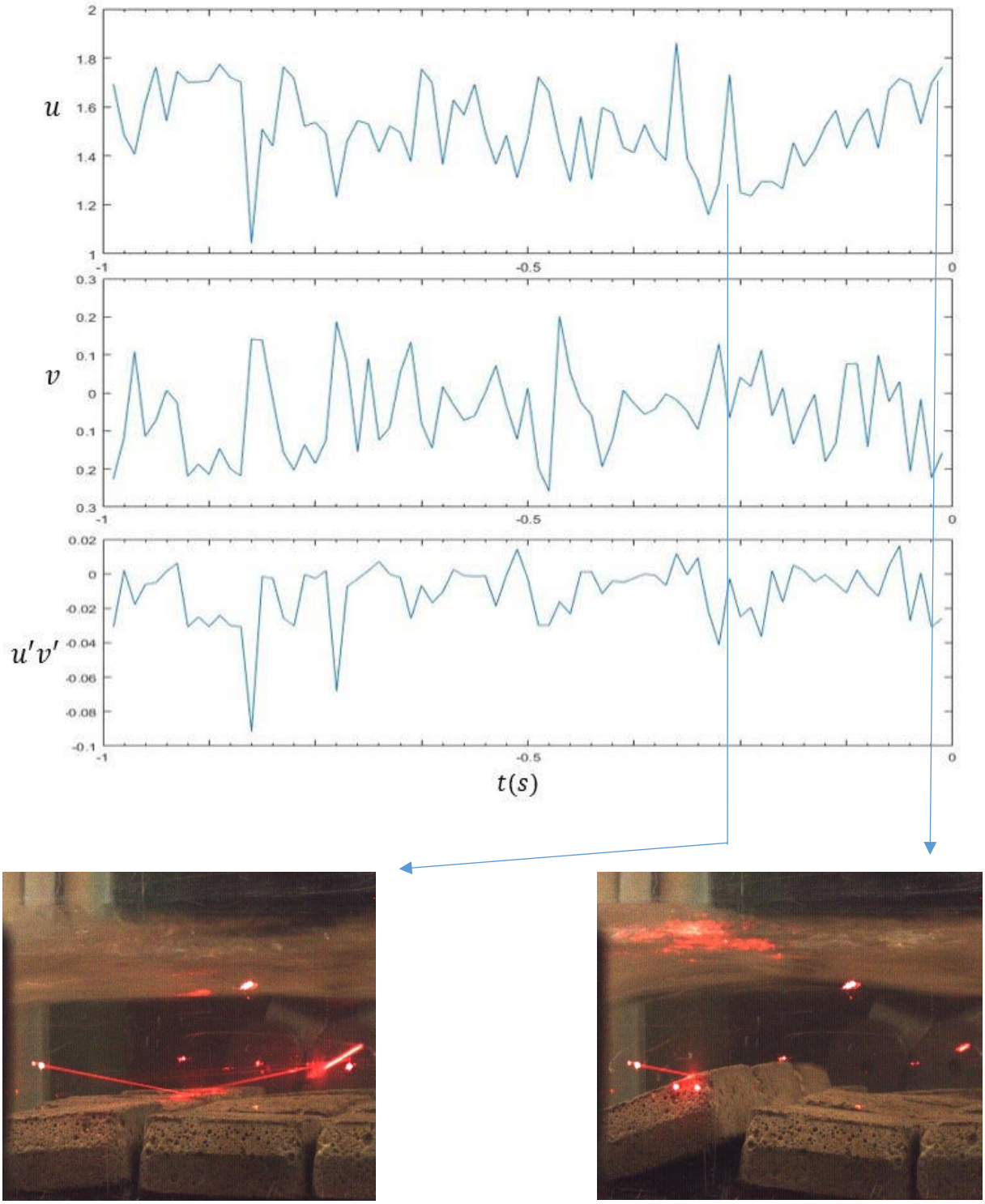

Figure 5.3: Typical synchronized velocity signals and recorded images for the second pattern

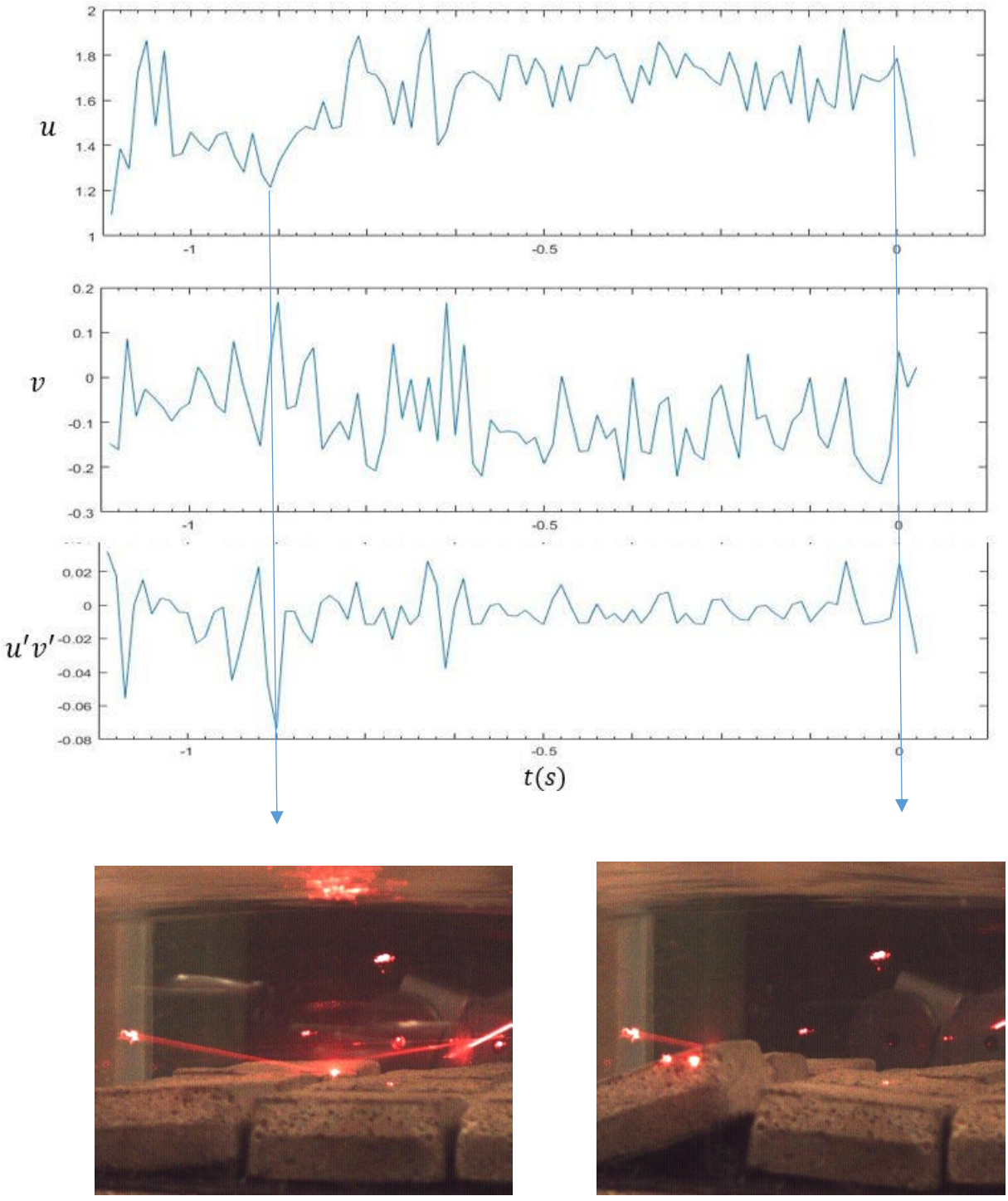

Figure 5.4: Typical synchronized velocity signals and recorded images for the second pattern

Note: failure moment is located at t=0 position in the velocity signals.

The velocity signal for the first pattern shows a clear increase from the initial exposure(the left image) to the failure moment(the right image). during this period, peaks of shear stress occur, especially at the maximum velocity time node. This coherent structure is also found in the second pattern. A sudden increase of flow velocity, along with a peak of shear stress present right at the initial exposure moment. Thus the coherent structure with sudden increase of velocity associated with a peak of shear stress is considered responsible for initial exposure.

5.1.3 Quadrant analysis

In previous chapter 5.1.2, velocity and shear stress structure were studied. To have a more in-depth understanding, in this section, even smaller structures were looked into to see how turbulence structures play a role here.

Quadrant analysis is considered simple but useful for addressing the generation of turbulence structure. The quadrant analysis was conducted for a previously found coherent structure that responsible for failure in section 5.1.2, namely at the time node with the sudden increase of flow velocity and the peak of shear stress. The result was presented in Figure 5.5.

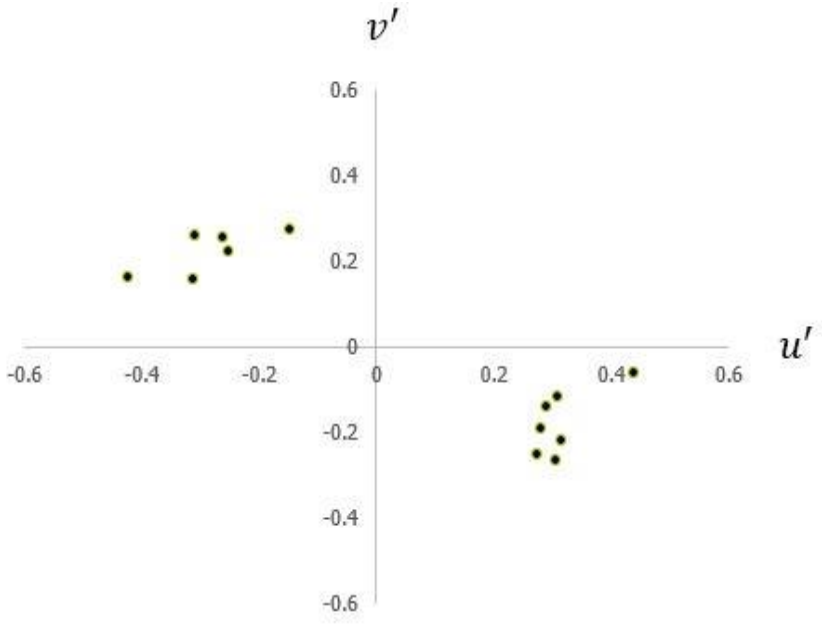

Figure 5.5: Quadrant analysis for all failures

As expected, Q2(ejection) and Q4(sweep) are mostly found to be responsible for instability of bed material, as they are linked to the positive instantaneous Reynolds stress, $-u'v' > 0$. Moreover, in present flow, sweep (Q4) and ejection (Q2) seem to be equally important. However, for rough wall situation, sweep is expected to have more contribution according to Raupach (1981). This can be explained as that the measured flow property was modified by the block movement. At moment of uplifting of block, the upwards force will be induced on the flow above it, thus causing positive vertical motions ($v' > 0$). Under this circumstances, the obtained ejection can actually be the 'ejection' of block. Therefore it is hard to draw the conclusion if the ejection is the cause or the consequence of the failure.

Moreover, for a sweep event the fluctuation lift force is positive (upwards), thus will contribute to the instability of block. However, in the ejection event, fluctuation lift will deduct the mean lift force, thus stabilize the block. Therefore, the sweep event and so caused lift force are considered responsible for the failure.

The quadrant analysis also gives information on the magnitude of fluctuation part of velocity, i.e., magnitude of u' and v'. Next, a force analysis including fluctuated quasi-steady force and time dependent acceleration will be conducted. Still, only the lift force is considered here since we are still focus on the cause of initial exposure. The block is still completely shielded from the neighboring one, thus the exposed area is not exist yet.

Fluctuation lift force is calculated by Equation 2-13. For the sweep event in the current flow condition, the average $u' = 0.32m/s$ and $v' = -0.18m/s$, with $\bar{u} = 1.4m/s$. With the affected area, $A_{F_L} = 4.5cm \times 7.5cm$ and parameter $a, b \approx 1$, giving $F_L' \approx 0.017N$. Force caused by acceleration is calculated by Equation 2-14. The time-dependent streamwise acceleration term can be derived from velocity signals in Appendix B, as well as from Figure 5.3 and 5.4. Taking an average gives a value of $a \approx 2m/s^2$. With mass coefficient $C_m = 2.67 \sim 3.75$ (Tromp 2004), giving $F_a = 0.62 \sim 0.8N$.

Since $F_a \gg F_L'$, it is clear that the time dependent acceleration plays a larger role than turbulence induced fluctuation force here.

5.2 The failure moment

After the initial exposure, the block deviated from its balance position and not going back. The turbulence contributions are relatively small for the initial exposure, as proved in section 5.1.3. Thus it is logical to expect its contribution to continuous lifting is still small. Thus more macro-scale structure is expected to cause to continues lifting of block from initial exposure to the failure moment.

One hypothesis is considered here to explain the failure. The flow above the block mattress was compressed after the initial movement of block. According to Bernoulli effect, local flow velocity goes up with smaller water depth, as shown in Figure 5.6. Thus it makes lifting force much larger, leading the failure. On the contrary, the turbulence structure is playing a less important role here.

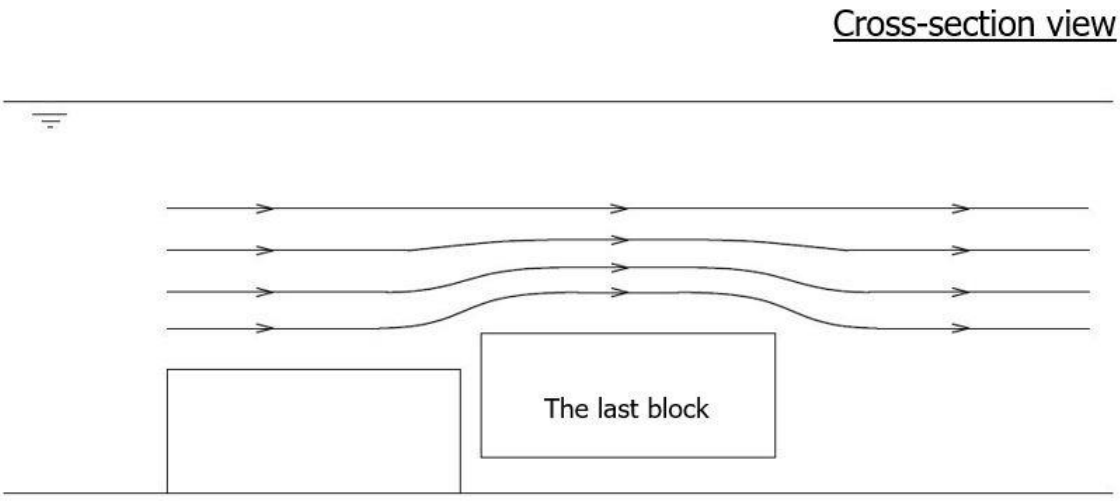

Figure 5.6 Bernoulli effect on the last block right after the initial exposure

To verify the hypothesis, the force analysis including all terms of Quasi-steady forces was conducted. Note that the velocity used here was obtained at the instantaneous failure time node from data directly. The average instantaneous flow velocity was $1.55m/s$, giving the instantaneous lift force 1.33N. With exposure area start to exist now, the drag force start to play a role. The exposed area was chosen to be $7.5cm \times 0.95cm$, according previously defined failure moment. Thus the obtained mean drag force is 0.19N.

The contribution of Bernoulli effect can be determined by addressing the relative increase of mean lift force. The mean lift force increased from $0.87N$ to $1.33N$, by 52.9%. The

contribution of turbulence structure can be shifted to the relative importance of fluctuation lift force over mean lift force, which is approximately $\frac{0.017}{0.87} = 2\%$.

In conclusion, the Bernoulli effect induced lift force together with drag force are responsible for the continuous lift after the initial exposure to the final failure moment.

5.3 Last row of block mat analysis

The failure always occurred at the last row of block mattress, so-called the free edge. To have a better understanding of the weakness of the last row block. The result of Test series 3 that focused on the last row was studied. A summary of flow velocity and turbulence intensity will be presented in the Appendix C. Figure 5.7 gives a sketch on the flow condition over the last row of block mattress.

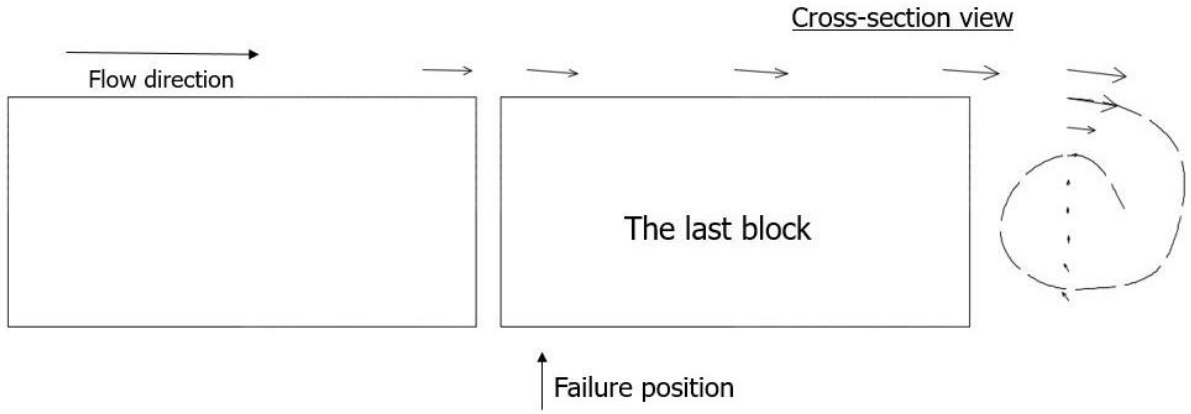

Figure 5.7: Flow condition over the last row of block mattress

Note that the lengths and the directions of arrows indicate the local flow velocities and directions.

It is clearly observed that the flow accelerated over the block surface and dropped right behind it. Besides, the recirculation zone presented over the block. Thus one can conclude that the backward facing step (BFS) effect occurred here. Next, the analysis on whether the BFS plays a role in failure will be addressed.

The recirculated flow will inject backward flow beneath the block, namely, the flow will penetrate backward under the block. This injection flow will induce backward force to lift the block. Therefore theoretically, the failure should present at the very end of bock mattress, if the BFS effect was severe. Thus the magnitude of backward flow velocity and induced force were checked. With magnitude of local flow velocity 10^{-1}, giving the magnitude of lift force 10^{-4}. This BFS induced lift force is way too small to lift the block by itself. However, it is possible that BFS cooperated with Quasi-steady force will contribute to the generation of the observed initial exposure. The hypothetical theory is discussed as follows, and a sketch of the process is present in Figure 5.8.

1. The BFS induced lift force will induce minor upwards movement to the very end edge.
2. The minor motion will increase the affected area for drag force in the flow direction.
3. This drag force will push the block away from its stable position.

4. Once the block deviates from the stable position, the initial exposure at the observed failure position (as shown in Figure 5.7) occurs.

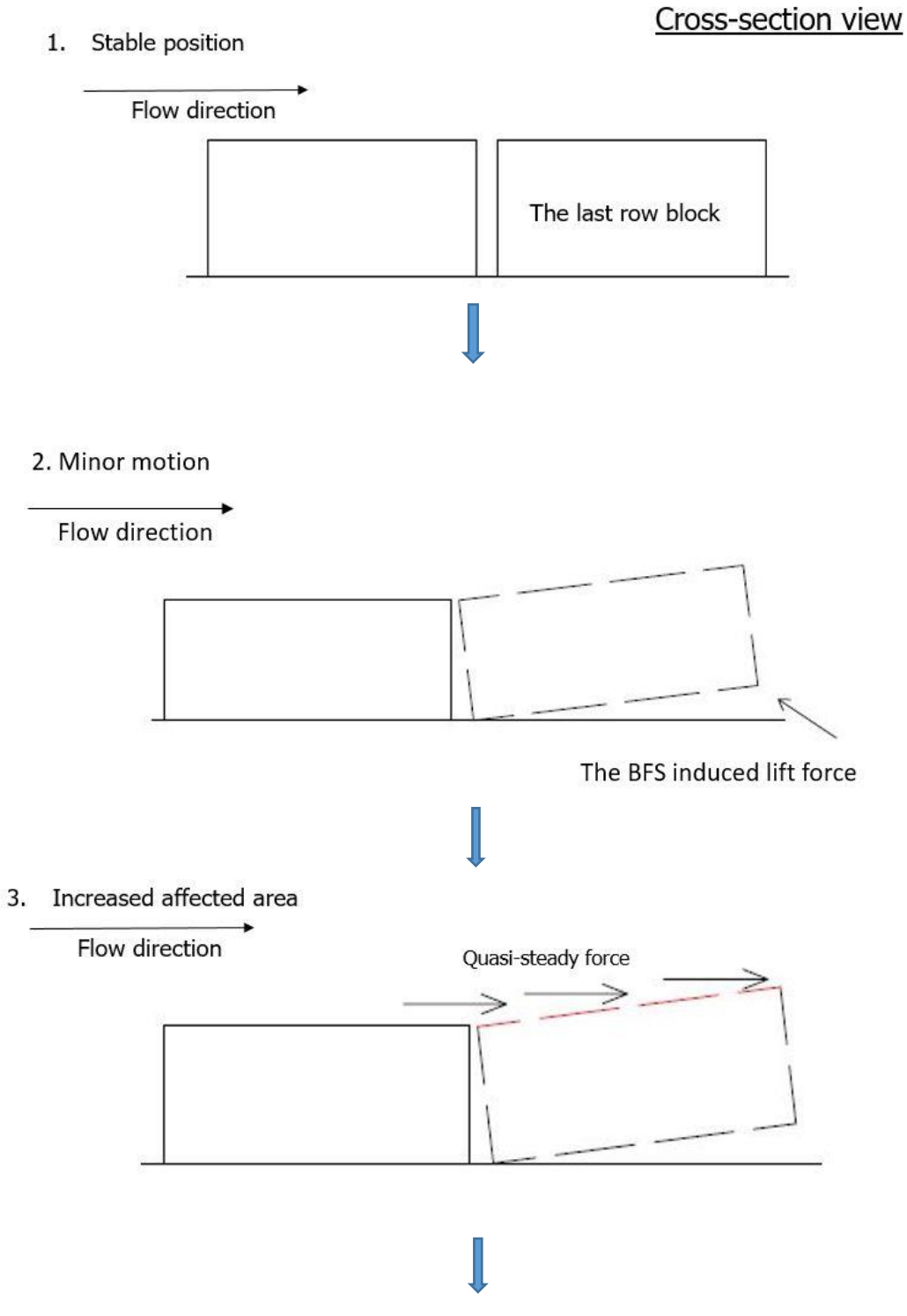

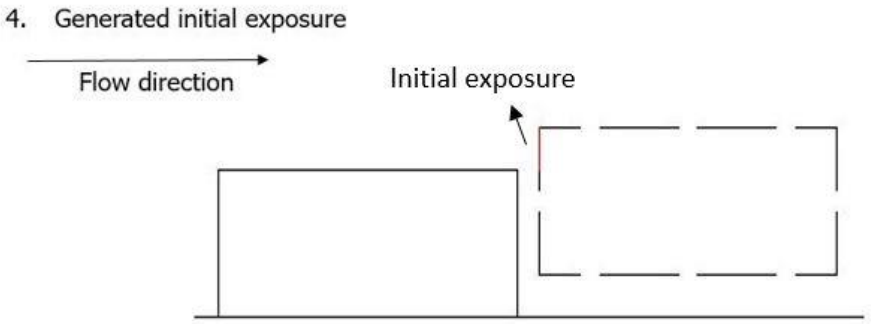

Figure 5.8: The generation of BFS induced initial exposure

Note that the sketch is not in scale, simply to give an impression of the process.

Apart from the recirculation effect, acceleration above the block surface was also observed. The mean acceleration of flow significantly improves the description of stone stability (Remco Steenstra 2016). Thus, in Chapter 6, the stability formula including the acceleration term will be discussed.

5.4 Concluding remarks

Based on the observation that the failure always and only occurred to the last row of block mattress, in this chapter, the detailed analysis was conducted to diagnose the failure mechanism.

Firstly, the cause of initial exposure was studied. The synchronized velocity signals with recorded failure images were checked to find the responsible flow structure for the force on block mattress. Next, a series of force analysis based on the quadrant analysis was conducted to evaluate the magnitude of forces.

The velocity signals showed a pattern of responsible flow structure, with a sudden increase of flow velocity following by a peak of shear stress. The following force analysis showed that larger scale flow structures, i.e., pressure gradient, time-dependent acceleration, can be more responsible in comparison to small-scale flow structure (turbulence), both in terms of the cause of initial exposure and continuous failure. Originally, the block mattress stayed stable under the mean Quasi-steady force. The lift motion was mainly caused by fluctuation and dynamic part. Whereas the dynamic part (time-dependent acceleration caused lift force) was 40 times larger than the fluctuation part (turbulence induced lift force). Besides, in turbulence scale, the quadrant analysis gave information on the responsible events, i.e., Q2 (ejection) and Q4 (sweep). Two events had similar possibilities of occurring. However, the present information is not sufficient enough to distinguish the Q2 (ejection) event was the cause or the result of the lift of block mattress. Due to the fact that the block is large enough to modify the flow properties, the quadrant analysis is not a sufficient tool to analyze the failure in this situation.

Secondly, the continuous failure process from initial exposure to actual failure moment was studied. As in the study of initial exposure, larger scale flow structure (Bernoulli effect) was also found responsible here. The evaluation was conducted by comparing the relative distribution to mean quasi-steady force. The lift force increased by 53% due to Bernoulli effect, whereas 2% by turbulence induced fluctuation.

Moreover, one more analysis was done targeting the local flow condition over the last row of block mattress. Here, the backward facing step was found, and can also account for the

occurrence of initial exposure. The failure process can be summarized as follows: the BFS injected flow under the block mattress form the very end edge, thus giving a minor motion of very end edge lifting; the exposure area was induced; quasi-steady force dragged the block to a horizontal position, thus the initial exposure occurred.

6 Stability formula and parameters

Following the main purpose of this thesis, an optimization needs to be done to Pilarczyk's. To solve the problem of the Pilarczyk's ill behavior in non-uniform flow condition, the main properties of non-uniform flow need to be considered. Therefore, the turbulence influence on the stability of block mattress was taken into consideration. Besides, considering the acceleration also plays an important role in lifting the block, this term needs to be included as well.

The chapter is structured as follows. In section 6.1, a new stability parameter based on Pilarczyk's formula was proposed. Next, in section 6.2, the final formulation of the proposed parameter was determined based on the present data. In section 6.3, the behavior of existing stone stability formula including the acceleration term in current block mattress situation was discussed. The performance of the new stability parameter was evaluated in section 6.4. Finally, the conclusions were presented in section 6.5.

6.1 The proposed stability parameter

The existing stability formula for block mattress, namely Pilarczyk formula, only introduced the turbulence effect as a numerical parameter K_T. Besides, this parameter were derived base on the experimental data for stone bed material. Thus it is to be expected and observed that the Pilarczyk formula was insufficient especially under the non-uniform flow condition. Firstly, to optimize the transport formula by introducing the turbulence effect fundamentally into it, Jongeling et al. (2003) proposed an approach that combined the mean flow velocity and turbulence intensity (i.e., $\bar{u} + \alpha\sqrt{k}$) to describe the peak of the force that present in the flow overpassing the bed material. This approach is widely used as the basis of latter proposed approaches. Later, Hofland (2005) found the maximum ($\bar{u} + \alpha\sqrt{k}$) local value weighted over mixing length L_m/y was responsible for instability. Thus the new form of mean velocity and turbulence combination, i.e., $< \bar{u} + \alpha\sqrt{k} >_{L_m} \frac{L_m}{y}$, was proposed. Hofland's approach was later used by R.S. Steenstra (2016) to describe the flow force one step further. In this formula, the acceleration terms was introduced, in the form of $C_{m:b} \frac{dp}{dx} d_{n50}$.

While the development of stone stability studying, the stability formula for block mattress still remains at the stage of merely taking the turbulence effect as a simple parameter. Thus taking a cue from the development of stone stability formula, introducing ($\bar{u} + \alpha\sqrt{k}$) into Pilarczyk's formula to describe the interaction between flow condition and block mattress behaviors seem to be logical. In the newly proposed formula, $(\bar{u} + \alpha\sqrt{k})^2$ will be replacing the existing $K_T \times u_{cr}^2$. Therefore, the new formula is formed as follows:

$$\varphi = \frac{\Delta D \times \Phi_s \times 2g \times K_s}{0.035 \times (\bar{u} + \alpha\sqrt{k})^2 \times K_h} \tag{6-1}$$

Where:

$\Delta = Relative\ density\ [-]$

$D = Characteristic\ dimension/thickness\ [m]$

$g = Acceleration\ of\ gravity = 9.81\ m/s^2$

$\alpha = turbulence\ magnification\ factor\ [-]$

$k = turbulence\ kinetic\ energy\ [m/s]$

$\varphi = Stability\ parameter\ [-]$

$\Phi_s = Critical\ Shields\ parameter\ [-]$

$K_h = Depth\ parameter\ [-]$

$K_s = Slope\ parameter\ [-]$

6.2 Final formulation of the proposed parameter

The formulation of proposed stability parameter was processed as follows: 1) recording the failure moment, mainly the failure discharge. 2) collecting the date to fill the database, focusing on the neighboring failure discharges region. 3) extracting the mean velocity and turbulence intensity information for all the failure cases, deriving the turbulence magnification factor α. 4) deriving new stability parameter.

6.2.1 Database

The main purpose of collecting the database was to prevent the interference by the lift of block mattress to the flow condition. A summary of Database for four set-ups was given in Figure 6.1, full information on velocity and turbulence properties was presented in Appendix D.

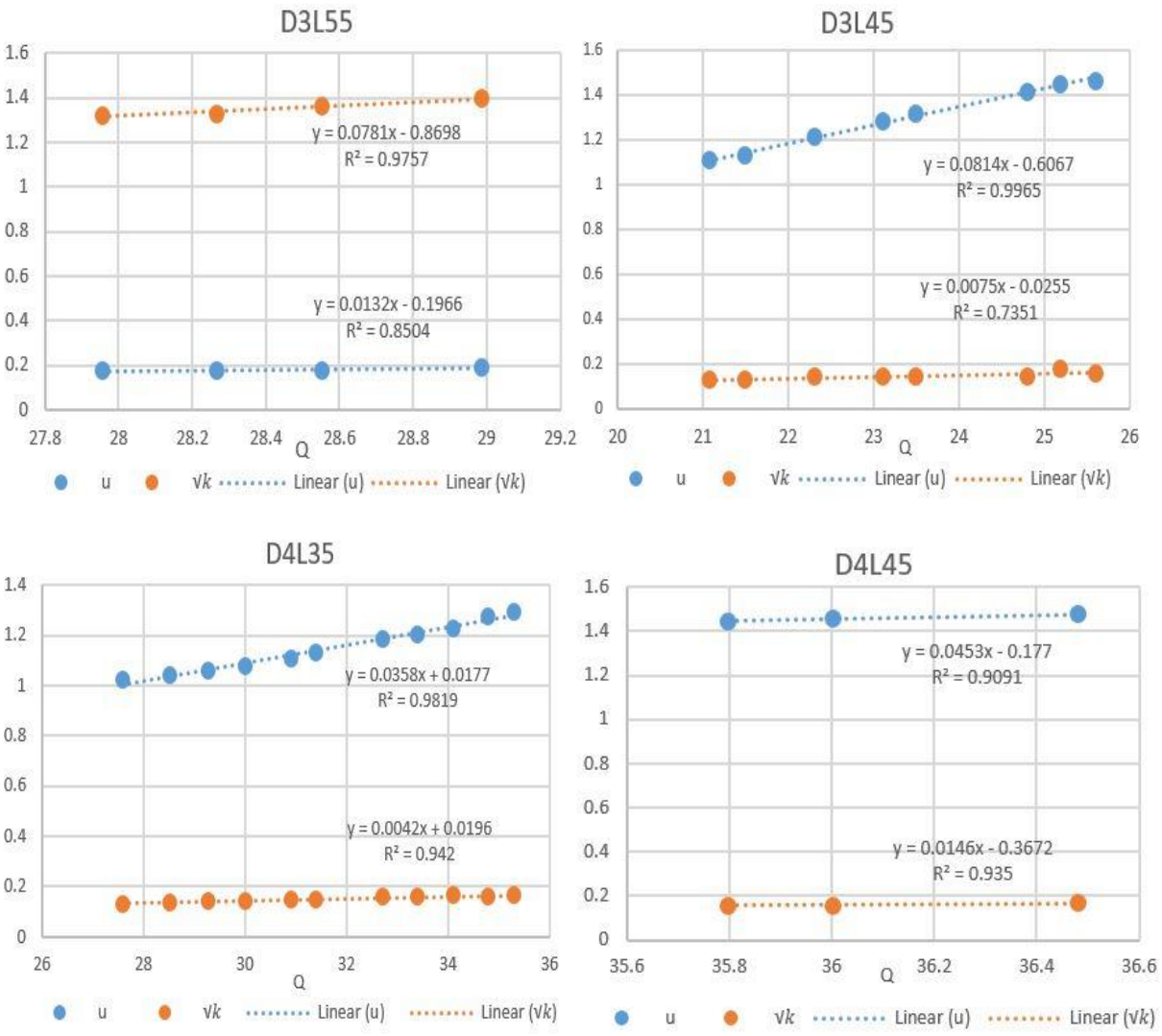

Figure 6.1: Summary of Database, along with the fitting linear function

As observed, the mean flow velocity increase with the increase of discharge, while the increase of turbulence intensity is very gentle. Besides, the fitting linear function behaves well with fitting coefficient $R^2 > 0.8$.

Next, the associated mean flow velocity and turbulence intensity at the failure discharge were derived from database. Table 6.1 presented the computed values for all failure case.

Table 6.1: Summary of flow characteristics obtained from database

Set up	Failure case	Discharge $[l/s]$	$\bar{u}\ [m/s]$	$\sqrt{k}\ [m/s]$
D3L55	1	28.24	1.34	0.176
	2	28.05	1.32	0.174
	3	28.25	1.34	0.176
	4	28.65	1.37	0.181
D3L45	5	25.15	1.44	0.163
	6	25.65	1.48	0.167
	7	24.54	1.39	0.159
	8	25.10	1.44	0.163
	9	25.20	1.44	0.164
D4L35	10	35.8	1.44	0.155
	11	35.95	1.45	0.157
	12	36.00	1.45	0.158
	13	35.95	1.45	0.158
	14	35.75	1.44	0.155
D4L45	15	38.20	1.39	0.180
	16	37.70	1.37	0.178
	17	37.80	1.37	0.178
	18	37.60	1.36	0.177
	19	37.65	1.37	0.178

6.2.2 Turbulence magnification parameter α

The method to determine the α value is given as following:

1 The relation between α and critical velocity is given: $u_{cr} = \bar{u} + \alpha\sqrt{k}$.
2 Assuming a single value of α exists to achieve a best fitting for 18 failure cases.
3 The value for α is expected to be between 0 and 7, as found by all previous researchers.

The information for $\bar{u}$ and $\sqrt{k}$ was collected in section 6.1.1, leaving the critical velocity u_{cr} to be the only unknown. The critical velocity can be treated as the maximum velocity at the failure moment. However, as studied in chapter 5, the responsible coherent structure that lead to the failure was not merely maximum flow velocity. Thus it will not be accurate to assume that $u_{cr} = u_{max}$. Another approach to derive the α value is to treat it as a fitting parameter, as illustrated by Hoan (2008). In this approach, the critical velocity is defined as the *failure velocity*. This failure velocity is rather a concept of the sum of flow conditions than merely flow velocity. Thus theoretically, for one type of block mattress under one type of hydraulic structure, there should be a fixed failure condition, i.e., a fixed failure velocity value. Based on the collected failure cases, a relation can be drawn as follows:

$$u_{cr} = u_{failure} = \overline{u_1} + \alpha\sqrt{k_1} = \overline{u_2} + \alpha\sqrt{k_2} = \cdots\cdots = \overline{u_n} + \alpha\sqrt{k_n} \quad (6\text{-}2)$$

Where the subscript numbers stand for the failure cases.

From the equation system 6-2, for different α value, different standard deviation of $u_{failure}$ for all failure cases will emerge. Thus the final α value will be chosen at the minimum standard deviation case. Figure 6.2 shows the trend for standard deviation under different α value conditions.

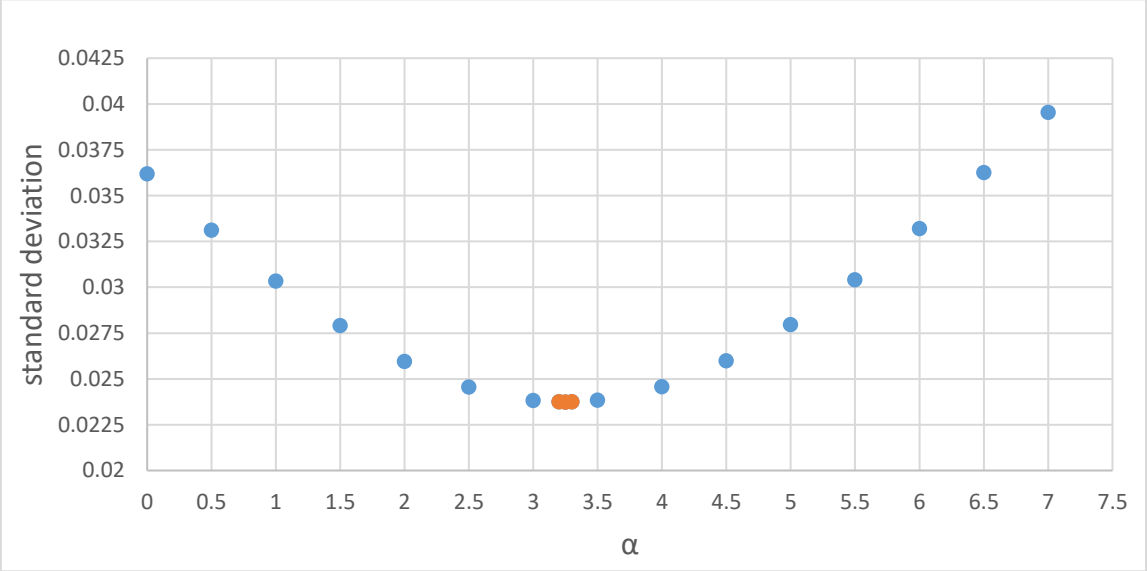

Figure 6.2: Standard deviation under different α value conditions

As can be observed from above figure, the best collapse of the failure velocity was at a α value of 3.25.

6.2.3 Stability parameter

In present flow condition and with the provided block mattress model dimensions, the values of associated parameters in Equation 6-1 are given in Table 6.2:

Table 6.2: Summary of parameter values in proposed stability formula (Eq. 6-1)

Parameter	Value	Reasoning
Δ	1.31	Relative density
D	$0.019m$	Thickness of block mattress
Φ_s	0.07	Suggested value by Pilarczyk
K_h	1	Measured velocity close to block mattress (approximately $0.5cm$)
K_s	1	Horizontal bottom

Along with the previously obtained α value, the proposed stability formula can therefore be simplified as follows:

$$\varphi = \frac{\Delta D \times \Phi_s \times 2g}{0.035 \times (\bar{u} + \alpha\sqrt{k})^2} = \frac{1.31 \times 0.019 \times 0.07 \times 2 \times 9.81}{0.035 \times (\bar{u} + 3.25\sqrt{k})^2}$$

With mean velocity and turbulence intensity given in Table 6.1, the stability parameter can be derived. Figure 6.3 shows the values of stability parameter under all failure discharges conditions.

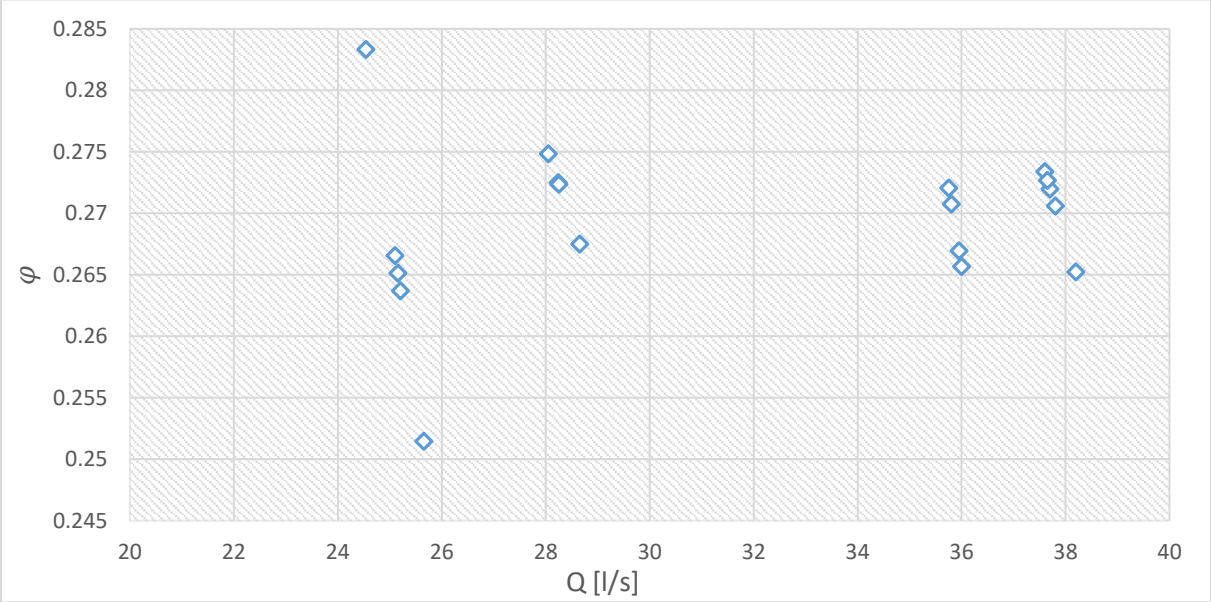

Figure 6.3: Stability parameter for all failure discharges

As can be observed from above figure, the obtained φ value spreads around a mean value 0.27. Normally during designs, deterministic and probabilistic approach will be conducted. For deterministic approach, taking the safer side is a better option, thus a slightly larger value of 0.3 is suggested. For probabilistic approach, a normal distribution with mean value of 0.27 and standard deviation of 0.02 is suggested.

6.3 Stability formula with acceleration term

Previously, the hydraulic force was given in the terms of flow velocity and turbulence effect and the stability parameter was derived explicitly incorporation of turbulence intensity. However, the acceleration in the flow also leads to a direct body force on bed material[Hoefel and Elgar (2003)]. In the present experiment, the water depth was observed to fluctuate along with the flow direction. Thus clearly the pressure gradient, i.e., the acceleration term, plays a role here.

Steenstra (2014) proposed a stone stability formula that included the flow velocity, turbulence properties, and pressure gradients. It described the influence of these properties explicitly and widened the application range of stability formula. The Steenstra's formula reads as follows:

$$\varphi = \frac{\left(\max\left[<\bar{u}+\alpha\sqrt{k}>_{L_m}\frac{L_m}{y}\right]^2\right)-C_{m:b}\frac{dp}{dx}d_{n50}}{K_\beta \times \Delta g d_{n50}} \tag{6-3}$$

Where:

$\bar{u}$: mean flow velocity $[m/s]$;

k: turbulence kinetic energy $[m/s]$;

L_m: Bakhmetev mixing length $[m]$;

y: height above the bed $[m]$;

d_{n50}: nominal stone diameter $[m]$;

K_β: correction for the bed slope in flow direction;

α: empirical turbulence magnification factor;

$C_{m:b}$: ratio of added mass coefficient to bulk coefficient;

$\frac{dp}{dx}$: pressure gradient; an approximation of $a_x = \frac{dp}{dx}$ was used in the paper.

The computation of parameter values was based on the data collected by Jongeling et al (2003), Hoan (2008), Huijsmans (2006) and Dessens (2004), mainly focusing on stone stability. A maximal correlation was obtained for $\alpha = 3.75$ and $C_{m:b} = 23$. The suggested values will be used to derive the stability parameter in this thesis.

Base on the flow and turbulence properties that studied in chapter 4, the mixing length model used here remains Bakhmetev distribution. In order to measure the pressure gradient, the approximation of $a_x = \frac{dp}{dx}$ was applied. Thus the measuring term shifted to acceleration, therefore mean velocity along the flow direction. Table 6.3 gives a summary of the measured acceleration term for four set ups.

Table 6.3: Summary of acceleration term and mean velocity for four setups

Set up	$a[m/s^2]$
D3L45	1.79
D3L55	0.09
D4L45	1.21
D4L35	1.66

The obtained acceleration value for set up D3L55 has a large deviation from those for other three. The data could be reasonable since this is the farthest measuring point away from the sluice gate. The flow may be experiencing the transition from supercritical to subcritical, and the acceleration stops. However, the Steenstra's formula only Only applicable for advective acceleration, thus this data set will be dropped.

Giving the explicit information on flow velocity ($\bar{u}$), turbulence intensity (k), mixing length (L_m), thickness of block mat ($0.019m$), bed slope correction (horizontal bottom $K_\beta = 1$), turbulence magnification factor ($\alpha = 3.75$), added mass coefficient to bulk coefficient ratio ($C_{m:b} = 23$), and acceleration (a from Table 6.3), the derivation of stability parameter is possible. Figure 6.4 shows the value of stability parameter under various discharge for set-up D3L45, D4L45 and D4L35.

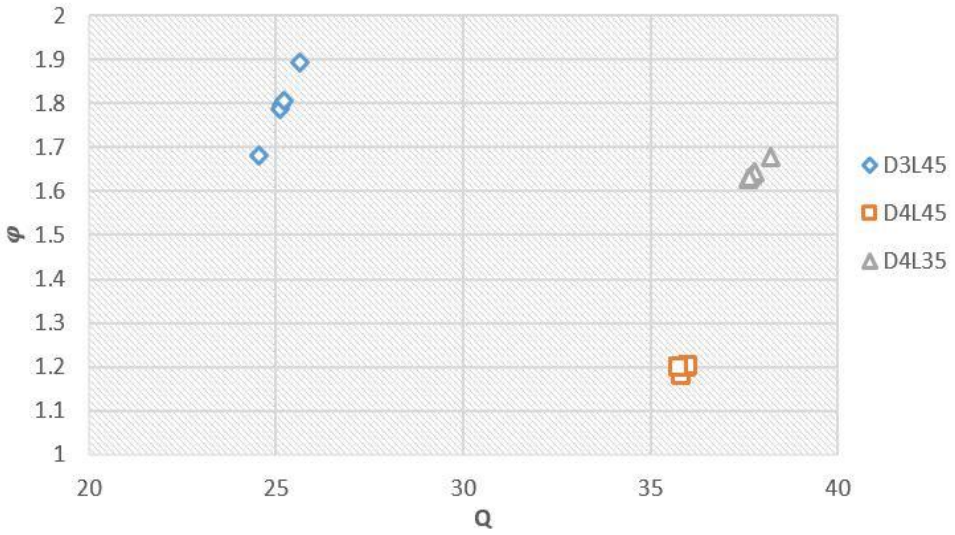

Figure 6.4: Value of stability parameter for different discharges

Note: the results are obtained from Eq. 6-3.

The value of obtained stability parameter spreads around a mean value of 1.54. A value 1.2 for stone material was suggested by Steenstra (2014). It is reasonable that a larger stability parameter for block mattress was obtained since it indicated that the block mattress is more stable than the stone type of bed protection.

The coincide of new stability formula and Steenstra (2014) formula not only verified the possibility of wider application range of Steenstra (2014) formula but also indicated that the current approach of including turbulence into Pilarczyk's formula is reasonable.

6.4 Evaluation of stability parameter

6.4.1 Comparison of stability equations

Comparing with Pilarczyk's formula

A common approach to evaluate the stone stability parameter is to compare the relationship between the stability parameter with the dimensionless entrainment rate. However, in block mattress situation, the failure happens as a snowball effect. It means that once the minor movement occurs, the whole block mattress will fail in 'snake shape', as observed by Smyrnis (2017). Hence the evaluation based entrainment rate is not valid here. Besides, the main purpose of this thesis is to optimize the Pilarczyk's formula. Therefore, a comparison between new stability formula and Pilarczyk's formula will be conducted as a reference of evaluation. Two methods to determine K_T value will be used here, the value suggested by Pilarczyk and the value proposed by Rock manual. The computed block mattress thickness under current flow conditions will be the indicator for the comparison.

Under the current flow conditions, the values for parameters in new stability formula as well as in Pilarczyk's formula are listed in Table 6.4:

Table 6.4: Summary of parameters in new stability formula and Pilarczyk's formula

Parameter	Pilarczyk	New proposed
Φ_s	0.07	0.07
φ	1 (Edges and transitions)	0.3
K_h	1	1
K_s	1	1
K_T	1.5 (increased turbulence)	-
	$\frac{1+3r}{1.3}$	
α	-	3.25

With all parameters, Figure 6.5 shows the obtained block mattress thickness by two approaches for all failure case.

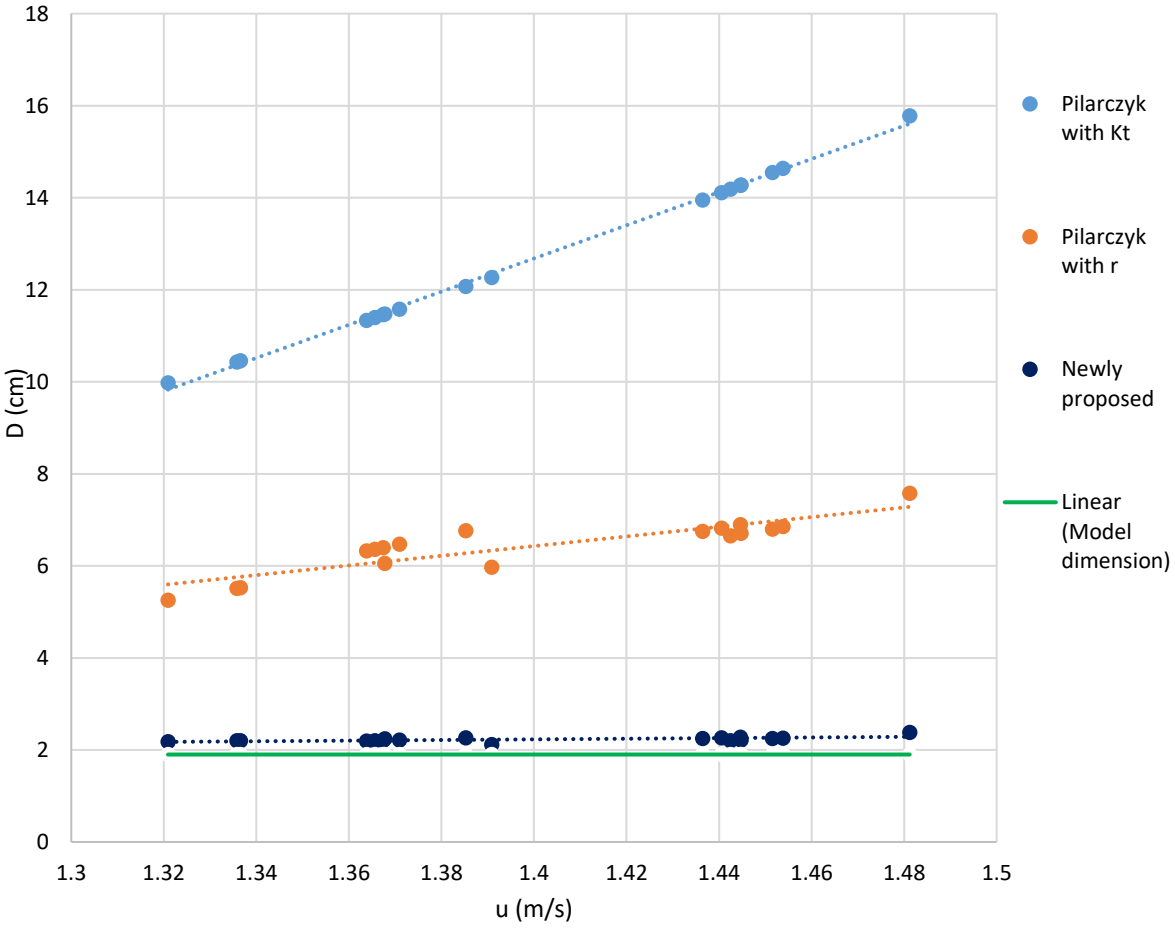

Figure 6.5: Computed block thickness by two stability formula for all failure cases, along with the real block thickness

Note that the new parameter is from Eq. 6-1.

As can be observed from above figure, the obtained block thickness values by Pilarczyk's formula deviate largely from the real dimension. The deviation is expected since Pilarrczyk

included safety coefficient into the formula. The relative turbulence intensity method gives significantly smaller scatter with model dimension, indicating this method has the ability to predict block mattress behavior more precisely. Moreover, the scatter grows with the increase of flow velocity. This means for higher flow velocity condition, the over-dimension problem will be more severe.

It is also clear that the block thickness values obtained by new stability parameter coincide well with the real dimension. However, it is not sufficient to draw the conclusion that the new formula behaves well since the stability parameter value is computed from the real dimension. For further evaluation, more data for various block mattress dimensions are required.

Comparing with Ortubay (2017)

Another set of experiment was done by Ortubay (2017) for the same purpose of present thesis. Whereas two experiments aimed at flow over different structures, weir and sluice gate. Due to different flow conditions, Ortubay gave different values on magnification factor and stability factor from the present thesis, i.e., $\alpha = 3, \varphi = 0.42$. This provides useful information for the proposal of safety factor. The detailed discussion will be presented in chapter *Discussion,* section 8.1.2.

Although two experiment tests gave different values on the parameter, the evaluations gave similar results. Figure 6.6 gives the testing results by Ortubay comparing with the original Pilarczyk's formula. The Original Pilarczyk's formula with K_T gave large scatter to model dimensions in both cases. Compare to the flow over weir structure, the flow under sluice gate has much faster velocity combining with low turbulence intensity. This resulted in large scatter of block mattress size if designing according to Pilarczyk's formula. Specifically, the designed thickness of block mattress is around 5.5 cm for weir structure, while 13cm for the sluice gate. This scatter verified the inaccuracy of Pilarczyk's formula when presenting different flow conditions. In addition, a clear shrink of scatter when using relative turbulence intensity can also be observed for both cases

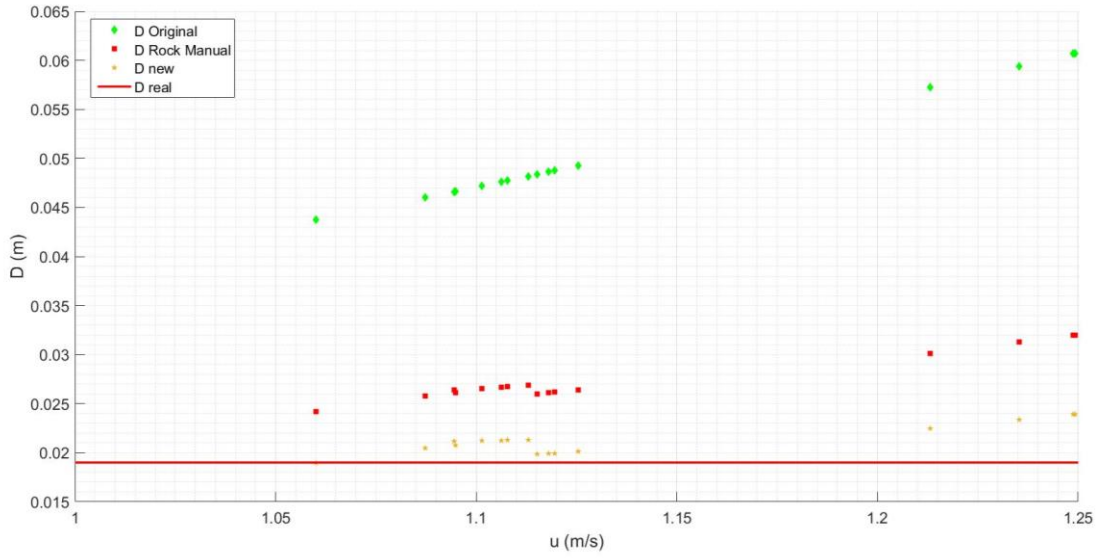

Figure 6.6: The computed block thickness by the 3 studied approaches and the real thickness for flow over weir structure, from Ortubay (2017)

6.4.2 Sensitivity analysis

For designing, it is useful to access the sensitivity of important parameters to adjust to different flow conditions. One should be aware that this is not the indicator of predicting block mattress dimensions for various flow condition, only to test the change of results with responding to the change of parameters.

The values for variants mean flow velocity $\bar{u}$, turbulence kinetic energy k, relative turbulence intensity r, Pilarczyk turbulence parameter K_T and turbulence magnification factor α will be treats in the following analysis. Reference value for each parameter was chosen as the characteristic value from the experiments, with $\bar{u} = 1.4m/s$, $k = 0.17m/s$, $r = 0.13, K_T = 1.5$.

Due to the turbulence parameter in three methods are different, the indicator T will be used for representing in general. Thus for original Pilarczyk's formula $T = K_T$, the relative turbulence intensity method $T = r$, the new approach $T = k$(turbulence kinetic energy). For analysis on flow velocity, $2u$ and $0.5u$ will be chosen as variant. Same goes for the turbulence effect analysis, $2T$ and $0.5T$ will be used. However, problems arise since doubling T maybe represent different flow conditions in three methods. For instance, increasing K_T from 1.5 to 3 means the flow conditions changes from increasing turbulence level to propeller induced turbulence level. Whereas for the other two methods, increasing r from 0.13 to 0.26 and k from 0.17m/s to 0.34m/s, may not revealing the change of flow as K_T indicated. This effect will be treated in Figure 6.8.

Parameters in newly proposed stability formula

This series of sensitivity analysis will be conducted to figure the sensitivity of important parameters in newly proposed stability formula. The results are given in Table 6.5, as well as the relative errors in Figure 6.7.

Table 6.5: Sensitive analysis on parameters in newly proposed stability formula

scenario		$\bar{u}\ (m/s)$	$\sqrt{k}\ (m/s)$	α	$D\ (cm)$	Relative error
0	(u, T, α)	1.4	0.17	3.25	2.20	-
1	$(u, 0.5T, \alpha)$	1.4	0.085	3.25	1.63	-0.26
2	$(u, 2T, \alpha)$	1.4	0.33	3.25	2.47	0.52
3	$(0.5u, T, \alpha)$	0.7	0.17	3.25	0.91	-0.63
4	$(2u, T, \alpha)$	2.8	0.17	3.25	6.54	6.19
5	$(u, T, \alpha = 3)$	1.4	0.17	3	2.12	-0.04
6	$(u, T, \alpha = 3.5)$	1.4	0.17	3.5	2.30	0.05
7	$(u, T, \alpha = 3.75)$	1.4	0.17	3.75	2.40	0.091
8	$(u, T, \alpha = 4)$	1.4	0.17	4	2.50	0.136

Note that the reference value for computing relative error is the diameter of scenario 0, with $(u, \sqrt{k}, \alpha)$.

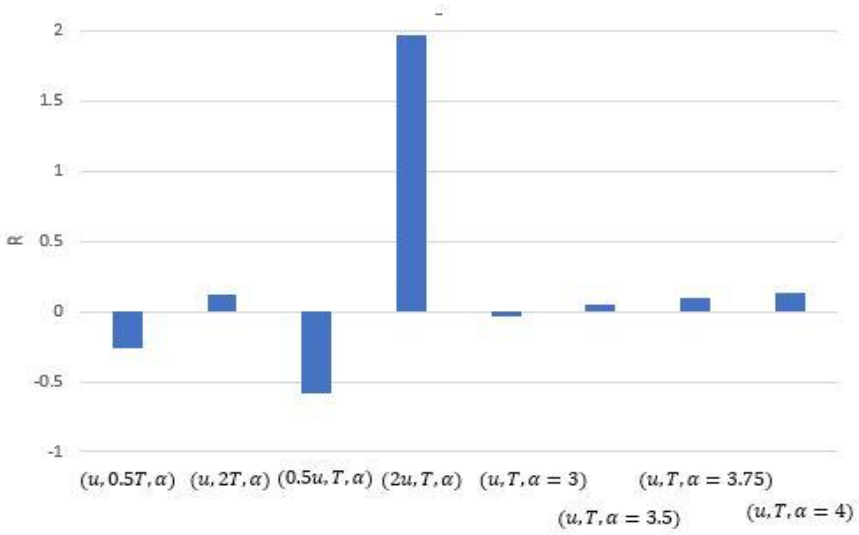

Figure 6.7: The sensitivity of three parameters with the indicator relative error

The most sensitive parameter, as can be seen from the chart, is the flow velocity. The increase of flow velocity, in comparison to the decrease, gives the largest deviation from the reference value. This is expected and can be measured accurately in practice. The influence of turbulence kinetic energy is fairly considerable, comparing to the magnification factor.

Three methods in different flow conditions

Three methods of predicting block mattress has been studied for now, the original Pilarczyk's formula with K_T, with relative turbulence intensity (r) and with turbulence kinetic energy ($u + \alpha\sqrt{k}$). As can be observed, three methods behaves differently under different flow condition. Therefore, another series of sensitive analysis will be conducted to compare these methods representing different flow conditions. Firstly, a comparison among three methods regarding the sensitivity to the change of flow conditions will be addressed, as shown in scenario 1 and 2. Next, their behaviors under two typical flow types will be studied. The flow types can be described as flow with high velocity and low turbulence (sluice gate) as scenario 3, as well as low velocity and high turbulence (reattachment point of weir) as scenario 4. The results of analysis is given in Table 6.6, as well as the relative errors in Figure 6.8.

Table 6.6: Comparison of three methods

Scenario		$D(cm)$ [K_T]	$D(cm)$ [K_T(r)]	$D(cm)$ [u + α$\sqrt{k}$]
0	u, T	12.6	6.4	2.2
1	$2u$, T	201.5	102.5	6.45
2	u, 2T	50.4	10.5	2.5
3	$2u$, 0.5T	50.4	75.8	5.5
4	$0.5u$, 2T	3.2	0.7	2.1
	Scenario	R [K_T]	R [$K_T(r)$]	R [$u + \alpha\sqrt{k}$]
0	u, T	-	-	-
1	$2u, T$	14.99	15.01	1.97
2	$u, 2T$	2.99	0.64	0.12
3	$2u$, 0.5T	2.99	10.84	1.50
4	$0.5u, 2T$	-0.75	-0.89	-0.18

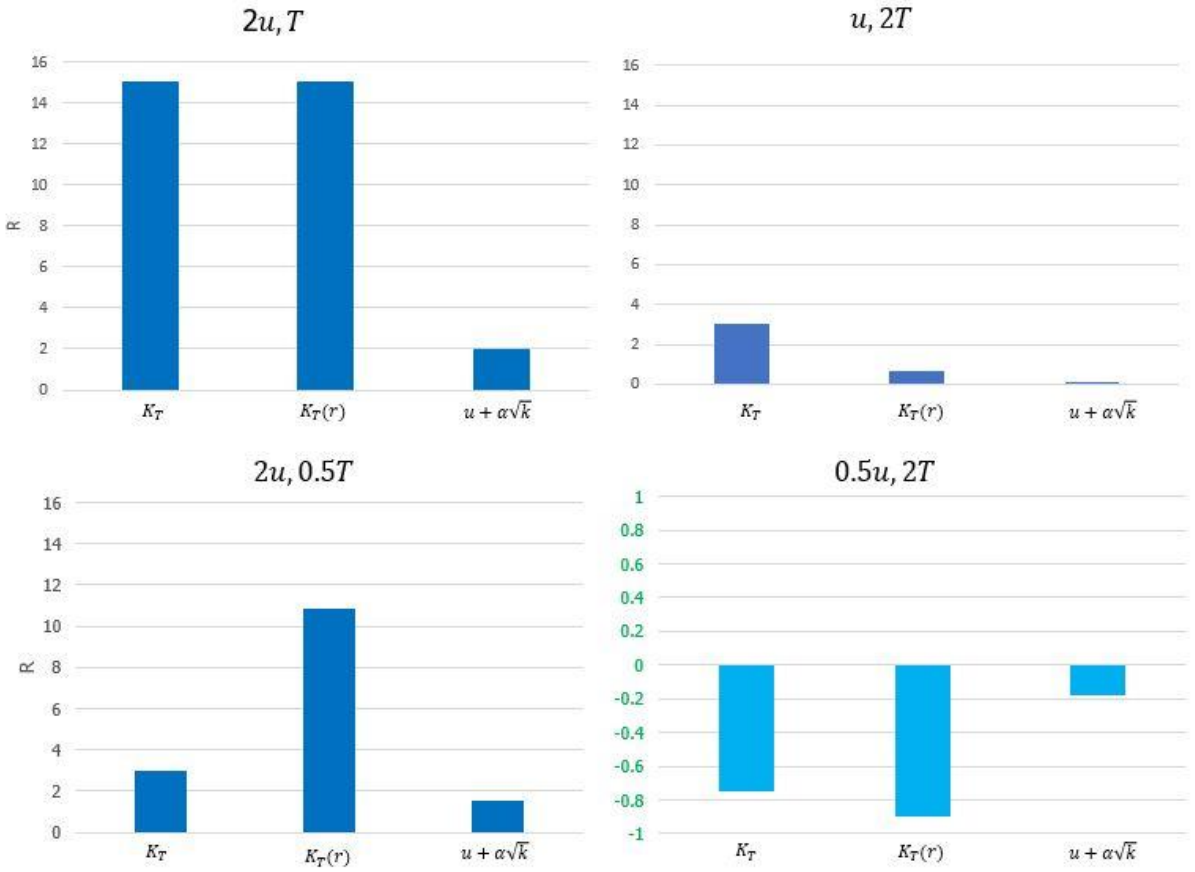

Figure 6.8: Comparison of three methods with indicator relative error

For the most sensitive parameter, flow velocity as shown in chart $(2u, k)$, the stability formula with K_T parameter gives significantly large deviation from the reference value. Whereas the kinetic energy approach is not deviating much. This result aligns with that from Figure 6.5 and 6.6, in which the design dimensions by K_T and $K_T\ (r)$ approach growing with the increase of flow velocity while the results from kinetic energy method remain stable.

For the turbulence effect, as shown in chart $(u, 2k)$, K_T shows much larger deviation than the other two methods. The influence of K_T increasing for low to high turbulence level is listed in Table 6.7. The values of K_T was chosen according to original Pilarczyk's formula.

Table 6.7: Influence of the increase of K_T

$u\ (m/s)$	K_T	$D\ (cm)$	R
1.4	1.5	12.6	-
1.4	2	22.4	0.78
1.4	2.5	36	1.86
1.4	3	50.4	3.00

The results increased by nearly 80% with K_T increases 0.5. whereas in Pilarczyk's formula, no more accurate values were given. This arises the uncertainty of predicting for block mattress.

The comparison among three methods under two typical types of flow conditions addressed in the chart $(2u, 0.5T)$ and $(0.5u, 2T)$. All three methods give same tendency of prediction, increase of design dimensions in sluice gate flow while decrease for weir flow. The difference

lies in the degree of changing. Despite the fact that K_T and $K_T(r)$ methods contain safety factor whereas kinetic energy method contains not, the extent of their deviation is still considered large. This means the safety factor embedded in the Pilarczyk's formula can be over large.

6.4.3 Evaluation of turbulence magnification factor

With the given conditions of flow characteristic and block mattress dimensions, one major determination of the accuracy of stability parameter is turbulence magnification factor α. Thus it is mandatory to evaluate the accuracy of parameter α. The turbulence magnification factor, by definition, is the value of turbulent velocity fluctuations represented by $\sqrt{k}$ relative to the mean velocity (Steenstra 2014). The present flow condition is non-uniform but steady, which allows it to be analyzed in statistical way. In statistics method, the α can be treated as the indicator of the skewness of the probabilistic density function of velocity signal. Hence by checking the velocity PDF, a rough impression of α value can be obtained. The same velocity signals for capturing the failure moment were used here. However, as illustrated in section 5.1.2, and Appendix B, the signals were interfered by bubbles. Hence manual elimination was applied. Since the flow is statistically steady, the remaining signal was considered undamaged and sufficient to represent the flow condition. Figure 6.6 gives the velocity PDFs for four set-ups.

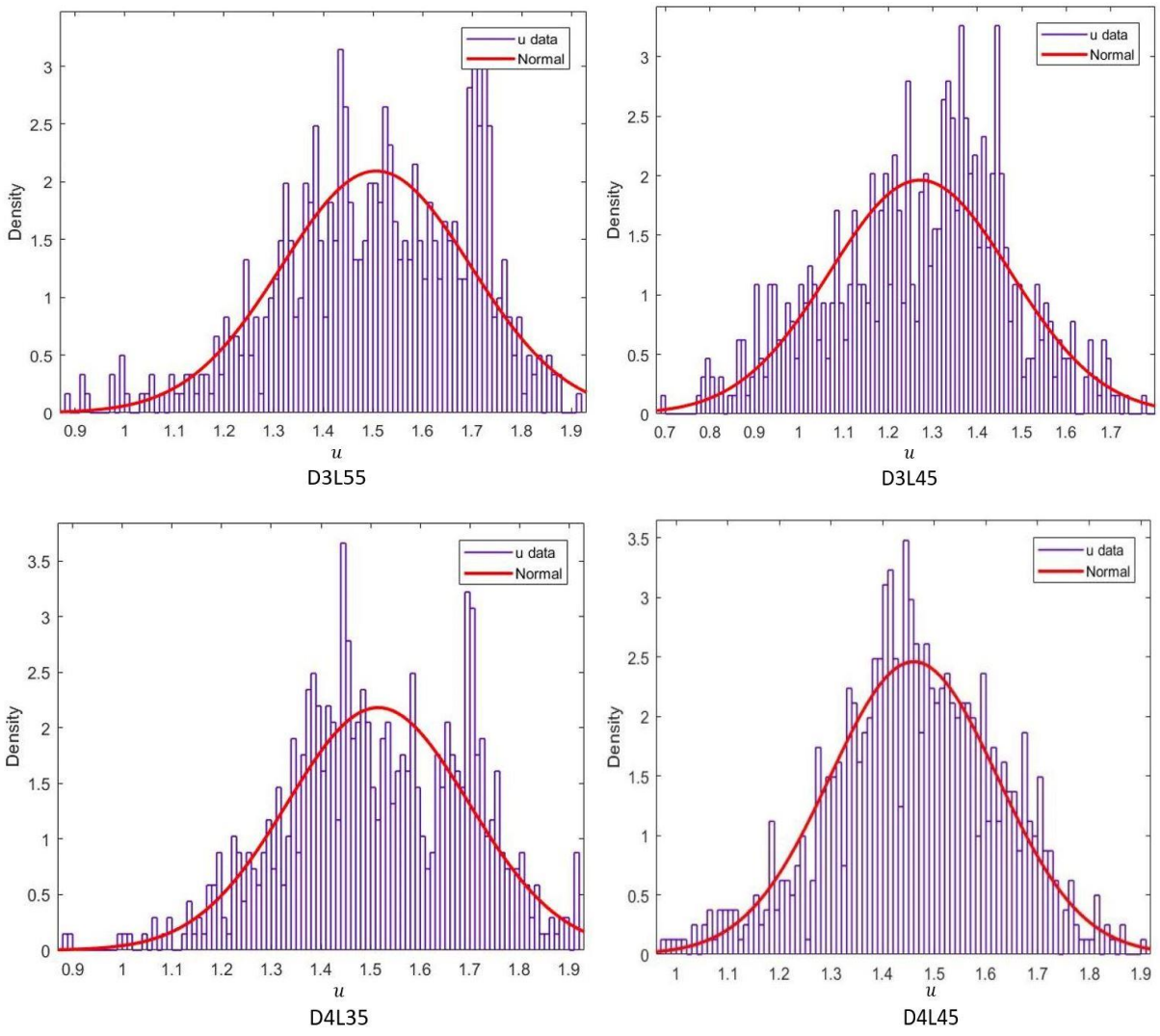

Figure 6.9: PDFs of velocity signals for four set-ups

As can be observed, clear negative skewness pattern exists for all four set-ups. The values for skewness is shown in Table 6.5.

Table 6.8: Skewness values of velocity signals for four set-ups

Set-up	skewness
D3L55	-0.48
D3L45	-0.24
D4L35	-0.23
D4L45	-0.20

The PDF is seen as a normal distribution with skewness smaller than 0.5, therefore 99.8% of the data is expected to be in the region of -3σ to 3σ (σ is the standard deviation). The α value relates to the standard deviation because it reveals the importance of the turbulent velocity fluctuations. Therefore from the velocity signal the, α value is expected to be around 3. This coincides with the previous computed value 3.25.

6.5 Concluding remarks

In this chapter, the optimization of Pilarczyk's formula in non-uniform flow was done by explicitly including the turbulence term into the formula, on the basis of the obtained data from the present experiment.

Following the path of stone stability formula development, the first step of optimization is to introduce turbulence in the form of turbulence intensity multiply by empirical magnification factor, i.e., $\alpha\sqrt{k}$. As concluded from previous chapter 5 on failure mechanism, the peak velocity was not responsible for the failure solely. Thus one can assume that under one hydraulic structure condition, for one block mattress, the failure condition should be the same for all experiments, as showed in Eqs. (6.2). By treating the α as a fitting parameter, a value of 3.25 was obtained with minimum standard deviation, as Figure 6.2. Next, the stability parameter φ was derived and a value of 0.3 was obtained deterministically. For probabilistic approach, a normal distribution with mean value of 0.27 and standard deviation of 0.02 is suggested.

The second step of representing the non-uniform flow was including the acceleration term into the formula. Steenstra (2014) proposed such a formula for the stone stability condition. Hence in this thesis, the examination of the behavior of this formula under block mattress situation was done. With all the empirical coefficient remaining the same, the obtained stability parameter had a value of 1.54. This value is considerably larger than the one for stone condition (1.2). the result was considered reasonable since the block mattress is by definition more stable than the stone type of bed protection. Base on the coinciding with the existing formula and present data, one can preliminary draw the conclusion that the current approach of representing the non-uniform flow characteristics was reliable. Moreover, the Steenstra (2014) formula can have a wider range of application, regarding representing block mattress stability.

The approach of evaluating the new stability parameter is by comparing it with the original Pilarczyk's formula. However, this evaluation cannot be completed with single block mattress model. What one can conclude from the evaluation is that the Pilarczyk's formula is on the over-safe side, meaning that the obtained block mattress size will be over-dimensioned. This information can be used for giving suggested safety factor under different flow conditions. By comparing the test results with Ortubay (2017), similar results regarding the conservation of Pilarczyk's formula with K_T. In addition, the relative turbulence intensity method narrowed the

deviation, indicating that it has the ability to represent flow conditions decently. Another indirect evaluation approach was to evaluate the empirical turbulence magnification factor (α), since with the given flow properties and block mattress dimensions, the α remained the only unknown. Due to the flow property that it is statistical steady, the α value can be seen as an indicator of the skewness of probabilistic density function of velocity signal. The obtained $\alpha = 3.25$ is considered reasonable, since it is close to standard normal distribution ($\alpha = 3$).

The sensitivity analysis shows flow velocity is the most sensitive parameter as expected, while the turbulence influence is also significant. The results were not very sensitive to α values changing. The comparison among three methods under various flow conditions gave the conclusion that the safety factor embedded in Piarczyk's formula can be over large.

7 Discussions

Following the path of study on stone stability parameters, as the first step to optimizing the Pilarcyk's formula, the combination of velocity and turbulence in a form of $(u + \alpha\sqrt{k})$ was proposed. However, as shown in Figure 6.4, a large scatter between newly proposed parameter and original Pilarczyk's formula was found. Besides, the evaluation of new parameter was also done by comparing with Steenstra (2014) formula, which included the accelerating term. A deviation was also found in this comparison. Therefore, in section 8.1, possible cause of remaining scatter will be discussed.

To preparing for introducing turbulence effect explicitly, the flow properties and possible failure mechanisms were also studied. Although as expected, the present flow condition was far from uniform, several unusual observations still worth to be discussed. this will be presented in section 8.2. when analyzing the failure mechanism for block mattress, numbers of uncertainties emerged. Thus in section 8.3, possible errors caused by those uncertainties will be illustrated.

Due to the fact that this is merely the first step attempting to include turbulence explicitly into Pilarczyk, some limitations still remain for this newly proposed formula. This will be discussed in section 8.4.

7.1 Cause of scatter

7.1.1 Scatter in stability parameter evaluation

Experimental configuration

1. Sample size
   In Jongeling et al. experiments, eight configurations were set up to collect data for the derivation of magnification factor(α). As well as in Hoan's experiment, three configurations with four measuring points for each one were conducted. Comparing the present data with previous data sets, disparity in sample size can be observed. In present experiment, four configurations with single measuring point for each one were collected. Besides, the α value is sensitive to obtained data, thus the small sample size may leads inaccuracy of α value.
2. Revealing 2D flow condition
   One major issue during the experiment was to reveal the flow condition, in reality, namely to ensure 2D flow condition. A special interface between block mattress and the still basin was used as shown in Figure 3.2. However, due to the different widths between block mattress and flume, a gap between mat and side wall still exist. This gap will induce vortex that hits the sides of block mattress, causing the instability.
3. Measurement device limitations
   The measuring by LDV device can go down to 5mm above block mattress. In current shallow water flow condition, water depth of 5.5cm to 6cm, 5mm is not negligible for some flow properties study. For instance, according to Froude number the flow is accelerating, thus typical accelerating velocity profile (as shown in Figure 2.1) is expected. However, the stretched boundary layer is missed in measure velocity profile (as shown in Figure 4.1).
4. Deviation cause by extrapolation
   During the experiment, bubble interaction was found to be severe in set-up D4L35. When collecting data for the database, flow information at the exact failure discharge could not be

obtained successfully. Therefore extrapolation was applied. However, the obtained values from linear extrapolation may have deviations from real ones.

5. Geotextile
   The geotextile using in the block mattress model was unscaled. The uncertainty of permeability and stiffness had an influence on the actual failure motion in revealing the real case. Less permeability will cause larger lift force, whereas higher stiffness will provide larger resistance. Therefore the general influence by geotextile to the failure motion is hard to determine.
6. Sudden increase in flow velocity
   During the experiments, it was found that the block mattress was highly vulnerable to the sudden increase of discharge, namely flow velocity. The controlling of discharge changing by the pump cannot be perfect, thus will influence the occurrence of failure motion. It was indeed recorded, for example unusually small corresponding discharge to the failure. But those records were considered irrelevant to stability parameter derivation.

Safety factor

As illustrated in section 6.4, Pilarczyk's formula included safety factor whereas the derived new stability parameter did not. This is the main reason that the large scatter between two stability parameters emerged. If now we also include safety factor into new stability formula and taking a new magnification factor as the method, another series and safer block mattress dimensions will be obtained. Regarding the new α value, one could use a value of mean+ 3×standard deviation as the extreme value. From the flow condition in present thesis and by Ortubay (2017), two α values were obtained for flow under sluice gate (α_s =3.25) and weir structure (α_w =3). Lacking sufficient information, a standard deviation $\sigma = \alpha_s - \alpha_w = 0.25$ is chosen. Thus the extreme α with a value of $\alpha_e = \alpha_s + 3\sigma = 4$ will be used as a safety for now. However, for more accurate information on mean and standard distribution of α value, more data on flow over different structures is needed. Figure 7.1 gives the values of computed block thickness with safety factor included.

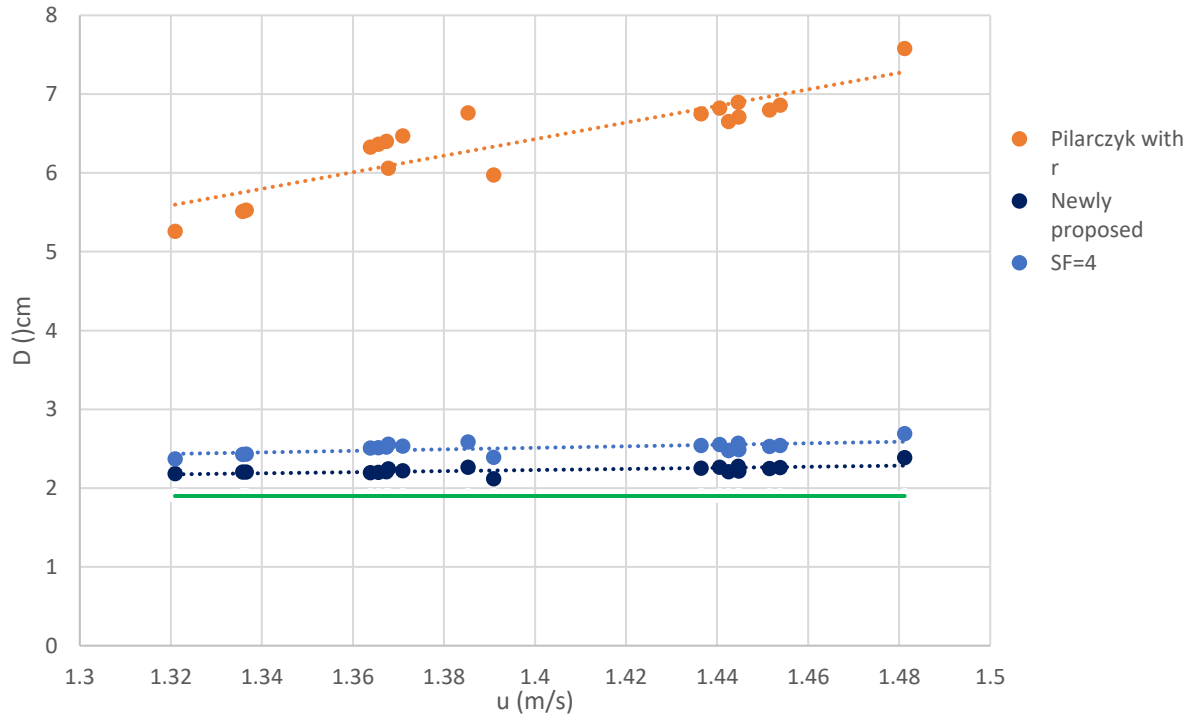

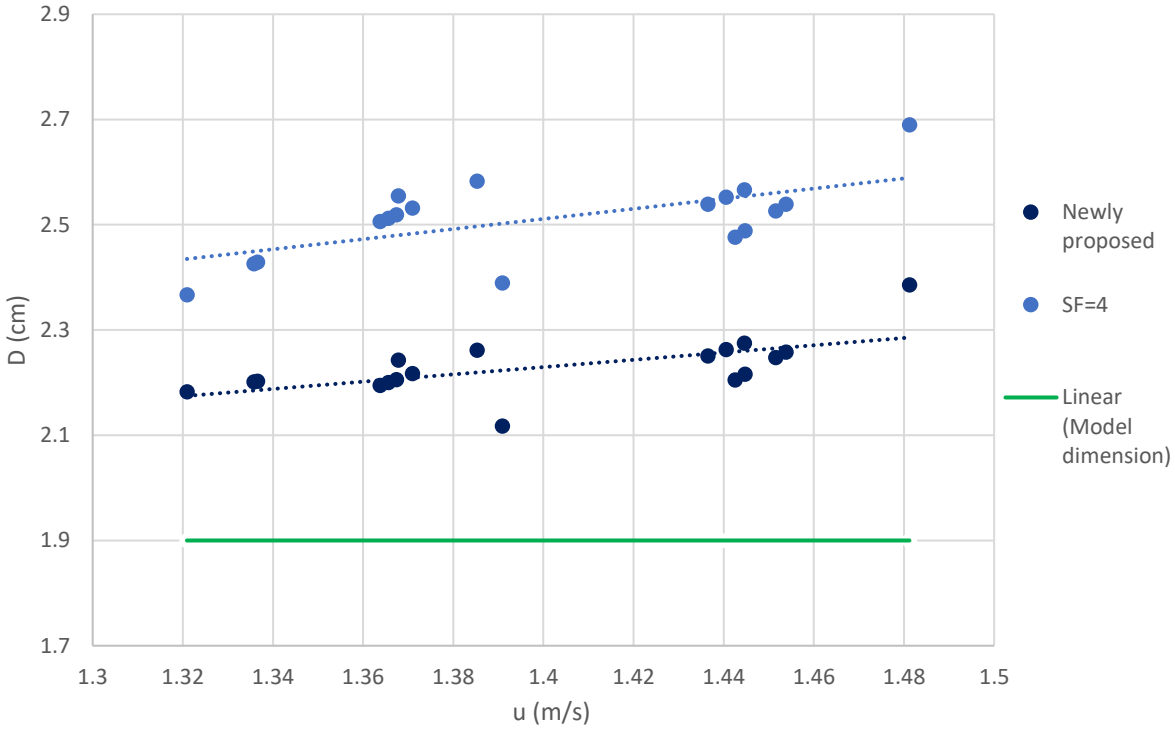

Figure 7.1: Computed block thickness by two stability formula, with SF in new formula

The above graph contains relative turbulence intensity method as a reference. The below one only shows the newly derived parameter with safety factor influence, in order to give more detailed information. The new stability parameter with safety factor increases by 25%, whereas the relative intensity method gives 1.9 times larger results.

Comparing with Steenstra (2014)

A small scatter also exist when comparing to Steenstra's formula. For stone stability, Steenstra found $\varphi = 1.2$ fitting best for the existing data sets. However, when applying this formula into present block mattress situation, φ with a value of 1.57 has been found. The possible cause of scatter is discussed as follows:

1. The acceleration term measurement
   The measurement results for acceleration term was listed in Table 6.3. One of them shows irregularity. This can be caused by experimental errors. While this data set was not included in the evaluation of Steenstra's formula also due to the limitation of the formula itself. It is only applicable for advective acceleration.
2. $C_{m:b}$ value
   Another limitation for Steenstra's formula is that it can only be applied for the condition when $C_{m:b}$ is known. However, the value is not explicit for block mattress, since there is not enough data to derive it. Currently, values for stone was used only to give an impression on the formula behaviour. For more detailed and precise evaluation, more data on block mattress is needed.
3. Magnification factor α value
   A value of 3.75 was used when applying Steenstra's formula for block mattress situation, whereas this value was derived for stone stability. This resulted in a difference of stability parameter. Now if the value for block mattress is used as 3.25, the gap shrinks. Table 7.1 shows the stability parameters with different α values.

Table 7.1: Stability parameters with different α values

	α	$C_{m:b}$	φ
Stone	3.75	23	1.2
Block mattress	3.75	23	1.57
	3.25	23	1.42

7.1.2 Scatter in flow characteristics study

1. Water level local fluctuation
   Among all the measuring devices, the accuracy of LDV is high enough for the current experiment. However, the water depth measurement done by a ruler is not accurate enough. Moreover, the water surface jumped making the accuracy even worse. This has an impact on the Reynolds shear velocity derivation using equivalent roughness method.
2. Deviation cause by extrapolation
   In chapter flow characteristics, the calibration of shear velocity was done by Reynolds shear stress method and TKE method. Both of them was established for fully developed flow, as well as using extrapolation to obtain the flow information at the bottom. Whereas in current flow condition (undeveloped), the boundary layer could be different than the fully developed flow. Thus this deviation may cause uncertainty of the calibration.
3. Measuring errors
   This may have an obvious impact on the study of flow characteristics. The water depth under current flow condition is very small, thus small inaccuracy when moving the measuring point through the water body vertically will cause deviation of velocity profiles.

7.2 Uncertainties in failure mechanism analysis

7.2.1 Force analysis

When conducting force analysis for block mattress, several uncertainties showed up that may have an impact.

1 The force coefficient, i.e., C_L and C_m, was valued roughly. Lacking sufficient information, the average value was chosen according to the suggested range. However, from literature study, for different stone types and different placement, different values were used. Thus it is reasonable to question the used value here.

2 The geotextile induced steady force was not taken into account quantitatively. This made it hard to distinguish the critical failure condition, especially for the initial motion analysis

3 The individuality of four blocks in the last row.
The four blocks in the last row move individually. Frequently, the ones on two sides of block mattress were lifted first, providing drag force to those two in the center, as shown in Figure 7.2. However, only the single-measuring-point measurement was used in this experiment, and it focused on the block in the middle. Therefore, the information is not enough to evaluate the force terms by neighboring blocks. This will leads inaccuracy for force analysis.

4 Bed material induced friction. When flow exerts drag force on block mattress, the geotextile will also receive friction caused by the bed. In this experiment, middle-sized gravel was chosen for the bed material lacking sufficient information. However, the friction force will be different for different type of bed, thus leading different critical flow conditions.

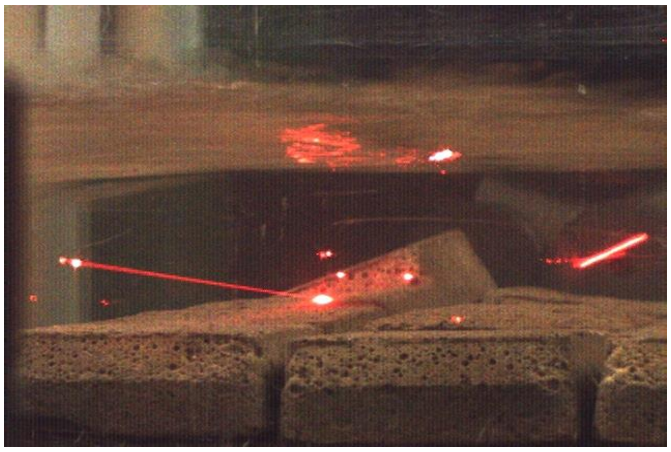

Figure 7.2: Individuality of four blocks in the last row of the mattress

7.2.2 Placement of block mattress

The placement of block mattress was observed to be essential for the failure occurrence during the present experiment. This was also concluded by Van Velzen and De Jong (2015) studying the block mattress behaviors under propeller-induced load. In this case, the placement played a role when some middle blocks were lifted earlier than the edge blocks. When it happened, the edge blocks failed at much lower discharge. It can be explained that the flow was modified by uplifted middle blocks. More turbulence was induced as well, leading the low failure discharge.

7.3 Limitations

1 Uncertainties on presenting different flow conditions.
In this thesis, only flow under sluice gate was studied. As to be expected, flow properties vary for those over different hydraulic structures. When comparing the results for flow over weir structure, different values for magnification factor and stability parameter was found already. Therefore, it is reasonable to believe that there will not be a single value to present all types of flow conditions.

2 Scaling effect
In the current experiment, only the model of block mattress was used. The scaling from prototype to model was done by Van Velzen and De Jong (2015), aiming at the block mattress behavior under propeller flow. At the experiment stage, the dimensions of block mattress have little to do with flow properties, thus it is reasonable to use the same model for the two experiments. However, as mentioned by Van Velzen and De Jong, the existing problem of scaling mainly lies in the geotextile, specifically the stiffness and permeability. Those two properties of geotextile have considerable influence on the block mattress behavior. For instance, the force provided by geotextile contributing to stability is related to its stiffness, and the lift force by flow associated to permeability. Without scaling down these two factors, the failure mechanism study is fairly influenced.

7.4 Practical application

Comparing the outputs new approach and Pilarczyk's formula, a smaller scatter for new approach presented. It is less conservative and gives smaller design dimensions, thus being economical and easy to produce and construct.

Another major advantage of the present approach is the feasibility under various flow conditions. As illustrated in the objective, this thesis is the first step to presenting various flow

conditions in a more certain way. Thus only one suggested value for turbulence magnification factor (α) and stability factor (φ) was obtained so far. By combining with the work done by Ortubay (2017) for flow over weir structure and following studies for other typical hydraulic conditions, a series of α and φ values can be obtained. The expected outcomes is shown as follows:

	Hydraulic condition	α	φ
1	Sluice gate	3.25	0.3
2	Weir	3	0.4
3	Condition 3	α_3	φ_3
…	…	…	…
n	Condition n	α_n	φ_n

Together with the turbulence kinetic energy, this table gives sufficient information on flow properties to predict the block mattress behavior with more certainty. From the previous sensitivity analysis (6.4.2), the most sensitive parameter is flow velocity following by turbulence kinetic energy. The obtaining of these two parameters is fairly simple and can be accurate, using field measuring and numerical model.

Moreover, the full collection of α and φ values also provides information for probabilistic design approach. With sufficient data, a probabilistic density function can be obtained. Although the α is not very sensitive to the flow condition, additional information for designing under unusual hydraulic conditions is still helpful. To achieve this, a method of applying extreme values as safety factors can be used.

8 Conclusions and recommendations

The stability of block mattress under non-uniform form was studied in this thesis. In this flow regime, the turbulence effect is of importance. From the literature study, fundamental research was done for the stone stability. However, regarding the interaction between flow and block mattress, most of the research still stays at the stage of observation instead of studying the flow force quantitatively. Moreover, the available formula was also developed adequately for uniform flow condition and only partly applicable for the non-uniform condition. For instance, the turbulence factor suggested by Pilarczyk can only be treated as a rule-of-thumb. To optimize Pilarczyk's formula, sufficient data is required. However, presently only very few experiments have been done aiming at the block mattress stability. Therefore, based on this situation, this thesis started with following research questions, as suggested in the first chapter:

Q1: What are the forces that exerted on the block mattress by the flow?

c. What are the flow properties in the current situation?
d. What flow structures exert forces on block mattress?

Q2: What is the responsible flow structure for the failure mechanism?

Q3: What are the forces can be expressed by the stability formula?

Q4: What is the most reasonable way to express the turbulence effect?

Q5: What data is needed from the experiments?

d. How many experimental set-up are needed?

e. How many failure cases is considered sufficient?
f. Which locations will be targeted for measuring?

Q6: How to derive required parameters with obtained data?

Q7: How well is the new stability parameter behave?

In this chapter, all the research questions will be conclusively answered in section 8.1. Next in section 8.2, recommendations for further research will be given.

8.1 Conclusions

8.1.1 What are the forces that exerted on the block mattress by the flow?

a. What are the flow properties in the current situation?

The flow in the current situation is fairly fierce, namely it is neither uniform nor fully-developed. Nevertheless, similarities were still found comparing to standard open channel flow. First of all, the logarithmic profile was found in the wall region, as well as the wake-log law in the outer region. Secondly, a calibration was done to shear velocity and equivalent roughness. It was found that the Reynolds shear stress method is more accurate for determining the shear velocity. Besides, the obtained equivalent roughness is larger than the suggested value by Pilarczyk. Moreover, a growing pattern of mixing length was found in the flow direction region. Bakhmetev mixing length model was found valid in the further downstream region.

b. What flow structures exert what forces on block mattress?

All the flow properties can be related to two velocity compositions, the mean and the fluctuation part. Therefore, all the forces exerted on the block mattress are also associated with theses two parts. In a nutshell, the mean flow velocity is responsible for mean quasi-steady force, namely mean drag force and mean lift force. The fluctuation part is account for the fluctuated quasi-steady force, meaning the fluctuated drag and lift force. The spatial change of mean velocity, i.e. steady acceleration, exert dynamic drag force.

8.1.2 What is the responsible flow structure for the failure mechanism?

Regarding the failure mechanism study, firstly, the failure was observed always happening to the last row of block mattress, so-called open edge. By synchronizing the failure images and velocity signals, a pattern of responsible flow structure was observed. A sudden increase of flow velocity following by a peak of shear stress always showed around the initial uplifting moment. Next, force analysis was conducted and showed that larger scale flow structures, i.e., pressure gradient, time-dependent acceleration, can be more responsible in comparison to small-scale flow structure (turbulence). Moreover, the backward facing step was also found can be account for the occurrence of initial exposure. In the period from initial motion to actual failure moment, larger scale flow structure (Bernoulli effect) was also found responsible. Quadrant analysis is not applicable in the current situation since the block motion is large enough to modify the flow properties.

8.1.3 What are the forces can be expressed by the stability formula?

The original Plarczyk's formula included mean quasi-steady force explicitly, in the term of u_{cr}^2. The fluctuating quasi-steady force was induced empirically, using parameter K_T. Rock manual proposed new form of K_T related to relative turbulence intensity. However this one still remain empirical, since the explicit expression should be in the form of squared velocity. Jongeling included full term of quasi-steady force, including mean and fluctuating part, in the term of

$(\bar{u}+\sqrt{k})^2$. The turbulence was expressed by turbulence kinetic energy. Later Steenstra included steady acceleration induced pressure gradient force , using $a \approx dp/dx$. The newly derived parameter followed the path of Jongeling, including the full quasi-steady force into Pilarczyk's formula. For now, no pressure gradient force was taken into account in the new parameter.

8.1.4 What is the most reasonable way to express the turbulence effect?

From the literature and failure mechanism study, it is concluded that the turbulence is of crucial importance to block mattress behavior. However, one major drawback of Pilarczyk's formula is that it fails to represent the flow condition with high turbulence but very slow flow velocity, for instance at the reattachment point downstream of weir-like structures. Besides, for the flow with high velocity but low turbulence, the Pilarczyk's formula tends to give over-dimensional results. Thus it is reasonable to separate the flow velocity and turbulence. From literature review and following the path of the development of stone stability formula, it is concluded that the combination $(\bar{u}+\alpha\sqrt{k})$ is the most accurate method to express turbulence effect. Therefore, in this thesis, the proposed stability formula is given as:

$$\Delta D = \frac{\varphi \times 0.035 \times (\bar{u}+\alpha\sqrt{k})^2 \times K_h}{\Phi_s \times 2g \times K_s}$$

With $\alpha = 3.25, \varphi = 0.3$.

The advantage of this approach can be summarized as follows: Firstly, it is able to predict the block mattress under various flow conditions more certainly. More specifically, the reattachment point with high turbulence and low flow velocity can be represented as well now, as well as the flow under sluice gate with high velocity and low turbulence. Secondly, the possibility of applying probabilistic approach on α will give more feasibility to adjust the block mattress dimensions under practical situations.

One disadvantage of this approach is that the turbulence kinetic energy needs to be obtained by simulation using numerical models. Whereas this can be done by

8.1.5 What data is needed from the experiments?

An experiment was done to collect data for the derivation of turbulence magnification factor and stability parameter, as well as to study the failure mechanisms and flow properties over under the sluice gate. Data of velocity signals and the precise failure moments synchronized with velocity were required. The main information needed from data was the mean and fluctuation compositions of velocity, corresponding to the exact failure moments.

To obtain this, four experiment set-ups were built and 18 failure cases were recorded. The set-ups of configuration were based on the feasibility of flume and the quality of velocity signals. Since the failure always occurred to the last row of block mattress during the experiments, the main target was set to be the last row of block mattress. For the purpose of deriving stability parameter, the measuring points were set to be as close as possible above the block mattress for data collection. For investigating the failure mechanism, flow conditions over the last row of block mattress needed to be studied. Thus measuring points were spread around the last row block.

8.1.6 How to derive required parameters with obtained data?

Based on the failure mechanism studying, the maximum of flow velocity was found cannot cause the failure solely. Thus the derivation of magnification value was based on the assumption that under one hydraulic structure condition, for one block mattress, the failure condition should be the same for all experiments. A value of 3.25 was found giving the best fit of obtained data. As for the stability parameter, with single block mattress given, a value of 0.3 was obtained deterministically. For probabilistic approach, a normal distribution with a mean value of 0.27 and standard deviation of 0.02 is suggested.

8.1.7 How well is the new stability parameter behave?

The evaluation of new stability parameter was done by comparing it with the original Pilarczyk's formula. However, this evaluation cannot be completed with single block mattress model. By combining the tests results from Orbutay (2017), one can conclude that the Pilarczyk's formula tends to give over-dimensional results. Besides, the optimization on original Pilarczyk's formula by relative turbulence intensity method behaves better for the flow with low velocity and high turbulence.

An application of stone stability formula including acceleration factor was also conducted in this thesis. Within the application range, i.e., only advective acceleration and given $C_{m:b}$, cooperating with obtained α value from this thesis, a stability parameter of 1.42 was found for block mattress. This value is considerably larger than the one for stone condition (1.2), since the block mattress is by definition more stable than the stone type of bed protection. The coincide of new stability formula and Steenstra (2014) formula not only indicated that the current approach of including turbulence into Pilarczyk's formula is reasonable, but also verified the possibility of wider application range of Steenstra (2014) formula.

8.2 Recommendations

Experiments on different block mattress dimensions

The evaluation of newly proposed stability parameter cannot be completed with single block mattress model. Therefore, other sets of models are needed. Since the relative density (Δ) and block thickness (D) are always coupled in the formula, either one of those can be chosen to change. The

Determine α value for different type of hydraulic conditions

Flow properties are expected to vary for different structures. Thus related α value needs to be checked for a larger range of flow conditions. By doing so, a distribution of α value can be obtained. It will provide more solid information on the choice of safety factor, as shown in section 8.1.2.

Experiments on the effect of bed roughness

During the experiment, the block mattress was found rather stable after the defined failure moment. Thus a gap between this failure moment and washing away failure, as observed by Smyrnis (2016), exists. In this process, another significant resistant force was provided bed material, i.e., the bed friction. For engineering design, it is relevant to know to what extent the block mattress will be washed away completely. Thus an experiment aiming at the bed roughness influence is suggested. Limited by the capacity of the flume in this experiment, no washing-away failure pattern happened. Thus flume with a larger capacity is preferred for later experiments.

Correction coefficient of acceleration term for newly proposed stability parameter

As an engineering approach, a formula with parameters easy to determine is optimal. In this regard, the newly proposed formula has two unknowns, i.e., mean velocity and turbulence intensity, to be determined. Whereas, in Steenstra's formula, additional mixing length distribution and acceleration term are also needed. In which the mixing length is not an easy term to find. Therefore, a combination of two formula is preferable. To do so, a correction coefficient for stability parameter is proposed. By applying Steenstra's formula and the formula proposed by this thesis to various flow conditions, two sets of stability parameters can be obtained. If a relation between two sets of parameters can be found, the correction coefficient for acceleration is obtained.

For decelerating flow condition

The limitation of Steenstra's formula showed up when applying for decelerating flow. However, for the flow under sluice gate, deceleration is a mandatory stage before the hydraulic jump. This is exactly the position where the bed protection applied. Therefore, it is preferable to collect data for this flow stage.

Influence of time-dependent acceleration

During the experiments, the block mattress showed vulnerability to the sudden increase discharge. It indicated that the time-dependent acceleration is of importance here. Besides, the dynamic drag force, which is considerably large among all force terms, also depends on this acceleration term. Thus to make the formula more general, this term should be included.

Reference

Arrieta Ortubay, Xabi. (2017). *Stability of block mattresses under non-uniform flow*. M.S. Thesis, Delft University of Technology.

B. Rodriguez & C. Escauriaza (2010). *Turbulent Flow in the Scour Hole Downstream of a Sluice Gate*: *Erosion induced by Görtler Vortices.* River Flow 2010 - Dittrich, Koll, Aberle & Geisenhainer (eds)

Coles, D. (1956). *The law of the wake in turbulent boundary layers*. J. Fluid Mech., 1:191-226.

G.J. Schiereck, H.J. Verhagen. *Introduction to bed, bank and shore protection.* Delft University of Technology.

Goldbold, J. (2014). *Stability design for concrete mattresses*. In Twenty-fourth (2014) International Ocean and Polar Engineering Conference, pages 302-308, Busan, Korea. Int. Society of Offshore and Polar Engineers.

G. van Velzen and M.P.C. de Jong (2015) *Stability of a block mattress in propeller-induced loads.* Deltares.

Einstein, H. and El-Samni, E. (1949). Hydrodynamics forces on a rough wall. *Reviews of Modern Physics*, 21(3): 520-524. In (Uitteenbogaard, R., Hoffmans, G. and Akkerman, G. 1999).

Ehab A. Meselhe, M.ASCE; and Kirby Hebert (2007). *Laboratory Measurements of Flow through Culverts*.

Hoan, N. T. (2008). Stone stability under non-uniform flow. *Ph.D. thesis*. Delft University of Techonology.

Hoan, N.T., Stive, M.J.F., Booij, R., Verhagen, H.J. (2011). *Stone stability in non-uniform flow*. Journal Hydraulic Engineering.

Hofland, B (2005). Rock and Roll: *turbulence-induced damage to granular bed protections.* Ph.D. thesis, Delft University of Technology

Huijsmans, M. A. (2006). *The influence of flow acceleration on the stability of stones*. Master's thesis, Delft University of Technology.

Izbash, S. V. (1935). *Constructions of dams by dumping of stone in running water*. Moscow, Leningrad.

Jongeling, T. H. G., Blom, A., Jagers, H. R. A., Stolker, C., and Verheij, H. J. (2003). *Design method granular protections*. Technical report, WL|Delft Hydraulics. In Dutch.

Keulegan, G. H. (1938). *Laws of turbulent flows in open channel flow*. Journal of Research of the National Bureau of Standards, 21:707-741.

Kim, J., Moin, P. and Moser, R. (1987). *Turbulence statistics in fully developed channel flow at low Reynolds number*. Journal of Fluid Mechanics, 177(-1), p.133.

Nezu, I. and Nakagawa, H. (1993). *Turbulence in Open-Channel flows. Balkema Rotterdam*. In (Hofland 2005)

Nezu, I. (2005). *Open-channel flow turbulence and its research prospect in the 21st century*. J. Hydraull. Eng, 131:229246.

Nikuradse, J. (1933). Strömungsgesetze in rauhen rohren. Forschungsheft 361, Verein Deutscher Ingenieure.

Pilarczyk, K. (2000). *Geosynthetics and geosystems in hydraulic and coastal engineering*. 1st ed. Rotterdam: A.A. Balkema.

Pilarczyk, K. (2001) *Unification of stability formulae for revertments*. In Porg. XXIX IAHR congress, Beijing

Pilarczyk, K.W. (2003). *Design of revetments*. Rijkswaterstaat, DWW.

Qingfu, X. and Zhiping, L. (2012). *Study on Flow Reattachment Length. Procedia Engineering*, 28, pp.527-533.

Raupach, R. M. (1981). *Conditional statistics of reynolds stress in rough-wall and smooth-wall turbulent boundary layers*. Journal of Fluid Mechanics, 108:363382.

Reynolds, O. (1883). *An experimental investigation of the circumstances which determine whether the motion of water in parallel channels shall be direct or sinuous and of the law of resistance in parallel channels*. Philos. Trans. R. Soc, 174:935U82.

Schiereck, G.J. updated by Verhagen, H.J. (2012). *Introduction to Bed, bank and shore protection*. VSSD.

Shields, A. (1936) Anwendung der Aehnlichleitsmechanik und der Turbulenz-forschung auf die Geschiebebewegung. Mitteilungen der Preussischen Versuchsanstalt fur Wasserbau und Schiffbau, Helft 26, Berlin. In German. In (Hoan, 2008)

Smyrnis, A. *Stability of block mats under flow conditions* M.Sc. thesis, Delft University of Technology.

Steenstra, R.S. (2014). *Incorporation of the effects of accelerating flow in the design of granular bed protections*. M.S. Thesis, Delft University of Technology.

Tennekes, H. and Lumley, J. L. (1972). *A First Course in Turbulence*.

The National Concrete Masonry Association (2010) *DESIGN MANUAL FOR ARTICULATING CONCRETE BLOCK (ACB) REVETMENT SYSTEMS*

Uijttewaal, W. S. J. (2011). *Turbulence in Hydraulics*. TU Delft, Delft.

Appendix A: Velocity signals interfered by bubbles.

The bubble interference can be diagnosed when the velocity signal suddenly drop to $u = 0$. It is due to the blockage of bubble body when it passing by, hence the loss of the velocity signals.

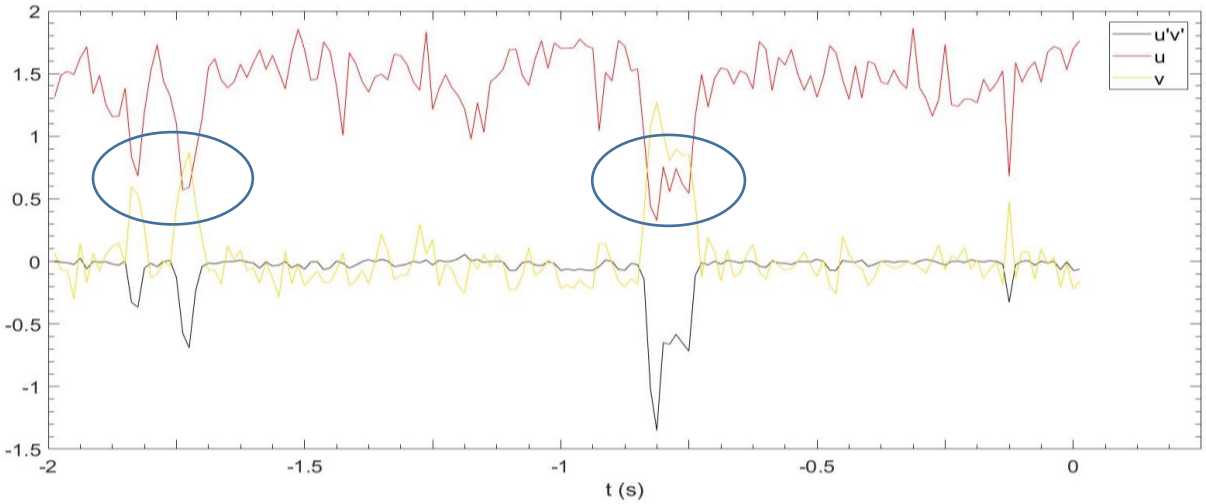

D3L55 F1

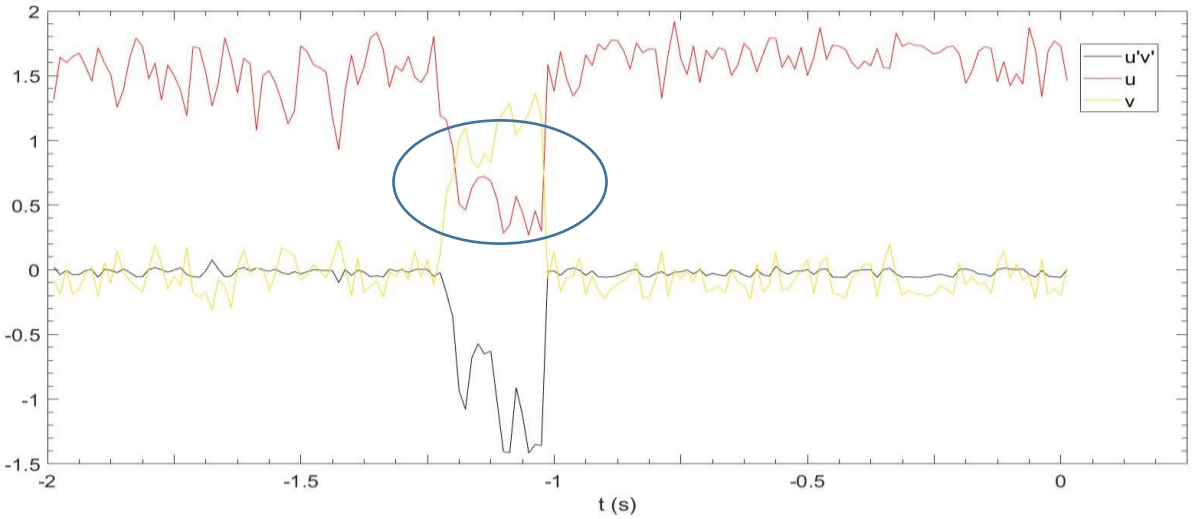

D3L55 F4

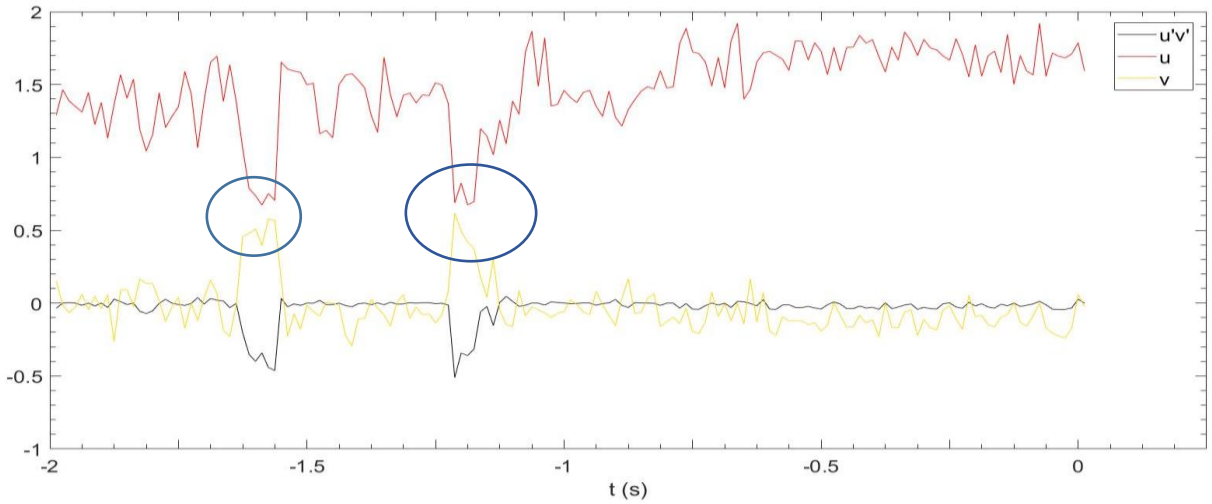

D4L35 F1

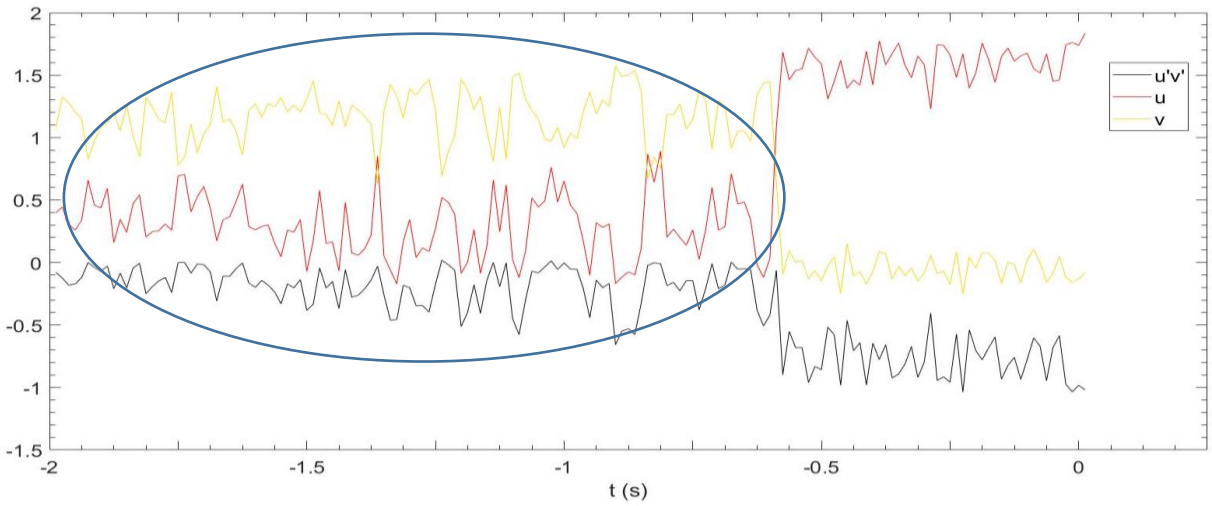

D4L35 F5

Note: the interfered part of velocity signal was marked by ellipse.

Appendix B: Velocity signals for all failure cases with actual failure moment at t=0.

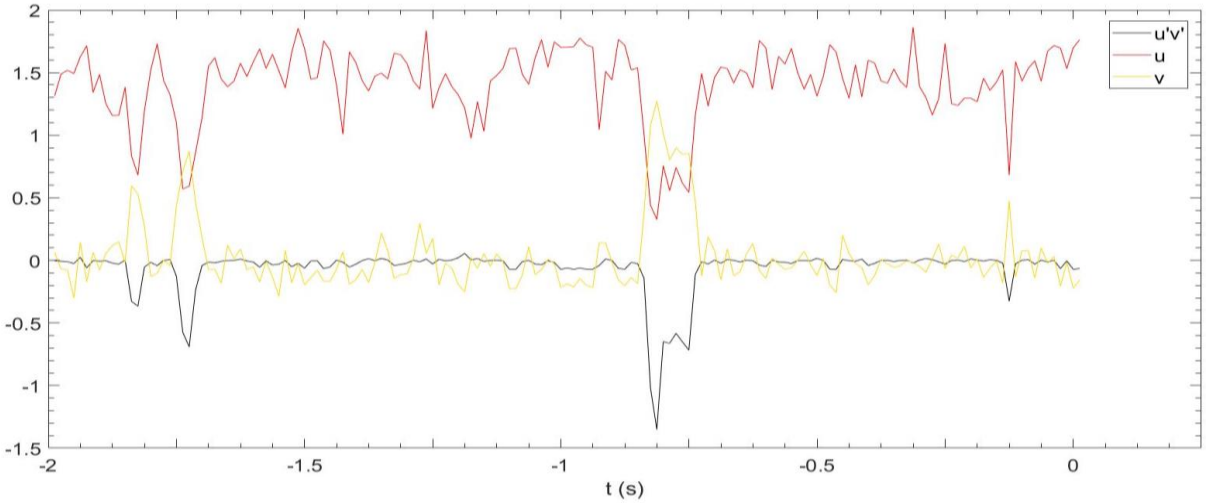

D3L55 F1

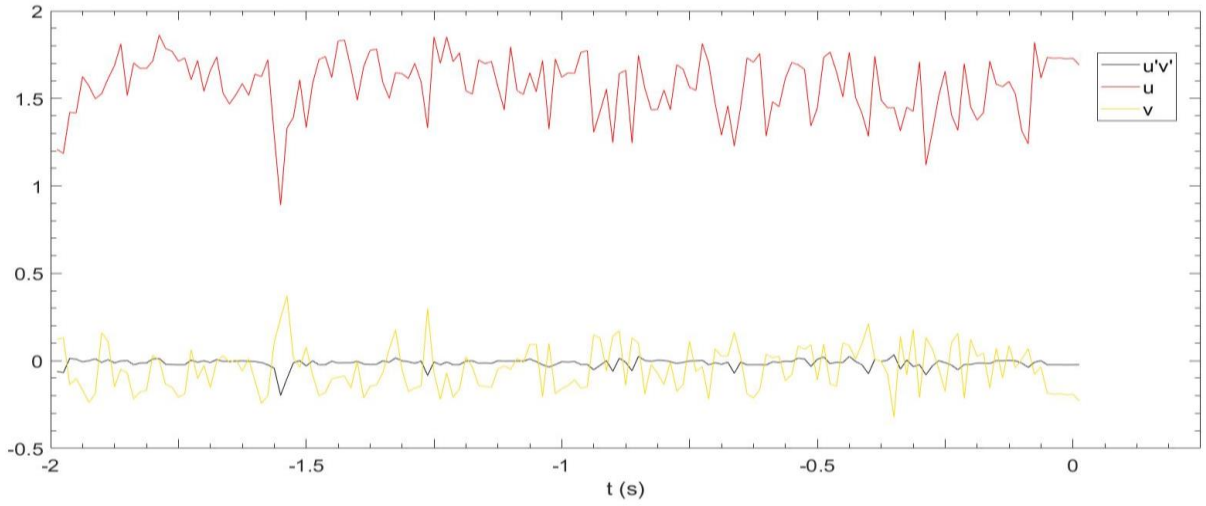

D3L55 F2

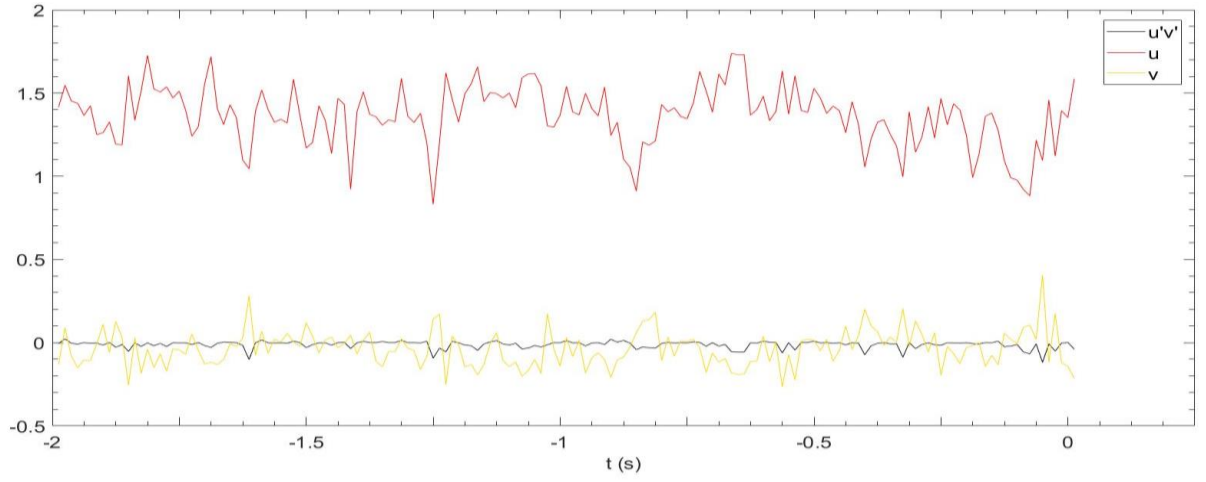

D3L55 F3

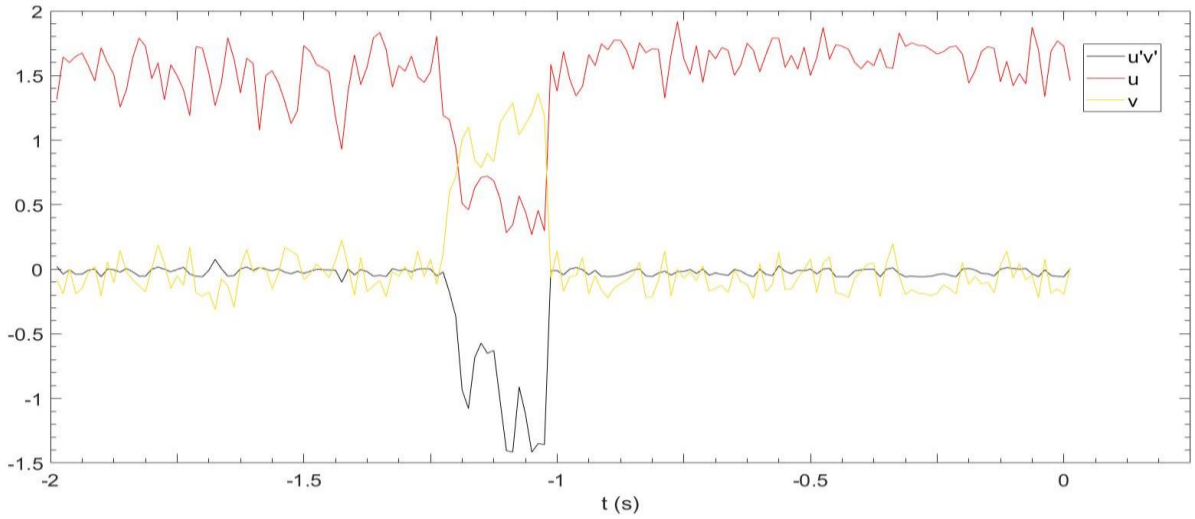

D3L55 F4

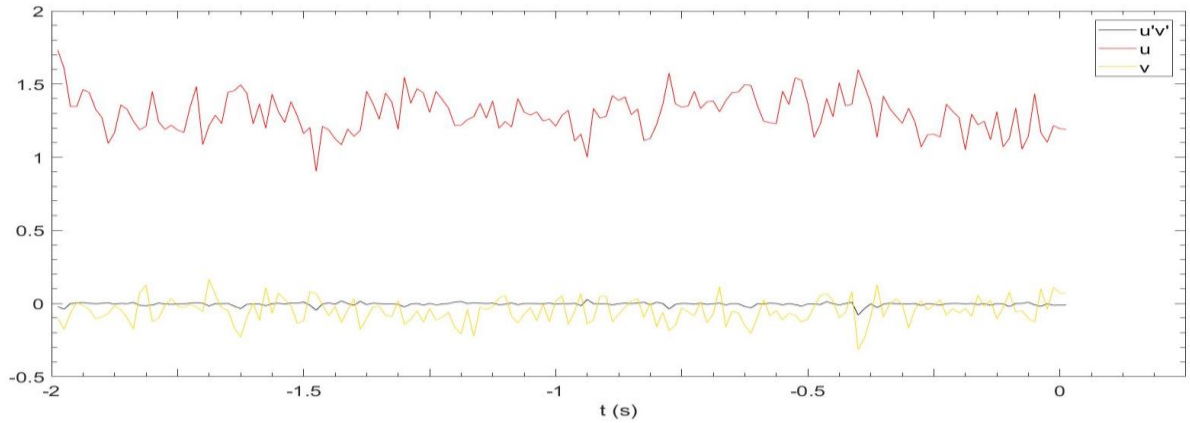

D3L45 F1

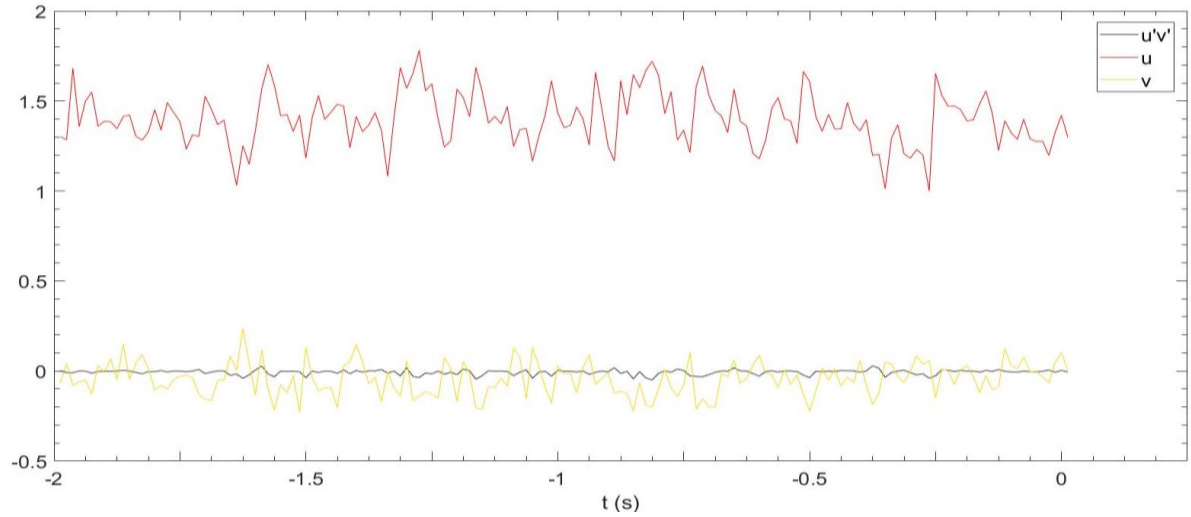

D3L45 F2

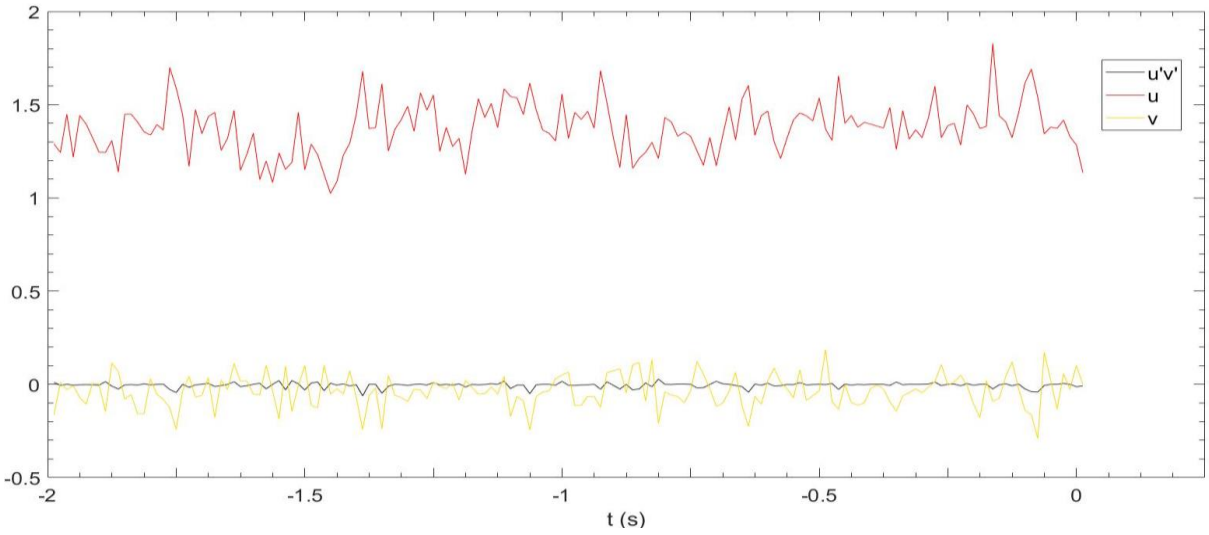

D3L45 F3

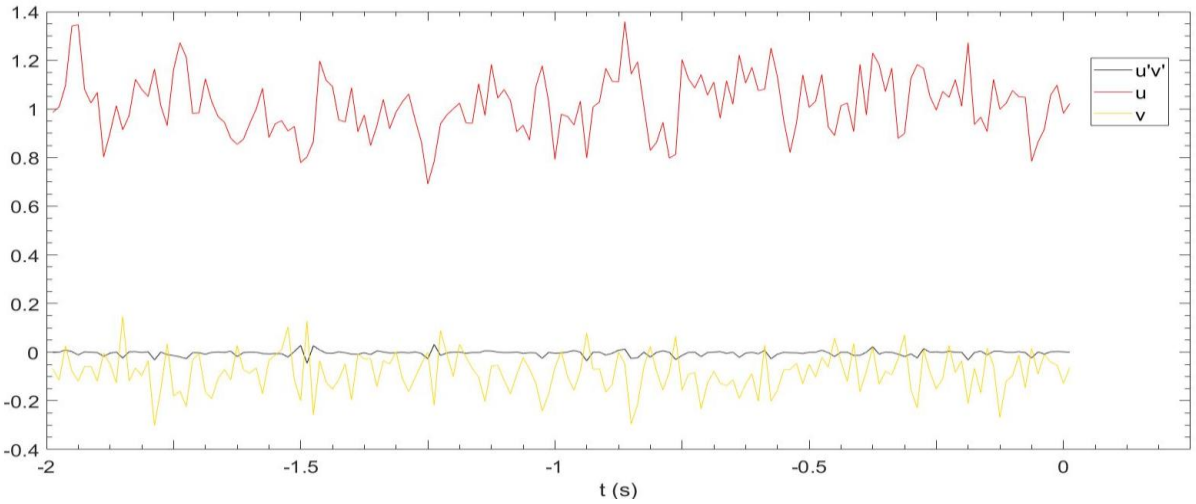

D3L45 F4

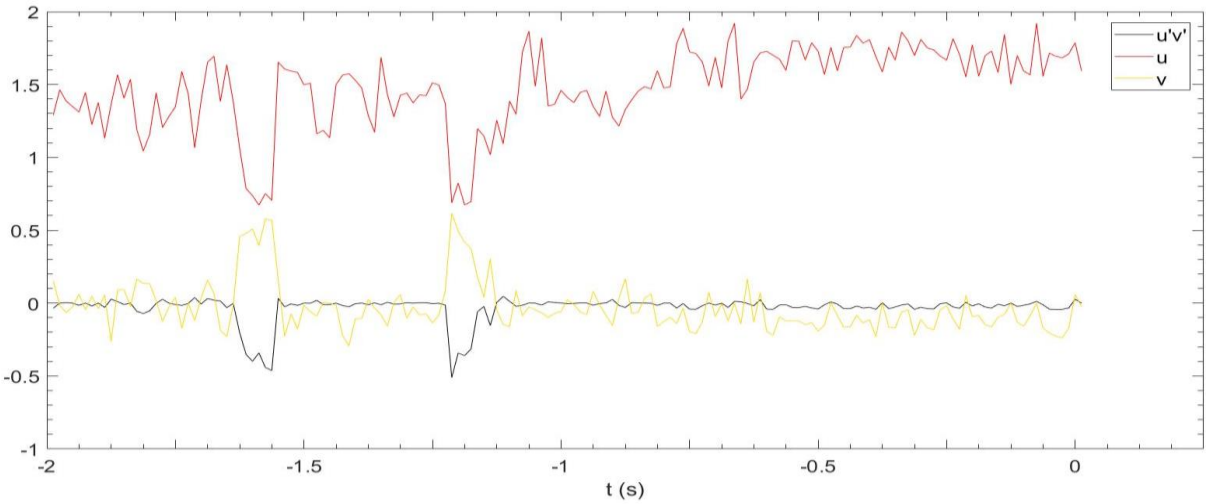

D4L35 F1

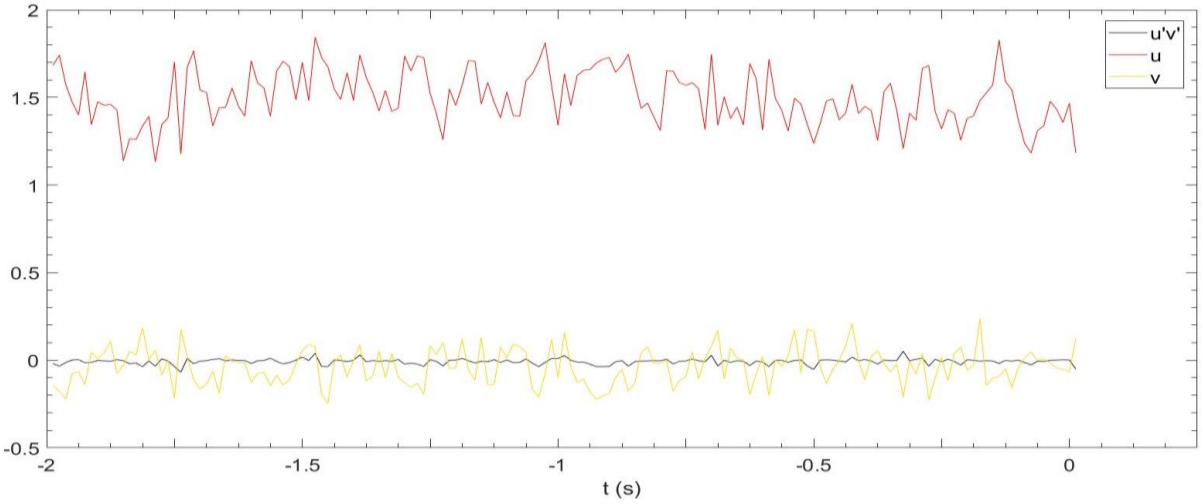

D4L35 F2

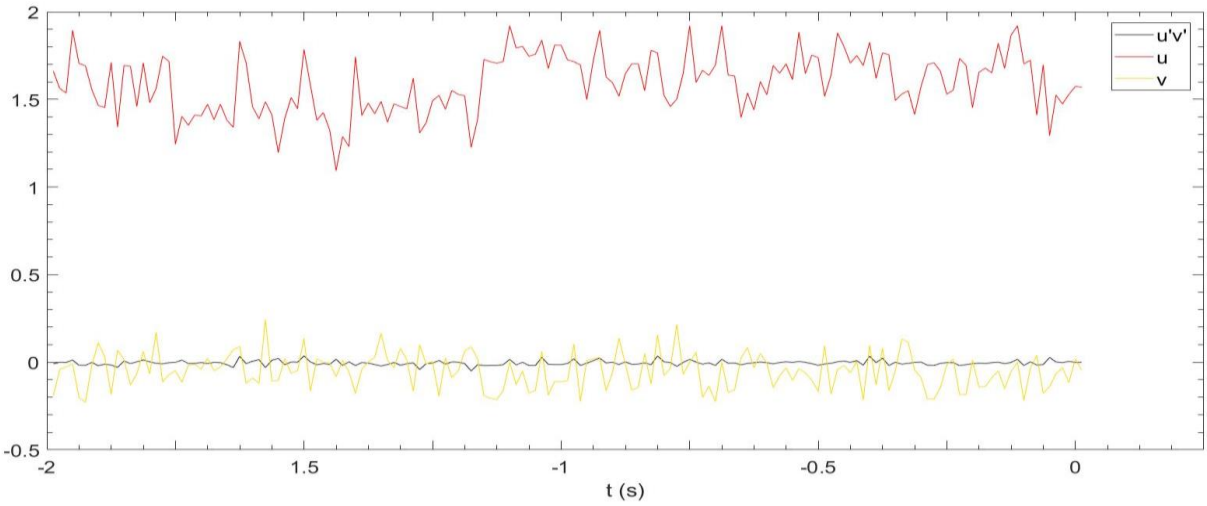

D4L35 F3

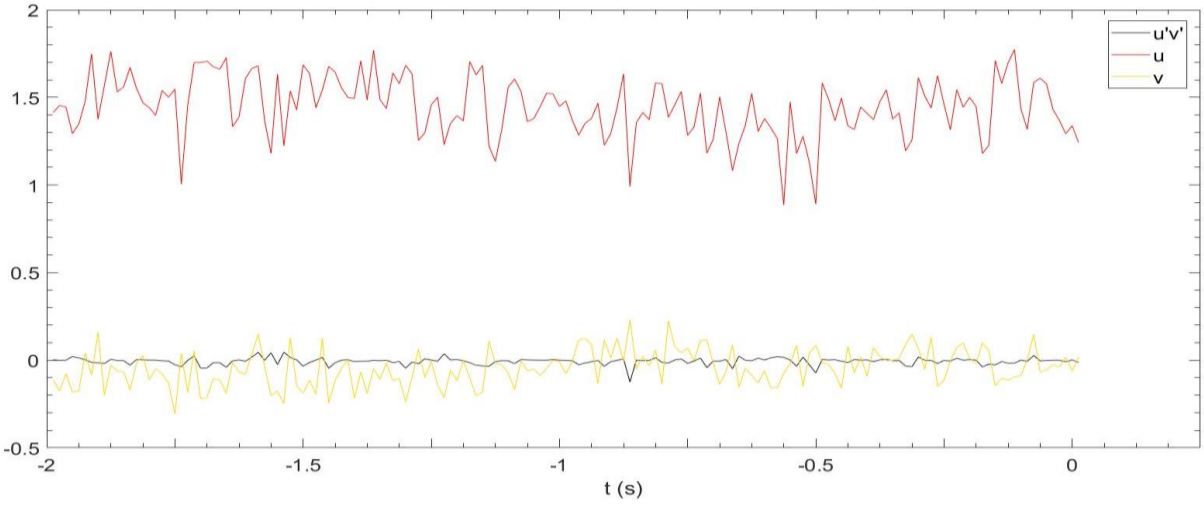

D4L35 F4

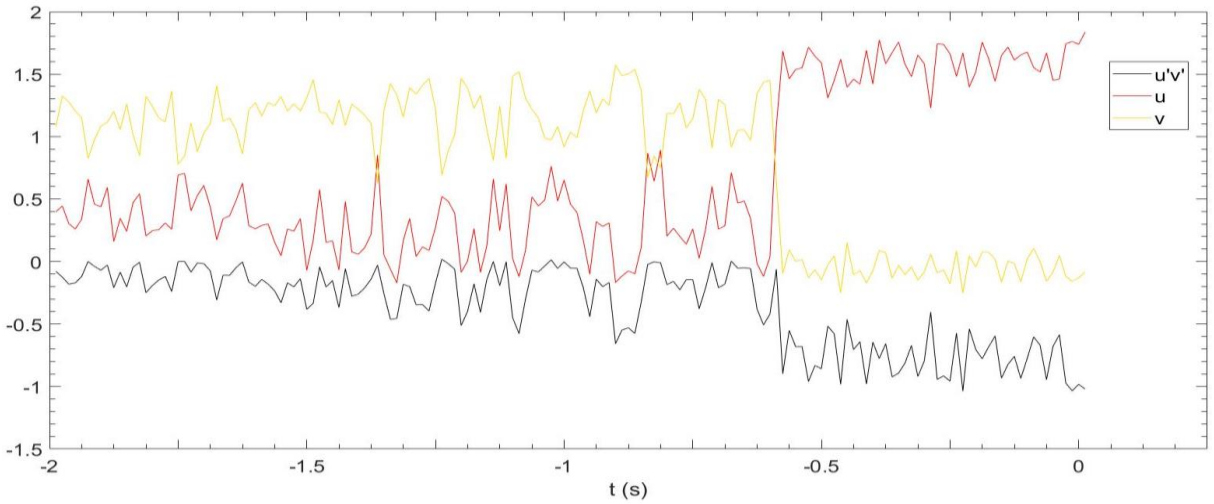

D4L35 F5

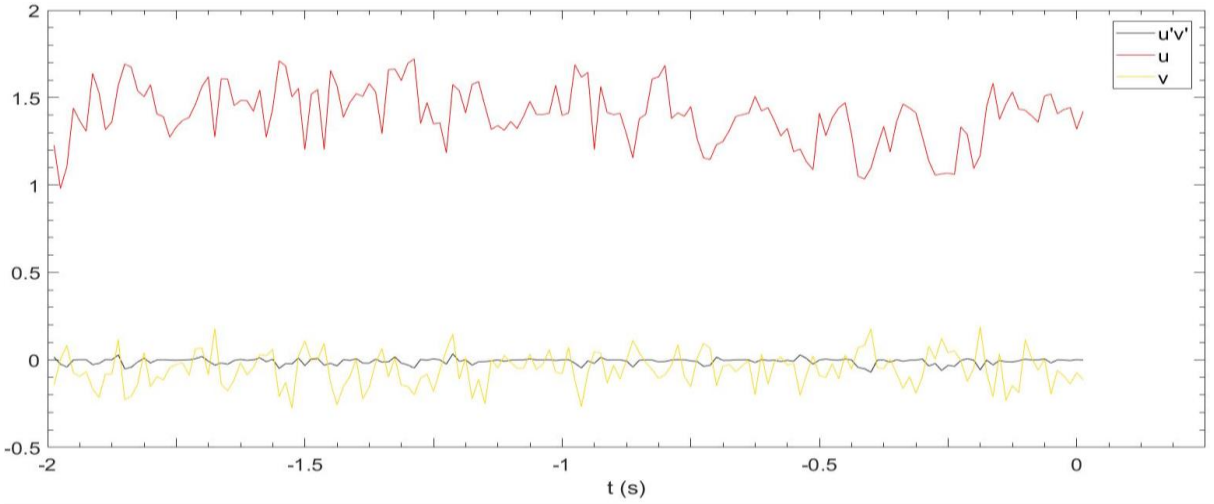

D4L45 F1

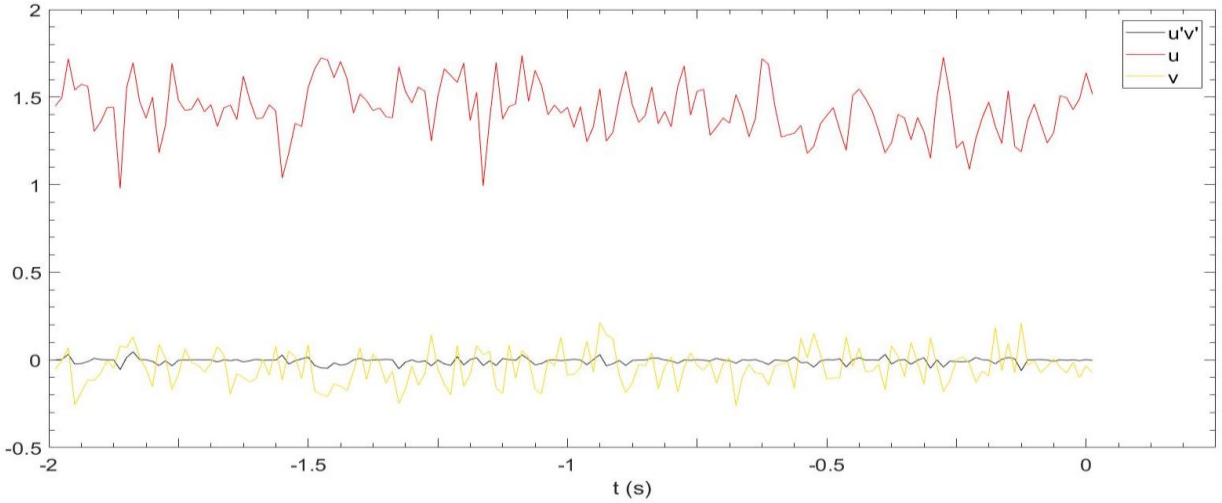

D4L45 F2

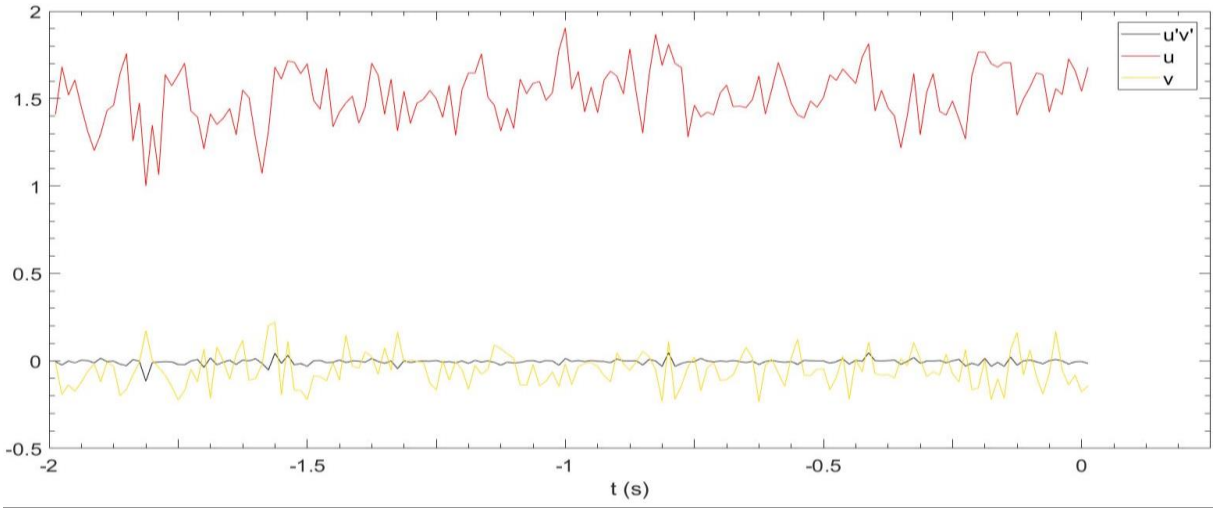

D4L45 F3

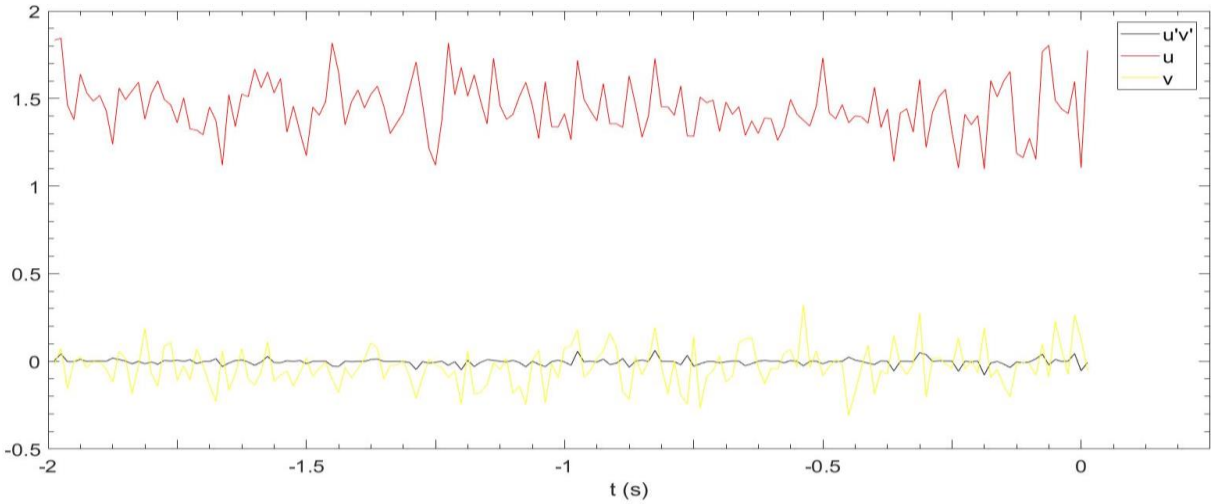

D4L45 F4

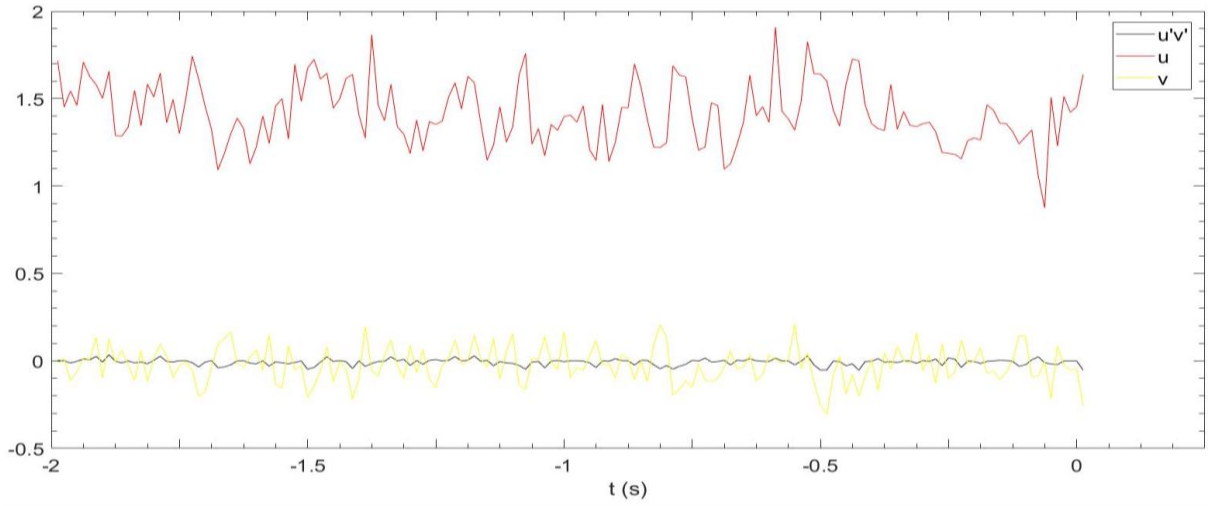

D4L45 F5

Appendix C: Data on the flow condition over the last row of block mattress.

Measuring point	$u[m/s]$	$v[m/s]$	$u'[m/s]$	$v'[m/s]$
1	1.167	-0.019	0.142	0.083
2	1.205	-0.092	0.132	0.077
3	1.254	-0.091	0.140	0.084
4	1.337	-0.085	0.131	0.079
5	1.393	-0.152	0.129	0.085
6	1.171	-0.152	0.174	0.122
7	0.655	-0.066	0.213	0.167
8	0.229	0.029	0.150	0.142
9	0.021	0.105	0.109	0.105
10	-0.030	0.137	0.100	0.091
11	-0.060	0.148	0.106	0.094
12	-0.115	0.163	0.110	0.092
13	-0.157	0.156	0.106	0.085

Appendix D: Database

The following table gives full information on discharge, velocity and turbulence properties of Database

Set-up	Q $[l/s]$	$\bar{u}$ $[m/s]$	u' $[m/s]$	v' $[m/s]$	$\sqrt{k}$ $[m/s]$
D3L55	27.95474	1.317971	0.186975	0.111213	0.172766
	28.26508	1.329776	0.192339	0.110246	0.175075
	28.55121	1.361942	0.192577	0.11106	0.175719
	28.98657	1.395126	0.201369	0.120875	0.186776
D3L45	21.0734	1.107352	0.137824	0.087665	0.131083
	21.49578	1.130885	0.146936	0.087746	0.135994
	22.30991	1.209194	0.156924	0.092931	0.144737
	23.10203	1.282151	0.16487	0.092893	0.149064
	23.48888	1.311923	0.15915	0.096514	0.148254
	24.79745	1.413698	0.156395	0.098261	0.147936
	25.19316	1.446218	0.178801	0.125772	0.178335
	25.59542	1.46224	0.169629	0.109896	0.162678
D4L35	27.57777	1.025898	0.136457	0.089482	0.131595
	28.51021	1.044586	0.146045	0.090944	0.137606
	29.26294	1.061615	0.148444	0.098692	0.144076
	30.00326	1.076626	0.150949	0.097715	0.14471
	30.89745	1.111679	0.159511	0.100731	0.151223
	31.40048	1.131929	0.159521	0.098365	0.149663
	32.71643	1.184514	0.172293	0.100853	0.158157
	33.40415	1.202426	0.171471	0.102354	0.158674
	34.10598	1.230676	0.181305	0.10652	0.16668
	34.77583	1.276568	0.17053	0.106095	0.160613
	35.28511	1.297008	0.176445	0.10713	0.164448
D4L45	35.76509	1.44519	0.161458	0.108012	0.157165
	35.798	1.441653	0.161785	0.106296	0.15616
	36.02525	1.460448	0.162062	0.106139	0.156197
	36.00197	1.460496	0.162887	0.106042	0.15656
	36.41548	1.475933	0.161261	0.105166	0.155121
	36.47996	1.474831	0.173498	0.111086	0.165502

Note:

1. The derivation of empirical turbulence magnification factor is sensitive to the accuracy of data, thus the original accuracy obtained directly from the LDV recorder remained.
2. For set-up D4l35, due to the bubble interference, it is not possible to collect the information on failure discharge. Thus extrapolation was applied. Therefore, more sets of data were collected to make the extrapolation more reliable.